USGS
science for a changing world

Prepared in cooperation with the Broward County Environmental Planning and Community Resilience Division

Drainage Infrastructure and Groundwater System Response to Changes in Sea Level and Precipitation, Broward County, Florida

Scientific Investigations Report 2022–5074

U.S. Department of the Interior
U.S. Geological Survey

Cover: Photograph showing flooding during a high-high tide event in Ft. Lauderdale, Fla. Photograph by Dorothy F. Sifuentes, U.S. Geological Survey.

Drainage Infrastructure and Groundwater System Response to Changes in Sea Level and Precipitation, Broward County, Florida

Edited by Jeremy D. Decker

Prepared in cooperation with the Broward County Environmental Planning and Community Resilience Division

Scientific Investigations Report 2022–5074

U.S. Department of the Interior
U.S. Geological Survey

U.S. Geological Survey, Reston, Virginia: 2022

For more information on the USGS—the Federal source for science about the Earth, its natural and living resources, natural hazards, and the environment—visit https://www.usgs.gov or call 1–888–ASK–USGS.

For an overview of USGS information products, including maps, imagery, and publications, visit https://store.usgs.gov/.

Suggested citation:
Decker, J.D., ed., 2022, Drainage infrastructure and groundwater system response to changes in sea level and precipitation, Broward County, Florida: U.S. Geological Survey Scientific Investigations Report 2022–5074, 99 p., https://doi.org/10.3133/sir20225074.

Associated data for this publication:
Decker, J.D., 2022, MODFLOW-NWT datasets for the simulation of drainage infrastructure and groundwater system response to changes in sea level and precipitation, Broward County, Florida: U.S. Geological Survey data release, https://doi.org/10.5066/P9ITQBFZ.

ISSN 2328-0328 (online)

Contents

Chapter D. Summary of Historical and Increased Sea-Level Scenario Simulation Results and Model Limitations

By Jeremy D. Decker

Chapter E. Numerical Model Construction

By Jeremy D. Decker

Figures

Chapter A

Chapter B

Chapter C

Chapter E

Tables

Chapter B

Chapter C

Chapter E

Conversion Factors

U.S. customary units to International System of Units

Multiply	By	To obtain
	Length	
inch (in.)	2.54	centimeter (cm)
inch (in.)	25.4	millimeter (mm)
foot (ft)	0.3048	meter (m)
mile (mi)	1.609	kilometer (km)
	Area	
square mile (mi^2)	259.0	hectare (ha)
square mile (mi^2)	2.590	square kilometer (km^2)
	Volume	
cubic foot (ft^3)	28.32	cubic decimeter (dm^3)
cubic foot (ft^3)	0.02832	cubic meter (m^3)
	Flow rate	
cubic foot per second (ft^3/s)	0.02832	cubic meter per second (m^3/s)
million gallons per day (Mgal/d)	0.04381	cubic meter per second (m^3/s)
million gallons per day per square mile ([Mgal/d]/mi^2)	1,461	cubic meter per day per square kilometer ([m^3/d]/km^2)
	Hydraulic conductivity	
foot per day (ft/d)	0.3048	meter per day (m/d)
	Leakance	
day^{-1}	1	day^{-1}

Datum

Vertical coordinate information is referenced to the North American Vertical Datum of 1988 (NAVD 88) and to the National Geodetic Vertical Datum of 1929 (NGVD 29).

Horizontal coordinate information is referenced to the North American Datum of 1983 (NAD 83).

Elevation, as used in this report, refers to distance above the vertical datum.

Abbreviations

CHD	Time-Variant Specified Head Boundary package
EDEN	Everglades Depth Estimation Network
ET	evapotranspiration
EVT	Evapotranspiration package
GHB	General Head Boundary package
GOES	Geostationary Operational Environmental Satellite
IPCC	Intergovernmental Panel on Climate Change
lidar	light detection and ranging
LWR	lower zone designation
MD	mean difference
MODFLOW	Modular Finite-Difference Groundwater Flow Model
NOAA	National Oceanic and Atmospheric Administration
NWT	Newton formulation
PEST	Parameter ESTimation software
PET	potential evapotranspiration
PEV	percent explained variance
PRD	production zone designation
RCH	Recharge package
RMSD	root mean square difference
SFWMD	South Florida Water Management District
SWR1	Surface-Water Routing process
UPR	upper zone designation
URO	Urban Runoff process
WCA	water conservation area

Drainage Infrastructure and Groundwater System Response to Changes in Sea Level and Precipitation, Broward County, Florida

Edited by Jeremy D. Decker

Executive Summary

Southeast Florida is highly susceptible to flooding because of its low topography and porous, highly permeable Biscayne aquifer. Rising seas will likely result in increased groundwater levels in parts of Broward County, Florida, that will reduce available soil storage and therefore increase the likelihood of inundation and flooding from precipitation events. Moreover, rising seas may also reduce the capacity of the coastal water-control structures to discharge inland waters to tidal areas, thereby increasing surface-water stage and nearby groundwater levels. Increased rainfall intensity will likely further increase peak surface-water stages and groundwater levels, more quickly fill the reduced soil storage capacity, and increase the likelihood for inundation. Managers and planners in Broward County, Florida, face the challenge of understanding and preparing for the consequent risk to residents, businesses, and critical infrastructure posed by increased sea level and precipitation.

The U.S. Geological Survey, in cooperation with the Broward County Environmental Planning and Resilience Division, has developed a groundwater/surface-water model to evaluate the response of the drainage infrastructure and groundwater system in Broward County to projected increases in sea level and potential changes in precipitation. The model was constructed using Modular Finite-Difference Groundwater Flow Model Newton formulation, with the surface-water system represented using the Surface-Water Routing process and the Urban Runoff process. The aquifer layering and flow parameters rely heavily on existing hydrologic flow models developed by the U.S. Geological Survey for the same model area. The surface-water drainage system within this newly developed model actively simulates the extensive canal network using level-pool routing and active structures representing gates, weirs, culverts, and pumps. Steady-state and transient simulation results represented historical conditions (2013–17). The simulated historical groundwater levels and upstream stage and flow at the primary structures generally captured the behavior of the actual hydrologic system. Simulation results incorporating increased sea level and precipitation were used to evaluate the effects of these projected changes on the surface-water drainage system and wet season groundwater levels.

Four future sea-level scenarios were simulated by modifying the historical inputs for both steady-state and the transient versions of the model to represent mean sea levels of 0.5, 2.0, 2.5, and 3.0 feet (ft) above the North American Vertical Datum of 1988. These mean sea levels correspond to sea-level rises of 1.05, 2.55, 3.05, and 3.55 ft, respectively, above the 2013–17 mean measured tidal stage. Additional simulations represented a 15-percent increase in rainfall rates using the transient model and a 15-percent increase in rainfall recharge using the steady-state model. The simulated results indicated that (1) the effects of increased sea level were more evident in the easternmost, coastal areas of the county where increases in groundwater levels are nearly equivalent to sea-level rise; (2) groundwater levels west of the coastal water-control structures only changed slightly in response to increased sea level for most scenarios; (3) when the control elevations of the gravity-controlled coastal water-control structures were surpassed by sea-level rise, the resulting increases in upstream stage in the connected primary canal resulted in increased groundwater levels that can propagate into the western parts of the county; (4) the historical west-to-east downward gradient in groundwater levels decreased with increased sea level, and groundwater levels were lower in central parts of the county than areas west and east for the higher sea-level scenarios; (5) simulated upstream stage for most of the primary coastal water-control structures increased with increased sea level, with the largest increases occurring at gravity-controlled structures having the lowest control elevations; (6) total flow through the primary structures increased as sea level increased because of additional groundwater leakage into the surface-water network; (7) the 3.0-ft mean sea-level rise scenario resulted in an increase of 37.10 square miles in area having a wet season average depth to groundwater of less than 2 ft, and an increase of 22.84 square miles in newly inundated areas compared to historical simulation results; and (8) a 15-percent increase in rainfall rate for the entire simulation period produced little increase in upstream stages at the primary structures and an increase in total flow through the primary structures proportional to the increase in rainfall.

Chapter A. Introduction

By Jeremy D. Decker

Background

In coastal Broward County, Florida, rising sea level has been empirically observed over the last decade, with increasingly frequent tidal inundation and increasing high-water elevations in low-lying and coastal areas. The increased sea level can substantially reduce the available soil water storage and drainage capacity because of the low elevation and flat topography of the county. The associated flooding risk is of particular concern during substantial precipitation events.

The relative sea-level trend observed at the Key West tidal gage from 1913 to 2020 was 0.0972 inches per year (in/yr), whereas the 50-year relative sea-level trend (1970–2020) shows a higher rate of 0.122 in/yr (National Oceanic and Atmospheric Administration, 2020). Sea-level rise projections for the next 100 years show, with time, an increasingly higher rate of sea-level rise leading to 10–17 inches (in.) of sea-level rise from 2020 to 2040 and a sea-level rise of 40–136 in. by 2120 (Southeast Florida Regional Climate Change Compact Sea Level Rise Work Group, 2020).

Projecting changes in future precipitation caused by changes in climate is more difficult than projecting future sea-level rise at the present time. Sea-level data present a clear, monotonically upward trend, whereas trends in rainfall are less clear and estimates of future precipitation characteristics are dependent on climate models with some degree of uncertainty. Possible climate change-induced increases in the frequency and (or) duration of rainfall events, coupled with decreased soil storage and drainage capacity caused by increased sea levels, could lead to increased vulnerability of both coastal and inland neighborhoods to surface ponding and flooding. The uncertainty in future climate coupled with the broad range in sea-level rise projections requires planners and managers to consider a range of possible changes in rainfall and sea level (Hallegatte and others, 2012; Weaver and others, 2013).

Understanding and mitigating the consequent risk of sea-level rise and (or) increased precipitation to residents, businesses, and critical infrastructure could support managers and planners in identifying areas of greatest vulnerability, testing management or adaptive actions, and projecting timelines for implementation of such actions. To help assess the current infrastructure and assist in possible adaptation and mitigation strategies, the U.S. Geological Survey (USGS), in cooperation with the Broward County Environmental Planning and Community Resilience Division, has developed a numerical surface-water/groundwater model of the urban areas of Broward County using Modular Finite-Difference Groundwater Flow Model Newton formulation (MODFLOW-NWT) (Niswonger and others, 2011), the Surface-Water Routing (SWR1) process (Hughes and others, 2012), and the Urban Runoff (URO) process (Decker and others, 2019). Steady-state and transient versions of the model were used to simulate the effects of projected changes to sea level and rainfall on surface-water stages, flow through the primary water-control structures, and groundwater levels.

These models can be used to help assess the capabilities of the county's current drainage network and the effectiveness of any proposed modifications to management practices or changes to physical infrastructure. The results produced by the numerical, physics-based surface-water/groundwater model provide insight into the behavior of the hydrologic system and can be used to assist decision makers and planners to weigh potential vulnerabilities and assess proposed changes. The hydrologic modeling tool can then be used to simulate additional scenarios involving changes in sea level, precipitation, and infrastructure. Results can be used to further analyze the system's response and evaluate potential adaptation or mitigation strategies.

Purpose and Scope

The purpose of this report is to provide simulation results and analyses that can be used to help evaluate changes to the drainage capacity and increased potential risk for landscape inundation for urbanized Broward County, Florida, under a range of sea-level projections and potential changes in precipitation. The study area extends south from the Hillsboro Canal, which defines the northern extent of Broward County, Florida, to the C-9 Canal, which crosses parts of southern Broward County and northern Miami-Dade County. The area is bounded to the west by the water conservation areas (WCAs) and to the east by the Atlantic coastline (fig. A1). The study periods consist of a historical 5-year period and four hypothetical, future 5-year periods defined by projected mean sea levels. Changes to groundwater levels, canal stages, and coastal structure flows caused by increased future sea levels are presented and analyzed to help understand the response of the hydrologic system.

This report documents the numerical models constructed using MODFLOW-NWT to simulate groundwater levels, surface-water stages, and coastal structure flows within the study area. Also included is a description of the components of the hydrologic system and the conceptual flow model. The changes in potential risk for landscape inundation caused by increases in mean sea level are quantified on the basis of simulated increases in groundwater levels resulting in decreased storage capacity between the water table and land surface. Potential increases in inland canal stages and changes to coastal structure flows caused by increases in sea level are also presented. Model inputs, executables, and post-processing tools required to reproduce simulation results and evaluate further changes to sea level, rainfall, and (or) changes to drainage infrastructure are provided in Decker (2022).

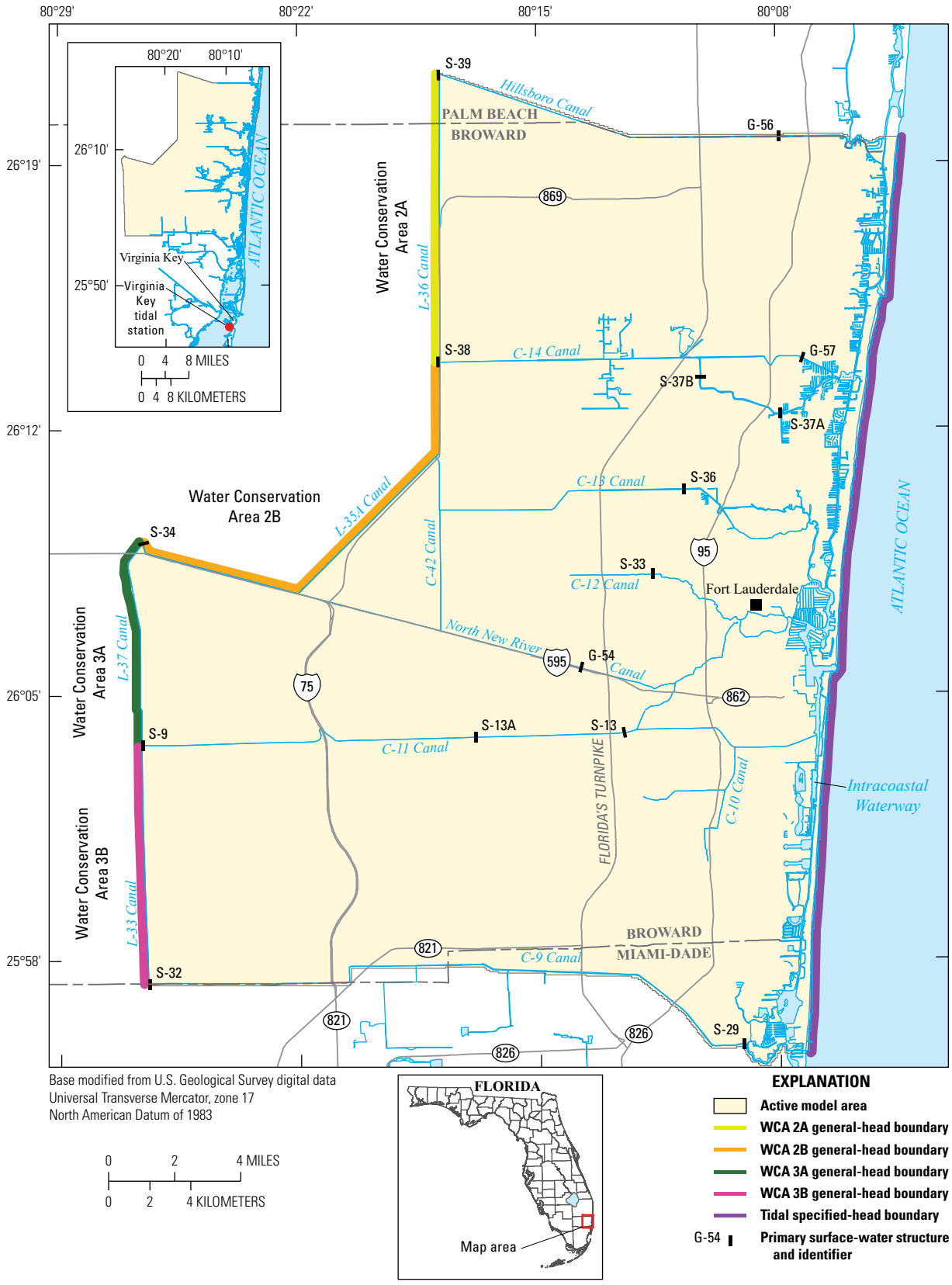

Figure A1. Model study area, Broward County, Florida.

Description of Study Area

Broward County is located on the southeast coast of the Florida peninsula and is the second most populous county in the State, with an estimated population of 1.9 million people as of July 2019 (U.S. Census Bureau, 2020). Broward County has a total land area of 1,225 square miles (mi^2) and is composed of a highly urbanized eastern third of the county and a largely undeveloped western two-thirds that includes the WCAs managed by the South Florida Water Management District (SFWMD). The urban area is separated from the WCAs by a protective levee, and water levels within the WCAs are maintained 4 feet (ft) higher, on average, than adjacent areas to the east (Broward County, 2019).

Broward County is generally low and flat, with most of the area being less than 20 ft above the North American Vertical Datum of 1988 (NAVD 88). The underlying, surficial Biscayne aquifer is shallow and composed of highly transmissive limestone (Renken and others, 2005). The aquifer is unconfined and largely recharged by infiltration from rainfall and surface-water flows. The average annual rainfall across the 18 rainfall measurement locations within the model extent (chapter E) during the 2013–17 historical period used for this study was 59.6 in., with the majority (41.8 in.) falling during the wet season (May 1–October 31) (SFWMD, 2022). In general, the year-to-year variability in rainfall can be high, with periodic wet and dry years. The groundwater and surface-water systems are well connected and the county has an extensive drainage system, which is designed and operated to accomplish several objectives. Excess water is routed from the WCAs to the coast to prevent flooding during the wet season or routed into the urban areas to recharge the groundwater system to meet water-supply demands during the dry season. The system is operated to prevent urban flooding while also maintaining sufficiently high groundwater levels to prevent salinity intrusion near water-supply wells (Renken and others, 2005). The county's drainage system consists of approximately 266 miles of primary canals managed by the SFWMD and an additional 1,800 miles of secondary and tertiary canals, many of which are managed by local drainage/water-control districts (Broward County, 2007). Despite the extensive and complex drainage infrastructure, flood-prone areas include the coastal areas east of the salinity control structures and the poorly drained areas in the western, urbanized areas that border the WCAs.

Related Studies

Models developed for three previous studies completed by the USGS with the cooperation of Broward County formed the basis for the current study: (1) a saltwater intrusion model of the northern part of Broward County, (2) a separate saltwater intrusion model of the central and southern parts of Broward County, and (3) a surface-water/groundwater model of the central and southern parts of Broward County. Langevin and Zygnerski (2013) developed the saltwater intrusion model for the northern part of coastal Broward County using SEAWAT (Langevin and others, 2008). This model was used to evaluate the sensitivity of well-field water quality to sea-level rise and well-field pumping rates. The model was calibrated using data from 1900 to 2005 and automated Parameter ESTimation (PEST) software, and sea-level rise was simulated using four different rates over 100 years. A saltwater intrusion model was developed separately for the central and southern parts of Broward County using SEAWAT (Hughes and others, 2016). The model was also calibrated using PEST to fit measured salinity and groundwater-level data from 1970 to 2012. A combination of coarse and fine discrete pilot points were used to increase pilot point coverage near the saltwater/freshwater interface. Individual cell-by-cell model parameter values were then spatially interpolated from these pilot points during the calibration process. Historical conditions were simulated from 1950 to 2012, and the sensitivity of the salinity distribution to sea-level rise and production well pumping was evaluated. The vertical layering within the surficial Biscayne aquifer was based on composite lithostratigraphic and conceptual hydrogeologic models.

The central and southern Broward County saltwater intrusion model relied on input datasets from two existing groundwater flow models during its development: (1) the Lower East Coast sub-Regional Model (Giddings and others, 2006) and (2) a groundwater/surface-water flow model of the urbanized areas of Broward County using the MIKE SHE and MIKE 11 simulator (referred to hereinafter as the "MIKE SHE model") (Islam and Dunn, 2006). The Lower East Coast sub-Regional Model was used to assist in projects involving water supply issues and the Comprehensive Everglades Restoration Plan. It was composed of smaller, high-resolution subregional groundwater flow models which were developed by the SFWMD and used the MODFLOW groundwater simulator. The subregional models were modified and combined into one larger model that spanned approximately 7,500 mi^2. The model was calibrated over a period of 14 years, from 1986 to 1999 (Giddings and others, 2006). The MIKE SHE model was used by Broward County to evaluate proposed water management plans (Islam and Dunn, 2006).

The third study (referred to hereinafter as the "inundation model"), which serves as a basis for the current modeling effort, involved the development of a surface-water/groundwater model of central and southern Broward County developed using MODFLOW-2005, the SWR1 process, and a newly developed URO process to calculate infiltration, recharge, and potential overland flow (Decker and others, 2019). A larger county-scale model with a 500-ft grid spacing and a local-scale submodel with a 167-ft grid spacing were developed to determine the benefits of grid refinement on model results. The groundwater-model layering and calibrated parameters from the salinity-intrusion model of central and southern Broward County constituted the model framework. The primary and

secondary canal systems within the central parts of the county were modeled dynamically using the SWR1 process. A combination of pumps, weirs, and underflow gate type water-control structures and level pool routing was used to simulate canal stage and structure flows for a historical (1990–99) period and for future (2060–69) scenarios. Three sea-level rise projections and the precipitation and potential evapotranspiration (PET) output of two dynamically downscaled general circulation models were used to evaluate possible changes in future groundwater levels, depth to groundwater, and the increased likelihood of inundation. The hydrologic model described in this report and used for the current analysis was constructed using the framework and parameters from these previous salinity intrusion and inundation models.

The SWR1 process within MODFLOW was first developed for and applied to a study area in Miami-Dade County, which is adjacent to southern Broward County (Hughes and White, 2014). The surface-water/groundwater model developed for the Miami-Dade County study was used to evaluate salinity intrusion during future scenarios involving changes to sea level and groundwater pumping. The model used the Seawater Intrusion package for MODFLOW to estimate the location of the saltwater/freshwater interface. This study also concluded that the SWR1 process adequately represented the connectivity between the extensive surface-water system within Miami-Dade County and the underlying groundwater aquifer, which is similar to the hydrologic system in Broward County.

Approach

For this study, a surface-water/groundwater flow model was developed using a modified version of MODFLOW-NWT (Niswonger and others, 2011), which included the previously developed URO process. The model area covers approximately 456 mi^2 of the urbanized, eastern part of Broward County (fig. A1), and the model uses a square 250-ft model grid spacing. The model uses the aquifer layering scheme developed for the central and southern saltwater intrusion models created for Broward County (Hughes and others, 2016). The vertical layering was reduced from 12 to 3 layers using the upper, production, and lower zone designations used during that saltwater intrusion model's calibration process by Hughes and others (2016). Calibrated aquifer parameters from the northern and the central and southern saltwater intrusion models were spatially interpolated and vertically averaged to obtain groundwater parameter values for the current model. Land surface elevations were derived from light detection and ranging (lidar) data collected as part of the Florida Division of Emergency Management Statewide Coastal LiDAR Project (SFWMD, 2007).

Steady-state and transient model scenarios were created using a modified version of MODFLOW-NWT (Niswonger and others, 2011). MODFLOW-NWT offers a Newton-Raphson formulation for MODFLOW-2005 (Harbaugh, 2005), which can improve the solution convergence of unconfined groundwater-flow problems. MODFLOW is a three-dimensional finite-difference groundwater model that can be used to simulate steady-state and transient three-dimensional groundwater flow based on Darcy's Law and the conservation of mass. For the transient simulations, the groundwater flow model uses daily stress periods with 25 time steps per day, the SWR1 process uses 3 time steps per groundwater time step resulting in 75 time steps per day, and the URO process uses 4 time steps per groundwater time step resulting in 100 time steps per day. The high number of time steps per day within the groundwater flow model reduces the number of iterations because the SWR1 and URO processes are linked to the MODFLOW model at the time step level.

The required model inputs include aquifer properties such as layer geometry and elevations, vertical and horizontal hydraulic conductivities, specific yield, and specific storage. Required groundwater boundary inputs include groundwater levels and flow-conductance values along the WCAs and specified tidal levels along the eastern boundary. The required groundwater flux input includes groundwater pumping and PET and recharge when using the Evapotranspiration and Recharge packages. The SWR1 process was used to dynamically simulate the canal stages, leakages, and structure flows in the modeled area. Required model inputs include canal locations and connectivity, canal cross-sectional information, canal leakance values, water-control structure locations and properties, specified-canal fluxes from the WCAs, and specified-canal stages for tidal and tail water locations. The URO process calculates the overland surface storage, infiltration, and recharge for the transient model simulations. The required inputs include rainfall rates, PET, and maximum infiltration and recharge rates.

The simulated surface-water model included primary, secondary, and some tertiary drainage features. Level-pool routing between specified surface-water structures was used. Each water control/drainage district was simulated as one or more level pools depending on that district's operational practices and infrastructure. Flow connections along primary drainage canals were simulated using flow connections defined by Manning's equation. Surface-water stages were specified for tidal and intracoastal SWR1 reaches using measured and projected sea levels. Canal stages downstream from the coastal water-control structures were also specified using measured tail water values and estimates for future scenarios. Measured discharges from the WCAs were applied as fluxes to the corresponding primary canals, and additional estimated fluxes were assigned along the Hillsboro and C-9 Canals (fig. A1) representing surface-water inflows from missing parts of the corresponding drainage areas.

The canal bed leakance values used by the SWR1 process to calculate leakage between the surface-water and groundwater systems were spatially assigned on the basis of water

control/drainage districts or drainage areas and were adjusted within the steady-state model using PEST automated calibration software. The general head boundary (GHB) conductance values along the western boundaries were calculated using previously calibrated hydraulic conductivity values from the central and southern saltwater intrusion model and were scaled using PEST. The evapotranspiration extinction depths used by the central and southern saltwater intrusion model were scaled using PEST as well. The average wet season observations during the historical period (2013–17) were used as steady-state model inputs for rainfall, PET, WCA water levels, and tidal levels. Input data were prepared for the same historical period and for several hypothetical, future 5-year periods defined by given projected sea levels and their associated potential ranges in arrival time. Datasets with modifications to existing rainfall were used to evaluate the potential effects on the hydrologic system as well. The resulting changes in canal stages, flow through the primary water-control structures, and groundwater levels for the various scenarios are presented and analyzed. The changes to average wet season groundwater levels and decreased depth to groundwater are presented as indicators of an increased likelihood for landscape inundation under future conditions.

The model was used to simulate changes in groundwater levels, canal stages, and structure flows for four future sea-level scenarios and possible changes to precipitation. The four sea-level scenarios were chosen on the basis of current coastal water-control structure elevations and the expected encroachment of tidal levels within the corresponding gate operational ranges. A range of expected arrival dates were generated for each possible future sea-level scenario on the basis of the "Unified Sea Level Rise Projection for Southeast Florida" document by the Southeast Florida Regional Climate Change Compact Sea Level Rise Work Group (2020).

Conceptual-Flow Model

The surface-water control volume has inflows that include precipitation, groundwater discharge within inundated areas, aquifer-to-canal discharge, and canal inflows from western control structures. The surface-water control volume has outflows that include evapotranspiration (ET), infiltration into the unsaturated zone, canal-to-aquifer leakage, and canal discharge through coastal and western control structures. The groundwater aquifer control volume has inflows that include infiltration into the unsaturated zone, canal-to-aquifer leakage, and fluxes from the eastern and western boundaries which represent the Atlantic Ocean and WCAs, respectively. The groundwater aquifer control volume has outflows that include aquifer-to-canal leakage, ET losses, groundwater pumping, and fluxes to the eastern and western boundaries which represent the Atlantic Ocean and WCAs, respectively.

Precipitation and Evapotranspiration

Rainfall was applied to the model through a spatially variable time series created using data from 18 rainfall measurement locations within the model extent (chapter E). Each model grid was assigned the rainfall zone value of the location nearest to the grid's center point. During the 2013–17 historical period, the annual rainfall for the average of these zones ranged from 52.3 to 73.5 in/yr, with an average of 59.6 in/yr (fig. A2). The average wet season (May 1–October 31) rainfall during this period was 40.8 in. or 0.222 inches per day. The spatially variable, average wet season rainfall values were applied as recharge to the steady-state model and ET was removed using the MODFLOW EVT (evapotranspiration) package.

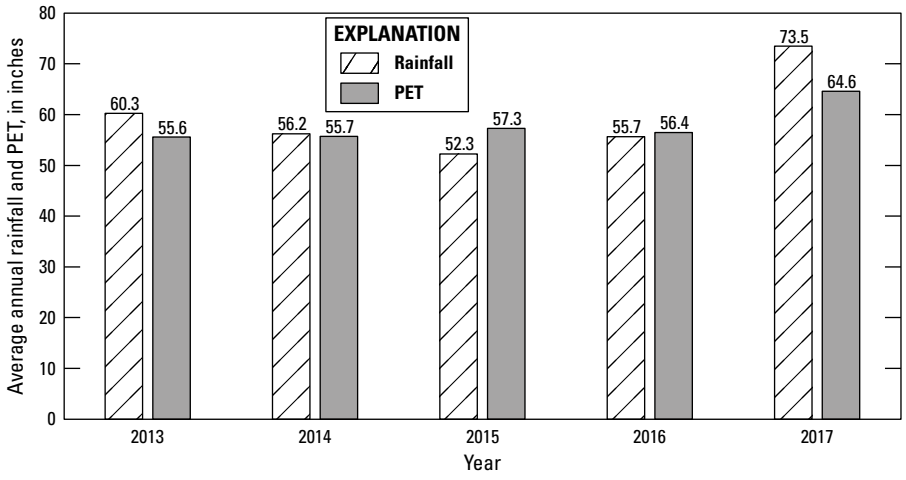

Figure A2. Average annual rainfall and potential evapotranspiration (PET) within the study area for the historical simulation period (2013–17).

PET data were used by MODFLOW to calculate the actual ET during the model simulations. The steady-state model uses the MODFLOW EVT package which calculates ET losses from the saturated groundwater model using a linear relationship and user-defined maximum ET rates, an ET surface, and ET extinction depths. The transient model uses the URO process to calculate the ET losses from the surface water, unsaturated zone, and the saturated zone. ET is removed at the full potential rate from the surface water, at a reduced rate based on the water content from the unsaturated zone, and from the saturated zone using the same methodology as the EVT package (Decker and others, 2019). The PET input dataset was calculated from 2-kilometer-scale Geostationary Operational Environmental Satellite (GOES) PET data for the State of Florida published by the USGS (Shoemaker, 2017; Mecikalski and others, 2018). The same zones established for rainfall were used for the application of PET. Daily values of PET for each rainfall zone were calculated as the mean of the GOES PET values contained within. The yearly PET for the average of these zones ranged from 55.6 to 64.6 in/yr, with an average of 57.9 in/yr (fig. A2). The maximum difference between the averages of the 18 zones was 2.5 percent during this time period. The average wet season PET was 36.2 in. per season or 0.197 inches per day. PET for the steady-state model was applied using a uniform average wet season value.

Groundwater Pumping

The surficial Biscayne aquifer is the primary water supply for Broward County. Water is removed from the groundwater model using monthly pumping rates at locations obtained from SFWMD databases (Kellie Madison, SFWMD, unpub. data, 2019).[1] An average of 215.9 million gallons per day is withdrawn from the study area during the historical simulation period (2013–17) (fig. A3). The pumping rates and locations from the historical period were used for all modeling scenarios.

Surface-Water System

The extensive canal system within the model area consists of primary, secondary, and tertiary drainage features. Surface-water control structures include gravity-controlled structures such as weirs and gates as well as pump structures. Drainage within the primary system is controlled by the SFWMD, whereas the secondary drainage can be controlled locally by water control districts, drainage districts, cities, or improvement/development districts (fig. A4). The tertiary drainage features consist of canals and features located on private lands and provide drainage into retention/detention areas or into the secondary system. Drainage from the secondary system into the primary system is typically controlled by pumps, gates, or fixed weirs to maintain target control elevations within the district or city. Pumps are simulated in the SWR1 process using a stage-discharge curve, and weirs and gates are simulated with formulations representing fixed-crest weirs or fixed-opening underflow gates. Coastal movable underflow gates represented by fixed gates in the model have specified invert elevations based on the gate opening and closing heights and only allow unidirectional flow from inland to coastal areas. Water can be pumped from or drained to the primary system from the WCAs that compose the western extent of the study area or drained or pumped from the system to tidal waters near the eastern extent of the study area (fig. A1). The surface-water system is operated to maintain high enough groundwater levels and gradients to prevent salinity intrusion and protect well-field water quality while preventing inland flooding.

The aquifer is well connected to the surface-water system. Leakage from the surface-water system can recharge the underlying aquifer when canal stages exceed groundwater

[1]At the time of publication, data were not available from South Florida Water Management District.

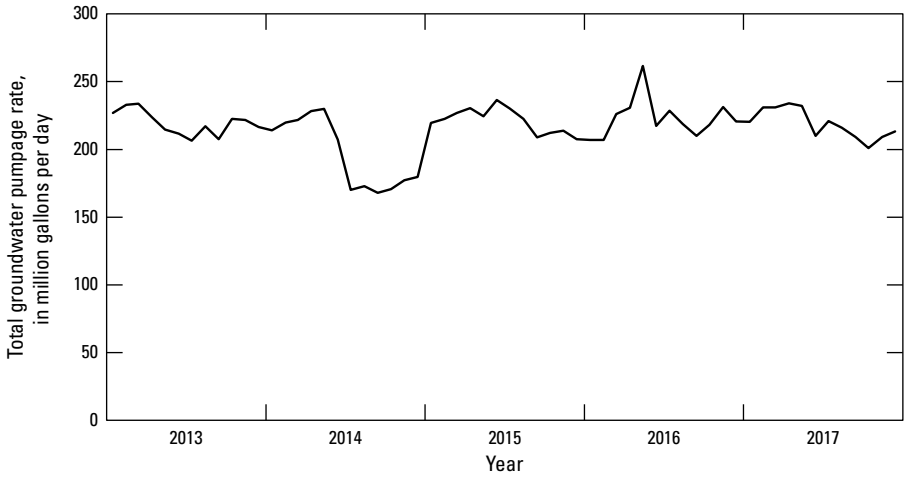

Figure A3. Total groundwater-pumping rate in the study area used for all simulations.

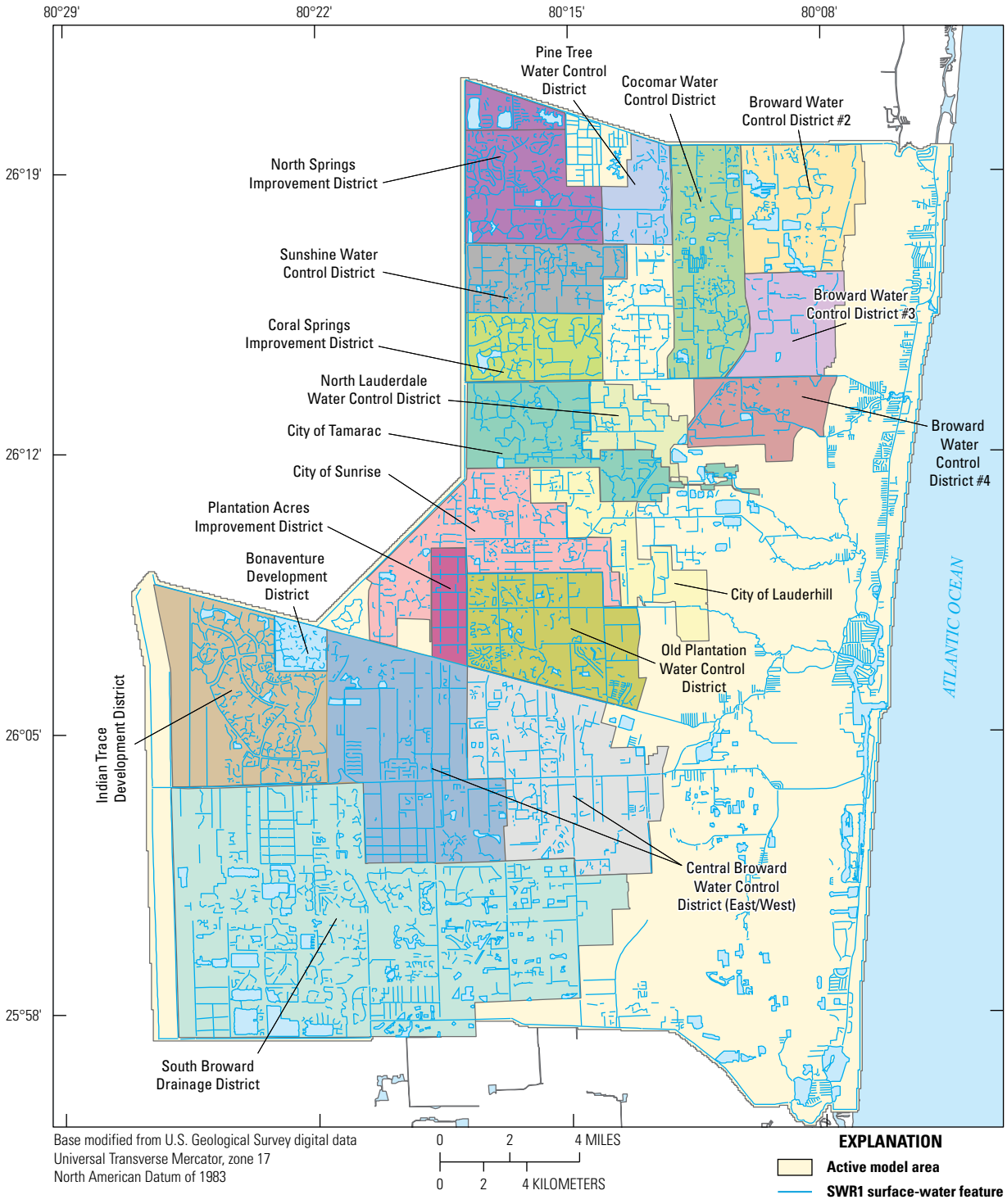

Figure A4. Surface-water features and water control/drainage districts simulated using the Surface-Water Routing (SWR1) process within the study area.

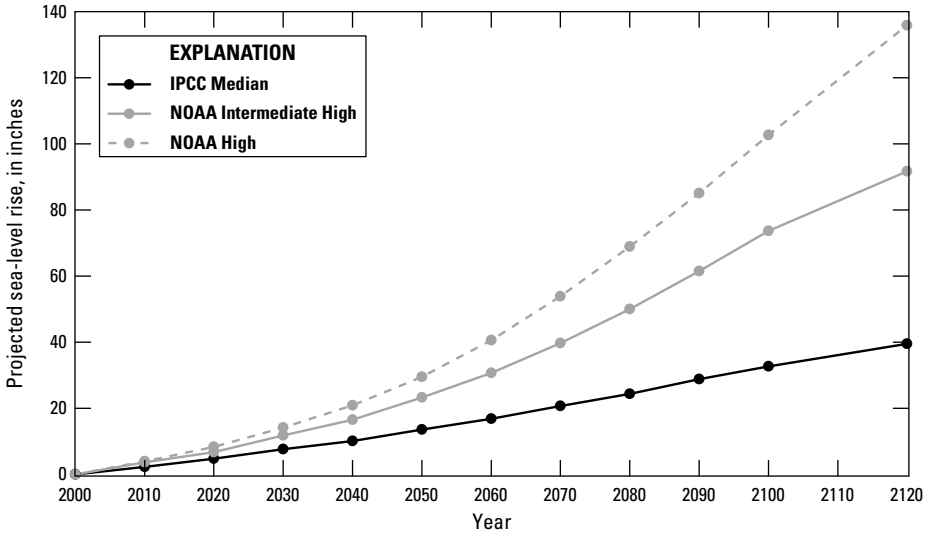

Figure A5. Projected mean sea-level rises in inches using the Intergovernmental Panel on Climate Change (IPCC) Median, the National Oceanic and Atmospheric Administration (NOAA) Intermediate-High, and the NOAA High curves (Southeast Florida Regional Climate Change Compact Sea Level Rise Work Group, 2020).

levels. The opposite occurs when groundwater levels exceed canal stages and groundwater discharges to the surface-water system. The directionality of canal leakage is localized and dependent on season and water-management practices.

Regional Groundwater Flow

The study area is bounded by the WCAs to the west and the Atlantic Ocean to the east (fig. A1). Groundwater levels are generally higher in the west compared to the east and higher in the north compared to the south, resulting in a potentiometric surface that slopes from northwest to southeast. The potentiometric surface is relatively flat with localized cones of depression formed around major production-well locations (Renken and others, 2005).

Future increases in sea level could alter existing regional groundwater levels, resulting in changes in groundwater/surface-water flows. Increased groundwater levels will likely reduce available soil storage and increase the likelihood of surface inundation. Additionally, possible reductions in groundwater level gradients can increase saltwater intrusion and result in water-quality issues near production-well locations. Future sea-level rise estimates produced by the National Oceanic and Atmospheric Administration and the Intergovernmental Panel on Climate Change and adopted by the Southeast Florida Regional Climate Compact Sea Level Rise Work Group indicate sea-level rise could reach 16.8–40.56 in. by 2060 and 39.48–135.84 in. by 2120 (fig. A5) (Southeast Florida Regional Climate Change Compact Sea Level Rise Work Group, 2020).

References Cited

Broward County, 2007, Broward County, Florida water quality atlas—Freshwater canals 1998–2003: Broward County Environmental Protection Department Technical Report Series, TR–07–03, accessed July 14, 2022, at https://www.broward.org/EnvironmentAndGrowth/EnvironmentalProgramsResources/Publications/Documents/water_atlas_19982003.pdf.

Broward County, 2019, 2019 Integrated Water Resource Plan update—Building resiliency in water management: Slide presentation, 79 p., accessed November 4, 2021, at https://www.broward.org/waterresources/pages/integrated-water-resource-plan.aspx.

Decker, J.D., 2022, MODFLOW-NWT datasets for the simulation of drainage infrastructure and groundwater system response to changes in sea-level and precipitation, Broward County, Florida: U.S. Geological Survey data release, https://doi.org/10.5066/P9ITQBFZ.

Decker, J.D., Hughes, J.D., and Swain, E.D., 2019, Potential for increased inundation in flood-prone regions of southeast Florida in response to climate and sea-level changes in Broward County, Florida, 2060–69: U.S. Geological Survey Scientific Investigations Report 2018–5125, 106 p., accessed November 3, 2021, at https://doi.org/10.3133/sir20185125.

Giddings, J.B., Kuebler, L.L., Restrepo, J.I., Rodberg, K.A., Montoya, A.M., and Radin, H.A., 2006, Lower east coast subregional (LECsR) MODFLOW model documentation: South Florida Water Management District draft report, 213 p., accessed November 4, 2020, at https://www.sfwmd.gov/sites/default/files/documents/lec_sr_draft_documentation.pdf.

Hallegatte, S., Shah, A., Lempert, R., Brown, C., and Gill, S., 2012, Investment decision making under deep uncertainty—Application to climate change: Washington, D.C., World Bank, World Bank Policy Research Working Paper 6193, 41 p.

Harbaugh, A.W., 2005, MODFLOW-2005, the U.S. Geological Survey modular ground-water model—The ground-water flow process: U.S. Geological Survey Techniques and Methods, book 6, chap. A16, 253 p.

Hughes, J.D., Langevin, C.D., Chartier, K.L., and White, J.T., 2012, Documentation of the Surface-Water Routing (SWR1) process for modeling surface-water flow with the U.S. Geological Survey Modular Ground-Water Model (MODFLOW-2005): U.S. Geological Survey Techniques and Methods, book 6, chap. A40 (ver. 1.0), 113 p.

Hughes, J.D., Sifuentes, D.F., and White, J.T., 2016, Potential effects of alterations to the hydrologic system on the distribution of salinity in the Biscayne aquifer in Broward County, Florida: U.S. Geological Survey Scientific Investigations Report 2016–5022, 114 p., accessed November 3, 2021, at https://doi.org/10.3133/sir20165022.

Hughes, J.D., and White, J.T., 2014, Hydrologic conditions in urban Miami-Dade County, Florida, and the effect of groundwater pumpage and increased sea level on canal leakage and regional groundwater flow: U.S. Geological Scientific Investigations Report 2014–5162, 175 p., accessed August 1, 2018, at https://doi.org/10.3133/sir20145162.

Islam, N., and Dunn, D., 2006, Recalibration and consolidation of integrated surface water and groundwater models for Broward County: Broward County Environmental Protection Department, Water Resources Division, 40 p.

Langevin, C.D., Thorne, D.T., Jr., Dausman, A.M., Sukop, M.C., and Guo, W., 2008, SEAWAT version 4—A computer program for the simulation of multi-species solute and heat transport: U.S. Geological Survey Techniques and Methods, book 6, chap. A22, 39 p.

Langevin, C.D., and Zygnerski, M., 2013, Effect of sea-level rise on saltwater intrusion near a coastal well field in southeastern Florida: Ground Water, v. 51, no. 5, p. 781–803.

Mecikalski, J.R., Shoemaker, W.B., Wu, Q., Holmes, M.A., Paech, S.J., and Sumner, D.M., 2018, High-resolution GOES insolation–evapotranspiration data set for water resource management in Florida—1995–2015: Journal of Irrigation and Drainage Engineering, v. 144, no. 9, 04018025, accessed November 3, 2021, at https://doi.org/10.1061/(ASCE)IR.1943-4774.0001312.

National Oceanic and Atmospheric Administration, 2020, Relative sea level trend— 8724580 Key West, Florida: National Oceanic and Atmospheric Administration web page, accessed November 3, 2020, at https://tidesandcurrents.noaa.gov/sltrends/sltrends_station.shtml?id=8724580.

Niswonger, R.G., Panday, S., and Ibaraki, M., 2011, MODFLOW-NWT—A Newton formulation for MODFLOW-2005: U.S. Geological Survey Techniques and Methods, book 6, chap. A37, 44 p.

Renken, R.A., Dixon, J., Koehmstedt, J., Ishman, S., Lietz, A.C., Marella, R.L., Telis, P., Rogers, J., and Memberg, S., 2005, Impact of anthropogenic development on coastal ground-water hydrology in southeastern Florida, 1900–2000: U.S. Geological Survey Circular 1275, 77 p.

Shoemaker, W.B., 2017, Daily reference (RET) and potential (PET) evapotranspiration data over Florida: U.S. Geological Survey data release, accessed May 27, 2020, at https://www.usgs.gov/centers/car-fl-water/science/reference-and-potential-evapotranspiration?qt-science_center_objects=0#qt-science_center_objects.

South Florida Water Management District (SFWMD), 2007, 2007 Broward 5-ft DEM in NAVD 1988, release version 1: South Florida Water Management District (SFWMD), accessed August 4, 2021, at https://geo-sfwmd.hub.arcgis.com/documents/broward-2007-fdem-5-ft/about.

South Florida Water Management District (SFWMD), 2022, DBHYDRO—Environmental data: South Florida Water Management District (SFWMD) database, accessed July 14, 2022, at www.sfwmd.gov/science-data/dbhydro.

Southeast Florida Regional Climate Change Compact Sea Level Rise Work Group, 2020, Unified sea level rise projection southeast Florida: Southeast Florida Regional Climate Change Compact Climate Leadership Committee, 36 p., accessed November 3, 2021, at https://southeastfloridaclimatecompact.org/unified-sea-level-rise-projections/.

U.S. Census Bureau, 2020, Annual estimates of the resident population for Counties in Florida—April 1, 2010 to July 1, 2019: U.S. Census Bureau, Population Division, March 2020, CO–EST2019–ANNRES–12, accessed November 3, 2020, at https://www.census.gov/data/tables/time-series/demo/popest/2010s-counties-total.html.

Weaver, C.P., Lempert, R.J., Brown, C., Hall, J.A., Revell, D., and Sarewitz, D., 2013, Improving the contribution of climate model information to decision-making—The value and demands of robust decision frameworks: Wiley Interdisciplinary Reviews, Climate Change, v. 4, no. 1, p. 39–60.

Chapter B. Simulation of Hydrologic System Under Historical Conditions (2013–17)

By Jeremy D. Decker

The groundwater/surface-water flow model was developed to simulate groundwater levels, surface-water stages, and surface-water control structure flows throughout the urbanized areas of Broward County. Steady-state and transient model realizations representing the 2013–17 historical period were prepared and simulated. The focus of the study was to produce accurately simulated wet season groundwater levels, stage, and flow through the primary structures. The wet season typically is characterized by the highest groundwater levels and the most frequent and intense precipitation events, making it the most vulnerable period for inundation and flooding. The steady-state model represented average wet season conditions for this period, and it was used to calibrate canal leakages, general head boundary conductance values, and evapotranspiration extinction depths used by the Modular Finite-Difference Groundwater Flow Model (MODFLOW) and the Surface-Water Routing (SWR1) process. Other parameters for the steady-state and transient models were derived from existing, calibrated models or estimated on the basis of published values. Details of model construction are provided in chapter E. Once developed, the models were then used to simulate possible future conditions involving increased sea levels and changes in precipitation (chapter C). Model input files, executables, and outputs described here are included in the associated U.S. Geological Survey data release (Decker, 2022).

Simulation of Steady-State Wet Season Conditions

Simulated groundwater levels at 23 groundwater monitoring locations and simulated upstream canal stages and flows at 10 primary water-control structures were compared to measured, wet season (May 1–October 31) averages from 2013–17 (fig. B1). Simulated wet season groundwater levels ranged from −0.481 to 9.324 feet (ft) above the North American Vertical Datum of 1988 (NAVD 88) (fig. B2) over the model area. The simulated wet season groundwater levels simulated at the groundwater monitoring locations ranged from 0.047 to 9.09 ft above NAVD 88 with differences in simulated groundwater levels and measured mean groundwater levels ranging from −1.430 to 4.545 ft, with a mean difference of 0.171 ft (table B1). The largest difference between simulated and measured values occurred at G-2395. The main reason for this large difference is that G-2395 is located within a production well field. The localized effects of production wells and their drawdowns may be underrepresented in the model because of the scale of model discretization. Excluding this groundwater measurement location from the analysis results in a mean difference of −0.028 ft. Additionally, some differences in groundwater levels can be attributed to the deviation in simulated surface-water stages in nearby SWR1 reaches compared to historical surface-water levels. The simulated surface-water stages and flows between level pool reach groups representing water-control districts and drainage areas are controlled by SWR1 structures having defined control elevations. Simulated structure operations likely deviate from actual operations, resulting in differences in simulated surface-water stages and flows when compared to measured values. Simulated groundwater levels near these surface-water features will then deviate from measured values because of the strong connection between the surface-water and groundwater systems. A focus on seasonal simulation results likely lessens the effects of the differences in the timing of structure operations. The simulated groundwater levels across four transects show a general west-to-east groundwater gradient with the highest groundwater levels located in the northern part of the county (fig. B3).

The invert elevations, which define the bottoms of the structure openings of the primary coastal structures, were adjusted to lessen the differences between simulated and measured mean upstream stages. Some invert elevations had to be adjusted out of their specified operational ranges to match the measured upstream stage value during the historical wet season, which is likely because of deviations in actual operations from those specified. The differences in simulated and measured mean upstream stage at the primary structures ranged from −0.031 to 0.839 ft, with a mean value of 0.150 ft. The differences in flow rate at the primary structures between simulated and measured wet season means ranged from −153.1 to 30.9 cubic feet per second (ft^3/s) (table B2). The largest structure flow error of −153.1 ft^3/s occurred at S-37A. The average wet season flow rate measured at S-37A is 141.4 ft^3/s greater than the average wet season flow rate measured at S-37B during the 2013–17 historical period and is not supported by the proximity of these two structures and the local hydrology. Therefore, the flow rate at S-37A was not included in the calibration process because of the likelihood of flow measurement errors and was replaced by the flow rate at S-37B. When flow at S-37B was used in place of S-37A, the mean difference in flow rate was −4.2 ft^3/s and the total difference in simulated and measured flow rate through the primary structures was −37.3 ft^3/s or −1.9 percent (table B2).

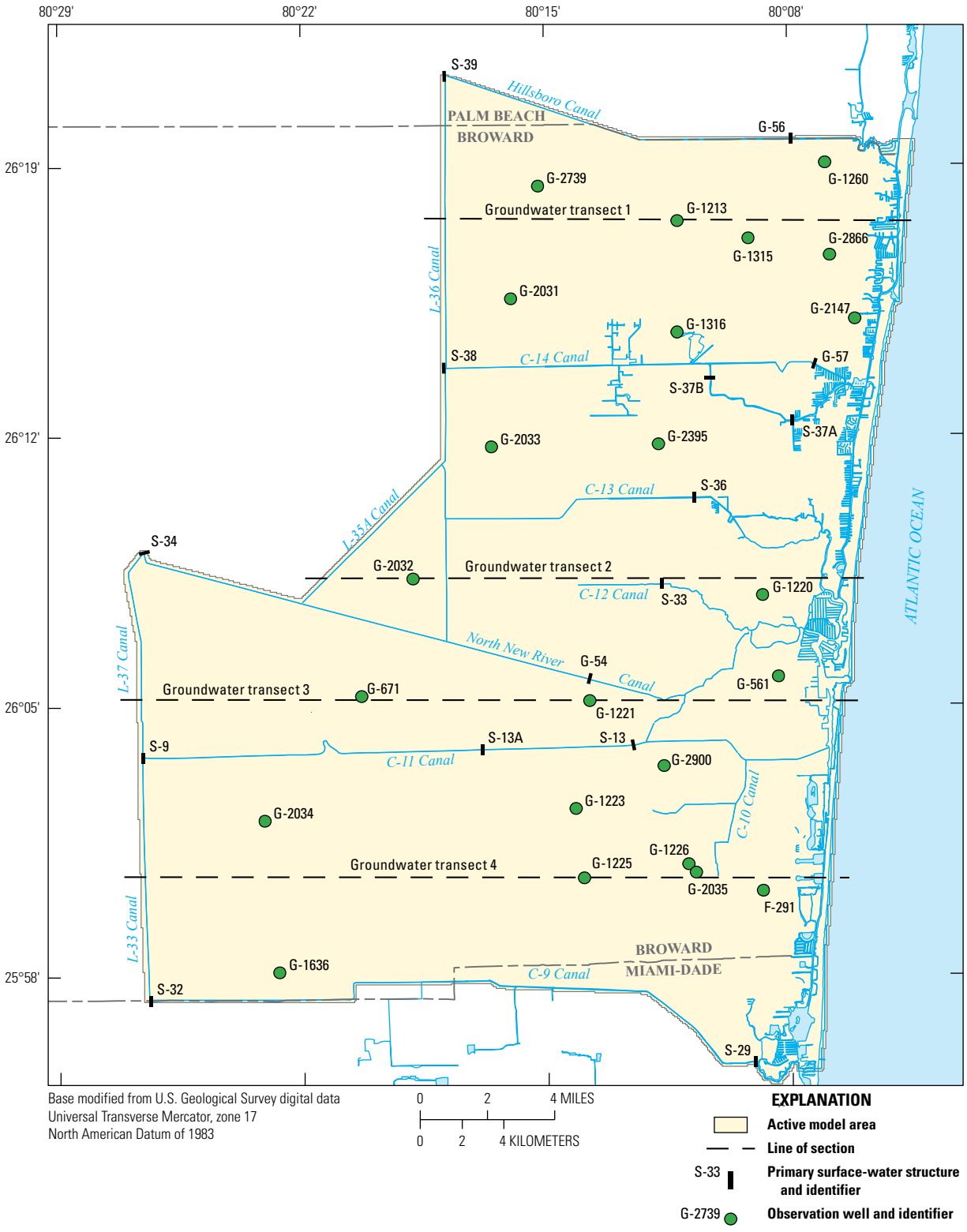

Figure B1. Groundwater monitoring locations, primary surface-water structures, and groundwater transects used for model comparison and analysis.

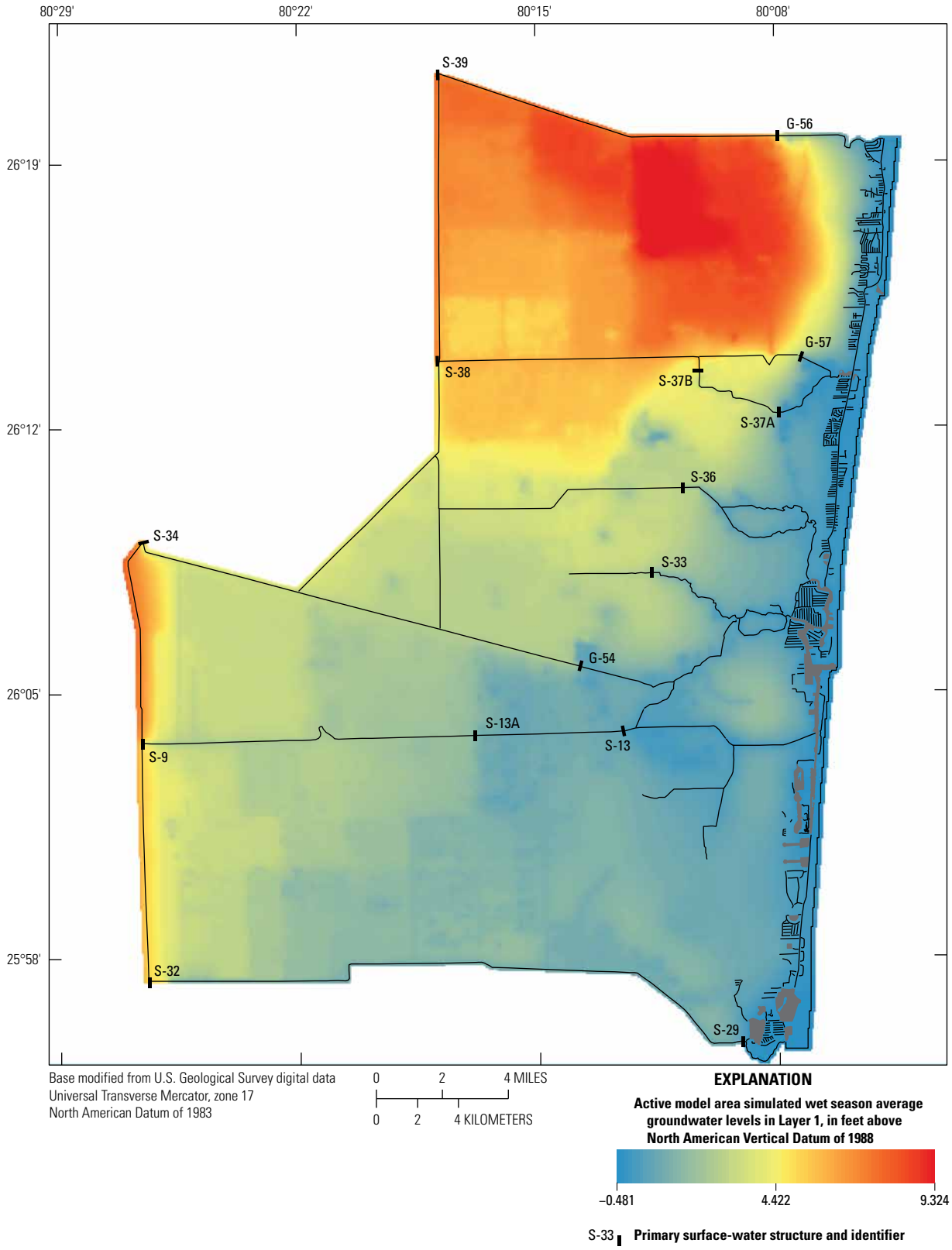

Figure B2. Simulated groundwater levels for the 2013–17 steady-state, wet season (feet above the North American Vertical Datum of 1988 [NAVD 88]).

Table B1. Groundwater monitoring locations, corresponding water control/drainage districts, and measured and simulated average wet season groundwater levels (2013–17).

[ft, foot; NAVD 88, North American Vertical Datum of 1988; N/A, not applicable]

Station name	Station location: Florida State Plane East Zone 901 (ft)		Water control/drainage district (control elevation, ft above NAVD 88)	Wet season groundwater level (ft above NAVD 88)		
	Easting	Northing		Measured mean	Steady-state simulated	Difference
G-2739	900879.3	718435.1	North Springs Improvement District (6.99)	6.436	7.042	0.606
G-1213	922784.0	713005.1	Cocomar Water Control District (9.49)	10.283	9.090	−1.193
G-1260	945960.7	722233.0	Broward Water Control District #2 (8.49)	3.863	4.435	0.572
G-1315	933951.4	710310.1	Broward Water Control District #2 (8.49)	8.853	8.556	−0.297
G-2866	946774.2	707749.1	None/coastal	5.207	5.566	0.359
G-2031	896641.0	700671.4	Sunshine Water Control District (5.99)	5.565	5.761	0.196
G-1316	922784.7	695506.3	Cocomar Water Control District (7.99)	6.321	7.370	1.049
G-2147	950735.5	697744.9	None/coastal	3.449	2.019	−1.430
G-2033	893602.4	677451.1	City of Tamarac (4.79)	5.057	5.167	0.110
G-2395	919870.7	677928.9	none (within well field)	−4.498	0.047	4.545
G-2032	881269.1	656665.1	Plantation Acres Improvement District (2.49)	2.676	2.752	0.076
G-1220	936277.4	654246.4	None/coastal	0.499	0.930	0.431
G-561	938777.4	641457.4	None/coastal	1.233	1.010	−0.223
G-671	873259.4	638146.4	Central Broward Water Control District (2.49)	2.234	2.072	−0.162
G-1221	909101.4	637548.7	Central Broward Water Control District (0.09)	1.136	0.771	−0.365
G-2034	858009.0	618564.9	South Broward Drainage District (1.99)	2.308	2.315	0.007
G-1223	906917.7	620589.1	Central Broward Water Control District (0.09)	1.181	1.030	−0.151
G-2900	920785.9	627369.2	None/coastal	0.398	0.007	−0.391
G-1226	924648.7	611882.8	None	0.59	0.764	0.174
G-2035	925843.0	610577.6	None	0.613	0.767	0.154
G-1636	860384.5	594728.0	South Broward Drainage District (2.49)	1.757	2.011	0.254
G-1225	908239.7	609662.8	South Broward Drainage District (0.99)	1.335	1.199	−0.136
F-291	936373.0	607754.0	None	0.883	0.637	−0.246
Mean	N/A	N/A	N/A	N/A	N/A	0.171

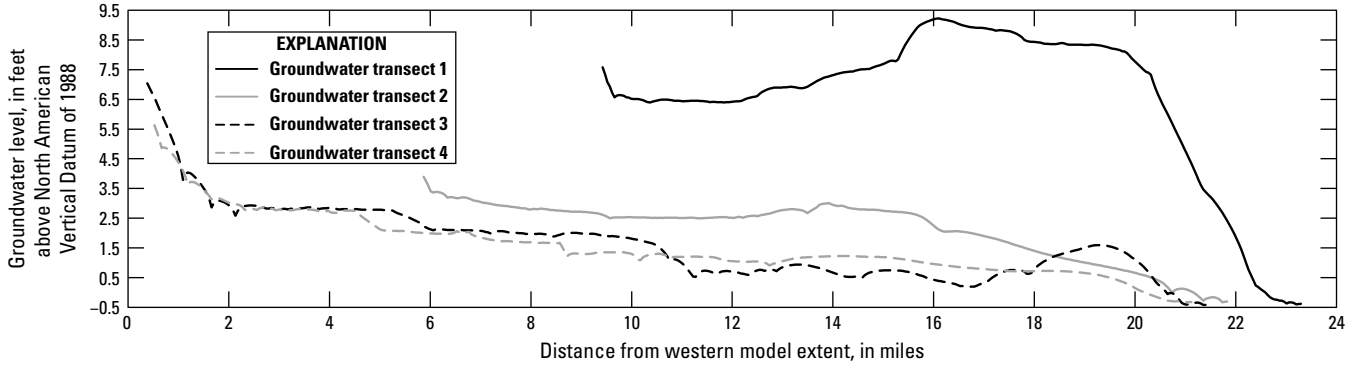

Figure B3. Simulated groundwater levels for the 2013–17 steady-state, wet season across four transects. Transects shown in figure B1.

Table B2. Measured and simulated wet season average (2013–17) upstream stages and flow rates for primary structures (2013–17). Mean and total differences do not include structure flow at S37A.

[ft, foot; NAVD 88, North American Vertical Datum of 1988; ft³/s, cubic foot per second; N/A, not applicable]

Structure name	Wet season upstream stage (ft above NAVD 88)			Wet season structure flow (ft³/s)		
	Measured mean	Steady-state simulated	Difference (ft)	Measured mean	Steady-state simulated	Difference
G-56	5.133	5.102	−0.031	351.1	346.8	−4.3
G-57	2.977	3.065	0.088	15.4	16.0	0.6
S-37A	2.112	2.414	0.302	614.3	461.2	−153.1
S-37B	5.098	5.937	0.839	472.9	445.1	−27.8
S-36	2.756	2.810	0.054	112.9	143.9	30.9
S-33	1.902	1.899	−0.003	9.5	8.9	−0.6
G-54	2.297	2.293	−0.004	166.6	163.4	−3.2
S-9	1.703	1.774	0.071	85.5	90.5	5.0
S-13	−0.042	0.094	0.136	272.1	283.7	11.6
S-29	0.482	0.681	0.199	453.2	403.6	−49.7
Total	N/A	N/A	N/A	1,939.2	1,901.9	−37.3
Mean	N/A	N/A	0.150	215.5	211.3	−4.2

Simulation of Transient Historical Conditions (2013–17)

Model inputs were prepared for a 5-year transient simulation representing a historical period (January 1, 2013–December 31, 2017). The groundwater levels were simulated using MODFLOW, the surface-water drainage network was simulated using the MODFLOW SWR1 process, and overland surface-water storage, unsaturated zone storage, infiltration, and recharge were simulated using the Urban Runoff (URO) MODFLOW process. The mean difference (MD), root-mean-square difference (RMSD), and the percent explained variance (PEV) were calculated for simulated and measured values of groundwater levels and flow through the primary structures. The MD describes how evenly the simulated values are distributed relative to measured values. Positive MD values indicate that the simulated values are greater than measured values, and negative MD values indicate that simulated values are less than measured values. The MD was calculated by using the following equation:

$$\mathrm{MD} = \frac{1}{n}\sum_{i=1}^{n}(X_s^i - X_m^i), \tag{1}$$

where

n is the number of simulated or measured values;
X_s^i is the simulated ith value; and
X_m^i is the measured ith value.

The RMSD indicates the magnitude of error between simulated and measured values; larger values of RMSD indicate larger model residuals (differences between simulated and measured values). The RMSD was calculated using the following equation:

$$\mathrm{RMSD} = \sqrt{\frac{1}{n}\sum_{i=1}^{n}(X_s^i - X_m^i)^2}. \tag{2}$$

The PEV indicates how closely the model simulates the variance within the measured values. The more similar the variances of the simulated and measured values, the closer the PEV is to 1.0. The PEV was calculated using the following equation:

$$\mathrm{PEV} = 1 - \frac{\sum_{i=1}^{n}\left[(X_s^i - \overline{X_s}) - (X_m^i - \overline{X_m})\right]^2}{\sum_{i=1}^{n}(X_m^i - \overline{X_m})^2}, \tag{3}$$

where

$\overline{X_s}$ is the mean simulated value, and
$\overline{X_m}$ is the mean measured value.

The PEV is similar to the commonly used Nash-Sutcliffe coefficient (Nash and Sutcliffe, 1970), except that all of the components are adjusted by their mean values.

Simulated Transient Groundwater Levels

Simulated daily groundwater levels were compared to measured daily values and model-fit statistics were calculated at 23 groundwater level monitoring locations for the entire historical period (table B3, fig. B1). Simulated groundwater levels exhibit similar trends and peaks to measured values at the monitoring locations (figs. B4 and B5). The simulated hydrograph for the G-2395 groundwater well exhibits the largest deviation from measured values (fig. B4). This is likely due to the presence of a production well field nearby that may be over- or under-represented in the model because of the scale of model discretization. The MD ranged from −2.02 to 3.71 ft (G-2147 and G-2395, respectively) with a mean of −0.29 ft. The RMSD ranged from 0.29 to 4.05 ft (G-1220 and G-2395, respectively), with a mean of 0.90 ft. The PEV ranged from −81.3 to 84.1 percent (G-1316 and G-1220, respectively), with a mean of 46.0 percent (table B3).

Simulated Stages and Flows at Primary Surface-Water Control Structures

Time series of simulated and measured daily upstream stages and flow through the primary structures were compared and model-fit statistics were calculated for the entire historical period. Within the model, the primary gated structures along the coast were represented as fixed-opening underflow gates with unidirectional flow to the downstream tidal reaches. The invert elevations were specified according to gate opening/

Table B3. Simulated groundwater levels and model-fit statistics for daily groundwater levels at 23 monitoring locations.

[ft, foot; NAVD 88, North American Vertical Datum of 1988; N/A, not applicable]

Station name	Groundwater levels (ft above NAVD 88)		Transient groundwater levels fit statistics		
	Measured mean	Simulated mean	Mean difference (ft)	Root-mean square difference (ft)	Explained variance (percent)
G-2739	6.369	6.459	0.083	0.56	39.2
G-1213	10.150	8.719	−1.43	1.54	37.8
G-1260	3.577	3.820	0.24	0.91	58.9
G-1315	8.949	8.215	−0.73	0.99	47.9
G-2866	4.816	4.293	−0.53	0.95	75.6
G-2031	5.680	5.566	−0.12	0.45	37.9
G-1316	6.315	6.763	0.45	0.72	−81.3
G-2147	3.168	1.150	−2.02	2.07	75.4
G-2033	5.057	4.684	−0.39	0.56	24.6
G-2395	−4.547	−0.845	3.71	4.05	34.6
G-2032	2.859	2.247	−0.63	0.79	−2.3
G-1220	0.496	0.385	−0.12	0.29	84.1
G-561	1.033	0.386	−0.64	0.71	81.9
G-671	2.406	1.685	−0.75	0.91	−28.1
G-1221	0.952	0.455	−0.50	0.59	67.9
G-2034	2.362	2.040	−0.35	0.70	38.1
G-1223	0.996	0.496	−0.51	0.59	70.5
G-2900	0.251	−0.155	−0.41	0.55	54.3
G-1226	0.401	0.124	−0.28	0.51	57.5
G-2035	0.453	0.128	−0.33	0.43	77.5
G-1636	1.764	1.554	−0.22	0.36	52.3
G-1225	1.120	0.576	−0.57	0.66	79.8
F-291	0.737	0.105	−0.63	0.70	74.7
Mean	N/A	N/A	−0.29	0.90	46.0

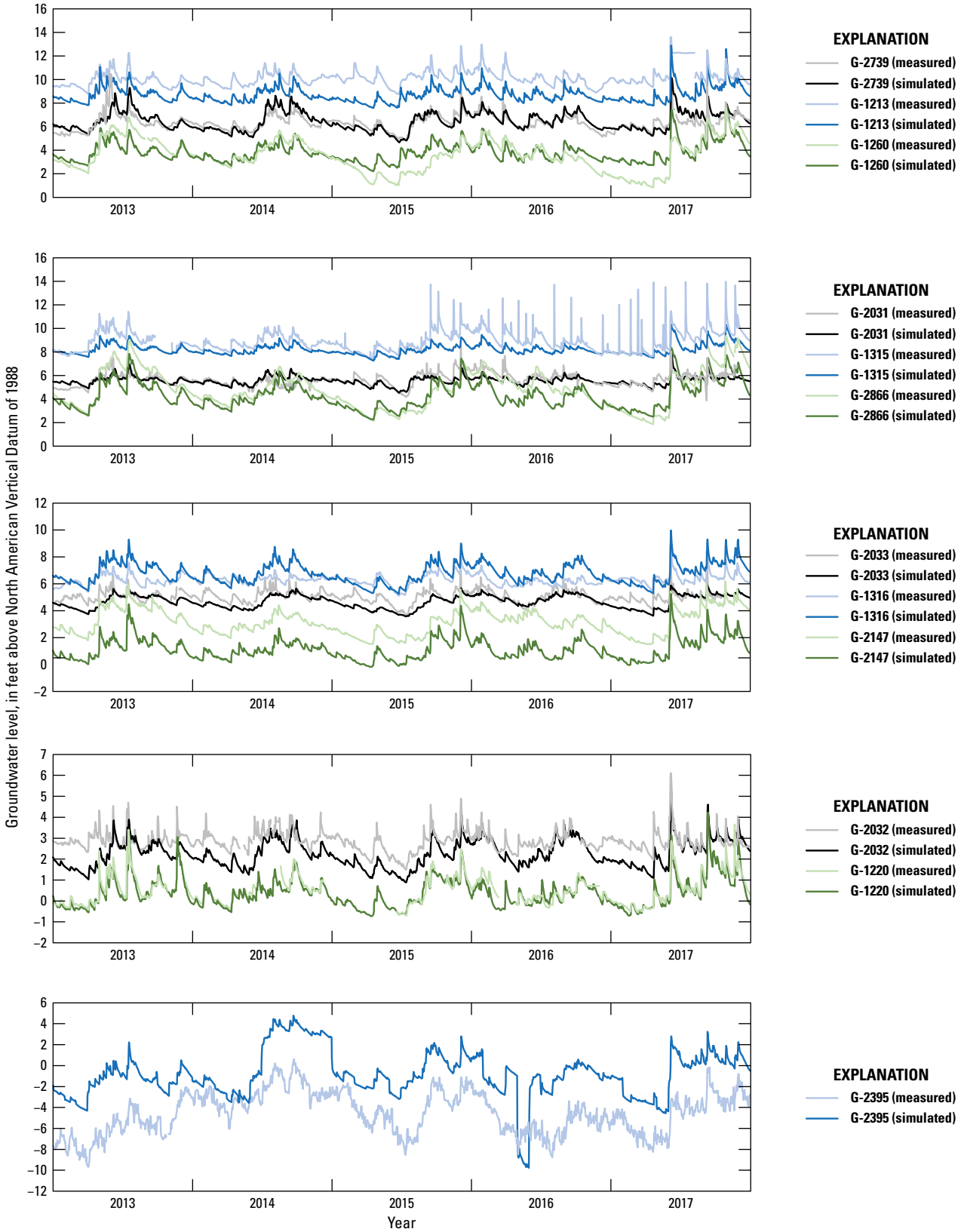

Figure B4. Simulated and measured daily groundwater levels for 12 monitoring locations during the historical period (2013–17).

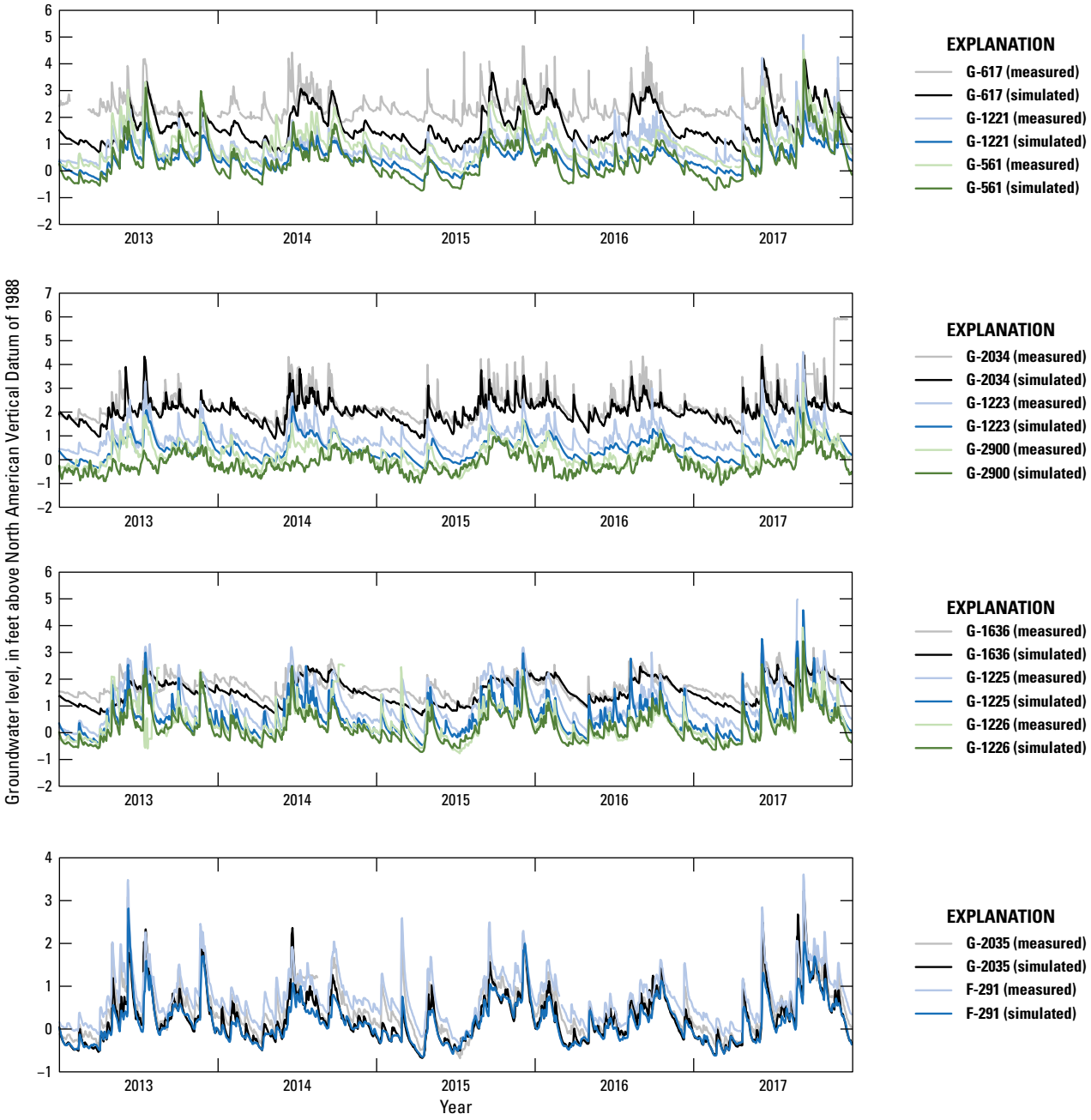

Figure B5. Simulated and measured daily groundwater levels for 11 monitoring locations during the historical period (2013–17).

closing heights, and structure widths were increased to allow additional flow area without substantial increases in upstream stage values (table E3, in chapter E). The use of an underflow gate formulation limits the maximum flow area of the structure to match the flow area available through the actual structure. In practice, these structures are operated on the basis of specified rules of opening and closing heights, and actual operations can deviate from these rules as adjustments are made to address specific conditions. Differences in these actual operations, compared to the calculated flow through structures represented as fixed gates, will result in differences between measured and simulated values. Upstream stage values would be expected to show the most deviation because of the opening and closing of the gates compared to continuous flow through a fixed opening. The MD for the daily upstream stage ranged from −0.679 to 0.461 ft (G-56 and S-37B, respectively) with a mean of −0.139 ft. The RMSD for the daily upstream stage ranged from 0.225 to 1.637 ft (G-57 and G-56, respectively) with a mean of 0.672 ft (table B4). Because of the difference in the timing of gate operations compared to the simulated flow through the representative weirs, the PEV was not calculated.

The time series of measured and simulated flow through the primary structures show similarities in trends and magnitudes (figs. B6, B7, B8, B9, and B10). Peak simulated flow rates are sometimes lower than peak measured flow rates, which is a common outcome with transient models because of the limited spatial and temporal resolution and a lack of precision in measured rainfall rates. Because of an unsupported increase in flow from S-37B to S-37A, the measured flow through the S-37A structure was not used during model calibration and is not considered in the discussion of model fit. This flow is still included in table B5 calculations for reference, however, because S-37A is a primary coastal structure. Ignoring the flow through S-37A, the MD for the daily structure flow ranged from −43.6 to 41.3 ft^3/s (S-29 and S-36, respectively), with a mean of −0.9 ft^3/s. Ignoring flow through S-37A, the RMSD for the daily structure flow ranged from 10.5 to 220.3 ft^3/s (G-57 and S-29, respectively), with a mean of 106.6 ft^3/s. Ignoring the flow through S-37A, the PEV ranged from −70.2 to 86.3 percent (S-9 and G-56, respectively), with a mean of 45.3 percent (table B5). The poor PEV calculated for flow rates through the S-9 structure is due to its representation within the model. The S-9 structure (fig. B1) is located along the western extent of the C-11 Canal and pumps water out of the canal and into the water conservation areas (WCAs) to the west. The specified operations of the pumping structure state that it is used to keep water levels in the C-11 Canal below 4.0 ft above the National Geodetic Vertical Datum of 1929 (NGVD 29) (2.49 ft above NAVD 88), but its actual operation is seasonal, with water levels typically maintained within a range of 1–3 ft above NAVD 88 (SFWMD, 2016) (fig. B10). The S-9 structure is represented as a stage-discharge curve within the model, with flow beginning to discharge out of the C-11 Canal at 1.75 ft above NAVD 88, which is close to the historical operations during the wet season. The stage-discharge curve reaches a peak flow of 2,880 ft^3/s at 2.5 ft above NAVD 88 and results in smaller variations in simulated upstream stage than variations in measured values. The simulated mean flow rate through the structure of 94.3 ft^3/s is similar to the historical mean flow rate of 90.6 ft^3/s (table B5).

The S-13 structure on the C-11 Canal (fig. B1) consists of a set of pumps and a gated spillway. The purpose of the structure is to prevent flooding of, overdraining of, and saltwater intrusion within areas west of the structure (SFWMD, 2016). The specified gate operational range is 1.6–1.8 ft above NGVD 29 (0.09–0.29 ft above NAVD 88). To prevent flooding upstream, the pumps are specified to operate when levels within the C-11 Canal exceed 2.5 ft above NGVD 29 (0.99 ft above NAVD 88). The gated spillway is represented as a fixed-opening underflow gate having an invert elevation of −0.30 ft above NAVD 88, which was based on the mean measured wet season upstream stage of −0.042 ft above NAVD 88. The pump is represented as a stage-discharge curve with flow beginning to discharge out of the C-11 at 0.00 ft above NAVD 88 based on historical pumping rates during the wet season. The measured and simulated flow rates through the S-13 structure in table B5 and figure B9 are the combined flows of the pumps and spillway (simulated stage-discharge and fixed-opening gate). The combined measured mean flow and simulated mean flow through the S-13 structure were

Table B4. Mean simulated and measured upstream stage and model-fit statistics for daily upstream stage at the primary structures.

[ft, foot; NAVD 88, North American Vertical Datum of 1988; N/A, not applicable]

Structure name	Upstream stage (ft above NAVD 88)		Transient fit statistics	
	Measured mean	Simulated mean	Mean difference (ft)	Root-mean square difference (ft)
G-56	5.454	4.775	−0.679	1.637
G-57	3.018	3.036	0.017	0.225
S-37A	2.193	2.211	0.019	0.603
S-37B	5.334	5.795	0.461	0.871
S-36	2.978	2.738	−0.240	0.584
S-33	1.892	1.488	−0.404	0.612
G-54	2.503	2.194	−0.309	0.667
S-9	2.009	1.777	−0.232	0.700
S-13	0.040	0.092	0.052	0.329
S-29	0.643	0.569	−0.073	0.491
Mean	N/A	N/A	−0.139	0.672

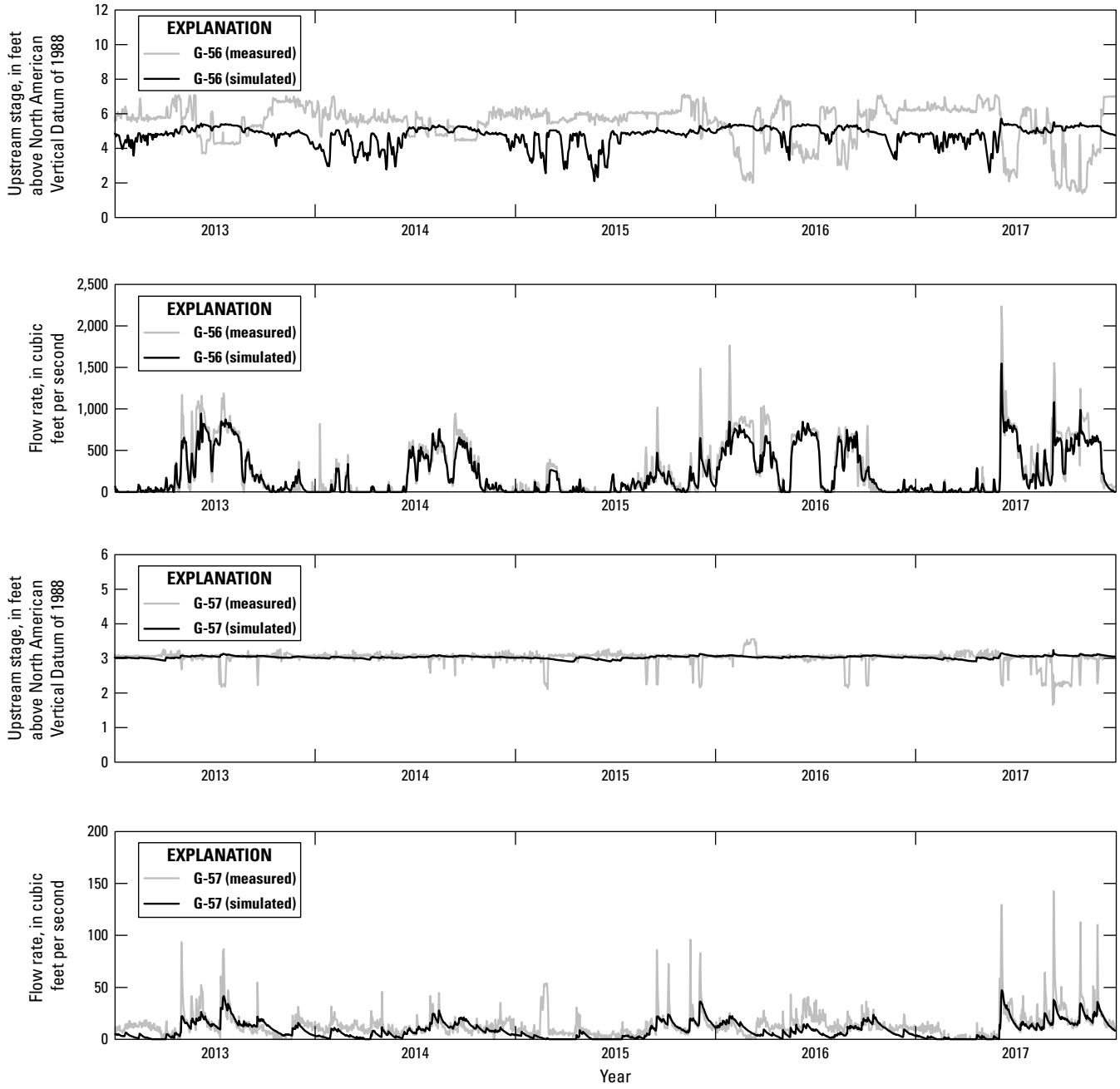

Figure B6. Simulated and measured upstream stage and flow through the G-56 and G-57 structures for the historical period (2013–17).

208.3 and 201.5 ft^3/s, respectively (table B5). The measured spillway flow and pump flow were 69.1 and 30.9 percent of the total flow, respectively (fig. B10). The simulated spillway flow and pump flow were 68.1 and 31.9 percent of the total flow, respectively. Large mean differences between simulated and measured upstream stage and the timing and magnitude of flow through the S-13 structure are likely due to deviations from the specified operational criteria.

The average inflows of rainfall rate during the historical transient simulation were 253.7 and 1,571.5 ft^3/s to the SWR1 and URO control volumes, respectively, resulting in a total of 1,825.2 ft^3/s or a yearly average of 60.0 inches per year (in/yr) over the area that is being simulated (fig. B11). The average rate of calculated outflows representing evapotranspiration (ET) from the SWR1, URO, and MODFLOW control volumes was 46.7, 343.6, and 407.0 ft^3/s, respectively, resulting in a total of 797.3 ft^3/s or a yearly average of 26.2 in/yr over the area that is being simulated. These volumes do not include outflows of ET from cells where tidal boundaries are being represented by SWR1 using specified stages. The net average aquifer exchange between the SWR1 and MODFLOW control volumes was 898.1 ft^3/s from MODFLOW while the

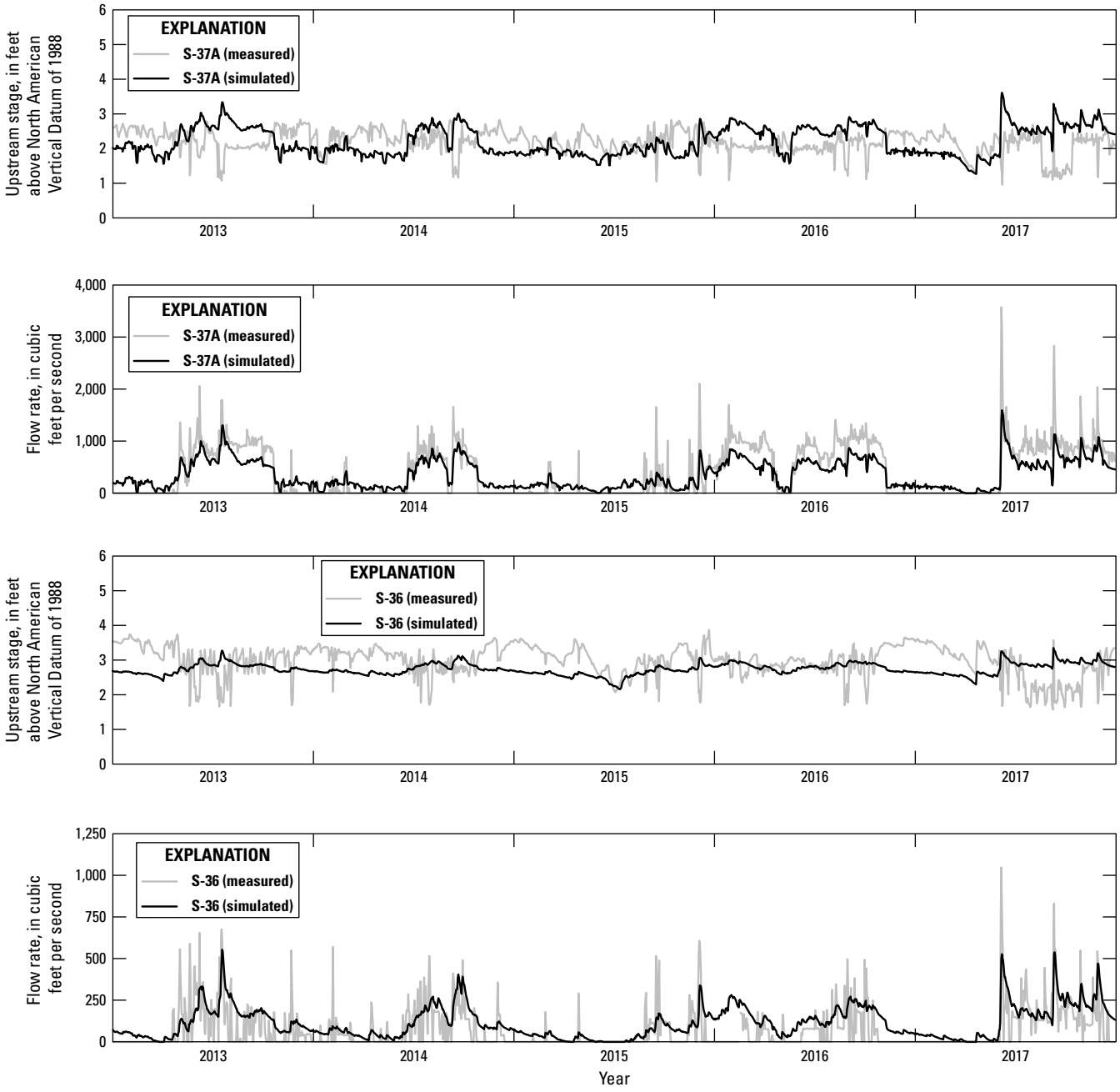

Figure B7. Simulated and measured upstream stage and flow through the S-37A and S-36 structures for the historical period (2013–17).

average recharge to MODFLOW from URO was 1,228.3 ft^3/s. The average specified inflows into the SWR1 control volume were 651.1 ft^3/s while the boundary flows and flow to specified stage reaches, which represent tail water and tidal areas, from the SWR1 control volume were 1,385.0 and 374.2 ft^3/s, respectively. The net average inflow to the MODFLOW control volume from the western, head-dependent flux boundaries representing the WCAs was 338.7 ft^3/s while the net outflow to the specified head boundaries representing tide was 22.3 ft^3/s.

While there are limited data available quantifying actual ET within the urban areas of south Florida, it is understood to be a substantial part of the overall hydrologic budget. ET has been independently estimated through indirect measurement techniques, but the uncertainty of those estimates is difficult to evaluate. There are currently no active actual ET measurement sites within the study area. One study conducted by the U.S. Geological Survey estimated the actual ET within Florida and parts of Georgia using an operational simplified surface energy balance model (Sepúlveda, 2021). The estimated actual ET for

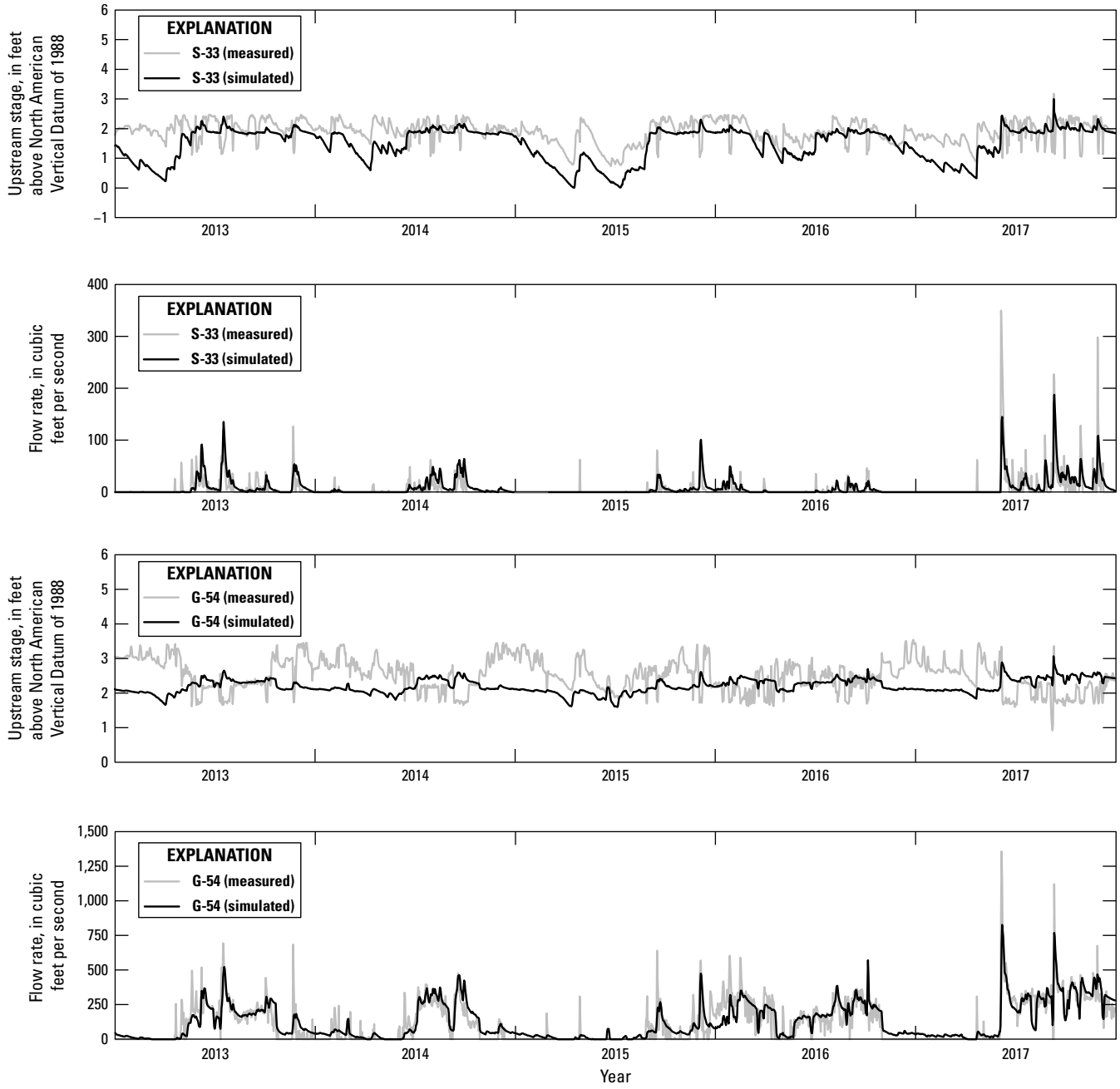

Figure B8. Simulated and measured upstream stage and flow through the S-33 and G-54 structures for the historical period (2013–17).

the study area ranged from 25.2 to 69.0 in/yr for the historical period (2013–17) with an average of 36.7 in/yr. Most of the study area within Florida and Georgia (82 percent) was considered to have a "shallow" water table of less than 2 ft. The simulated average wet season groundwater levels for the current study result in an average depth to water greater than 3 ft for the study area and the land use for most of the study area is classified medium- and high-density residential and commercial with an estimated 29 to 64 percent impervious area and shallow rooted vegetation (Decker and others, 2019). Measured ET values would likely be lower in areas with deeper water tables and increased impervious area. Only one measurement location in central Florida was available for reference and bias correction for urban land-use types. This measurement site was located at the University of Central Florida and estimated actual ET using the eddy-covariance method for an area with an 8-kilometer radius composed of 61 percent urban, 34 percent nonurban, and 5 percent open water (Sumner and others, 2017). The mean estimated actual ET for the study period (January 29, 2009–September 27, 2012) was

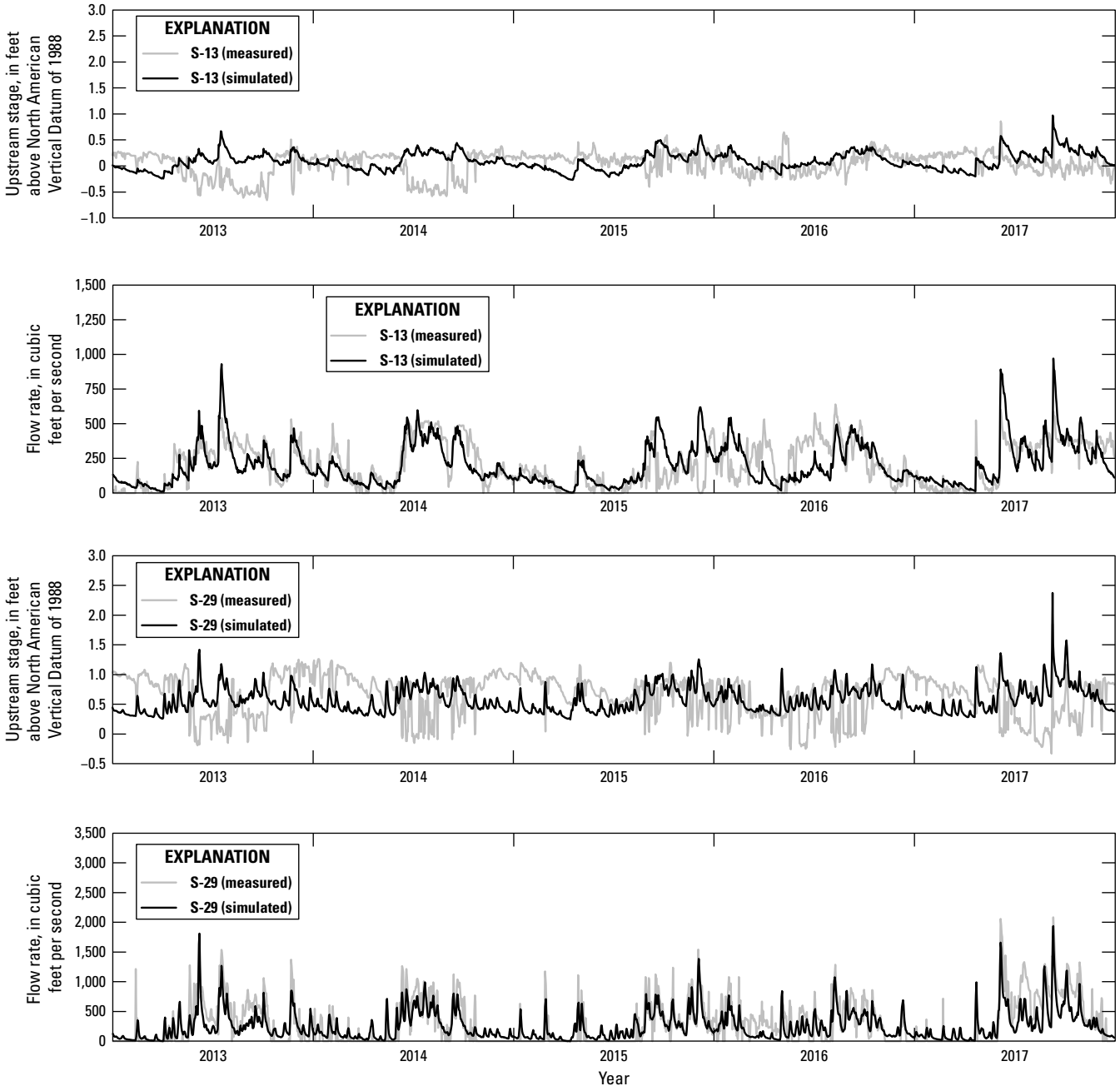

Figure B9. Simulated and measured upstream stage and flow through the S-13 (combined spillway and pump flow) and S-29 structures for the historical period (2013–17).

36.0 in/yr with estimates of 37.9 and 35.7 in/yr for the full years of 2010 and 2011, respectively. Additional measured actual ET data within the urban areas of south Florida would substantially improve the understanding and quantification of urban ET and could be used to develop improved techniques to estimated and simulated ET in south Florida.

If the model were adjusted to more closely match published values of estimated actual ET for the study area, a likely model result would be reduced flows at the primary structures because of the increased volumes removed from saturated and unsaturated storage. Groundwater and surface-water levels west of the primary control structures would likely not change substantially because of the operations of the surface-water system and the use of control elevations. Groundwater levels east of the primary control structures and groundwater flow to the SWR1 and specified head boundaries representing tidal areas could decrease as a result of increased ET volumes.

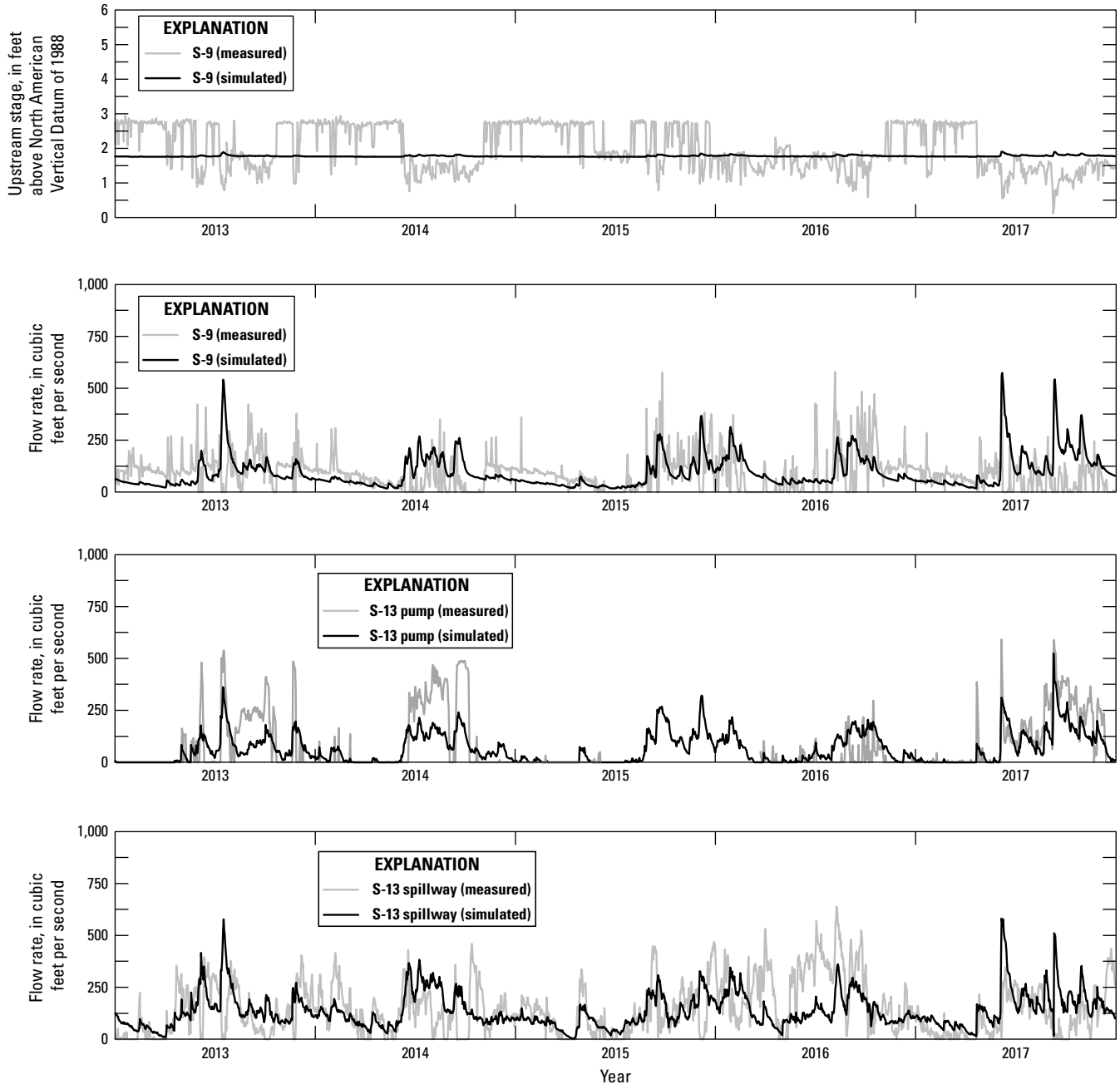

Figure B10. Simulated and measured upstream stage and flow through the S-9 structure and simulated and measured pump and spillway flow for the S-13 structure for the historical period (2013–17).

Table B5. Mean simulated and measured flow through primary structures and model-fit statistics for daily flow through the primary structures.

[ft^3/s, cubic foot per second; ft, foot; N/A, not applicable]

Structure name	Structure flow (ft^3/s)		Transient fit statistics		
	Measured mean	Simulated mean	Mean difference (ft)	Root-mean square difference (ft)	Explained variance (percent)
G-56	250.9	222.8	−28.1	124.2	86.3
G-57	13.6	9.1	−4.6	10.5	42.9
S-37A	415.2	355.6	−59.6	260.2	72.3
S-37B	321.4	343.6	22.3	175.6	79.0
S-36	72.1	113.6	41.3	100.7	40.4
S-33	6.2	7.9	1.7	15.2	54.8
G-54	117.2	123.3	6.1	75.4	74.4
S-9	90.6	94.3	3.8	109.1	−70.2
S-13	208.3	201.5	−6.8	128.7	33.7
S-29	299.5	255.9	−43.6	220.3	66.6
Mean	N/A	N/A	−0.9	106.6	45.3

Comparison of Simulated Steady-State Wet Season Conditions and Transient Historical Conditions

Steady-state, wet season, simulated average water levels and flow rates were compared to monthly average water levels and flow rates from the transient model. The differences in boundary forcings and inputs between the two simulations included differences in sea level, WCA groundwater levels, rainfall, evapotranspiration, and SWR1 inflows to the surface-water model.

The mean difference between the steady-state, wet season, simulated average groundwater levels and average wet season groundwater levels from the transient model at the 23 monitoring locations was 0.333 ft, indicating slightly higher values, on average, were simulated by the steady-state model (fig. B1, table B6). The simulated groundwater levels at the monitoring locations for the transient model were highest during the month of September with a monthly mean of 3.178 ft which is 0.078 ft higher than the results from the steady-state simulation. The magnitude of the mean differences in monthly average groundwater levels at these locations was lowest (0.037 ft) for the month of October.

Despite the statistical similarities between the transient model's averaged October results and the steady-state average wet season model results, some key differences exist in the groundwater levels and flow through the primary structures because of differences in model inputs. The primary differences in inputs include groundwater boundary elevations for the WCAs at the western extent of the model, tidal stages, rainfall, and SWR1 influxes into the primary canals (table B7). Differences in other model inputs, such as tail water stages and potential evapotranspiration, exist but are smaller in magnitude. The average groundwater boundary elevations for the month of October within the transient model were 1.01, 1.15, 1.43, and 0.57 ft higher than the elevations used in the steady-state wet season model for WCA 2A, WCA 2B, WCA 3A, and WCA 3B, respectively. The average tidal stage for the month of October within the transient model is 0.52 ft higher than the tidal stage used in the steady-state wet season model. The average wet season recharge rate used in the steady-state model is 0.018 foot per day, which is 44.7 percent greater than the average of the October rainfall values (0.013 foot per day) from the transient model. The estimated surface-water fluxes added to the Hillsboro and C-9 Canals representing inflows from missing parts of the drainage area are 59.1 and 149.3 ft^3/s in the steady-state wet season model compared to the transient model's average October values of 42.4 and 117.7 ft^3/s. Lastly, the surface-water inflows from the S-39, S-38, and S-34 structures used in the steady-state model are 208.5, 337.4, and 146.3 ft^3/s compared to October averages from the transient model of 128.7, 368.6, and 184.9 ft^3/s.

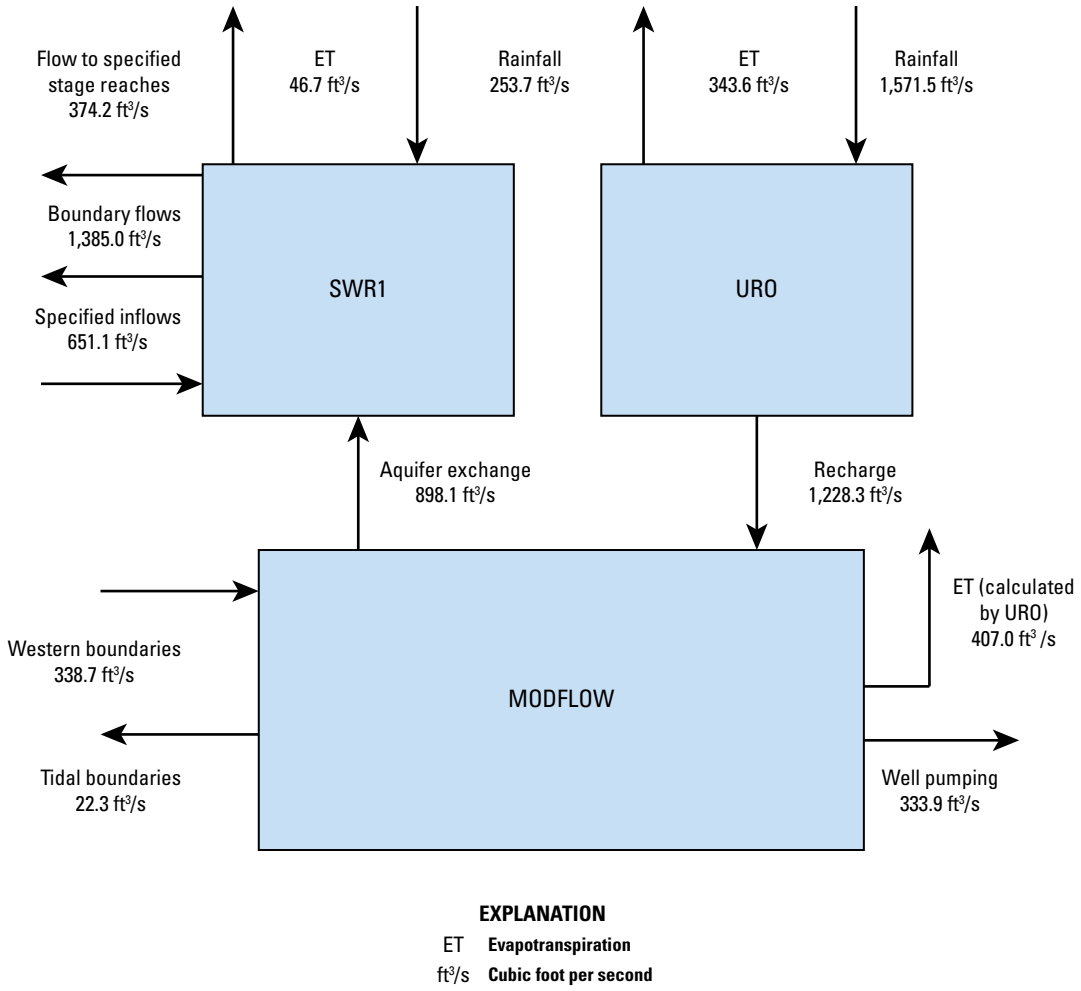

Figure B11. Simulated water budget for the Surface-Water Routing (SWR1) process, Urban Runoff process (URO), and Modular Finite-Difference Groundwater Flow Model (MODFLOW) control volumes for the transient model historical period (2013–17).

Table B6. Simulated average wet season groundwater levels for monitoring locations for the transient and steady-state models and differences in monthly average groundwater levels from the transient and steady-state models.

[ft, foot; NAVD 88, North American Vertical Datum of 1988; N/A, not applicable]

Station name	Average wet season groundwater levels (ft above NAVD 88)		Difference (ft)	Differences in monthly average and steady-state wet season groundwater levels (ft)		
	Steady state	Transient		August	September	October
G-2739	7.042	6.743	0.300	−0.024	−0.153	0.177
G-1213	9.090	8.905	0.185	0.237	−0.141	0.108
G-1260	4.435	4.068	0.367	0.552	−0.038	0.149
G-1315	8.556	8.337	0.219	0.266	0.016	0.164
G-2866	5.566	4.689	0.877	0.962	0.461	0.541
G-2031	5.761	5.661	0.100	−0.037	−0.107	0.080
G-1316	7.370	6.999	0.371	0.428	−0.154	0.018
G-2147	2.019	1.411	0.607	0.702	0.314	0.192
G-2033	5.167	4.811	0.356	0.238	0.008	0.072
G-2395	0.047	−0.499	0.546	−0.255	−0.978	−0.525
G-2032	2.752	2.425	0.327	0.227	−0.135	0.024
G-1220	0.930	0.599	0.331	0.513	−0.126	−0.154
G-561	1.010	0.611	0.400	0.592	−0.033	−0.036
G-671	2.072	1.886	0.186	0.175	−0.407	−0.058
G-1221	0.771	0.600	0.170	0.158	−0.115	−0.011
G-2034	2.315	2.195	0.120	0.068	−0.148	0.081
G-1223	1.030	0.704	0.326	0.360	0.039	0.199
G-2900	0.007	−0.038	0.045	0.115	−0.282	−0.511
G-1226	0.764	0.363	0.401	0.514	0.058	0.073
G-2035	0.767	0.364	0.404	0.517	0.077	0.066
G-1636	2.011	1.699	0.313	0.188	−0.056	0.016
G-1225	1.199	0.853	0.346	0.368	−0.002	0.244
F-291	0.637	0.287	0.350	0.479	0.111	−0.069
Mean	N/A	N/A	0.333	0.319	−0.078	0.037

Table B7. Differences between steady-state wet season model input values and average monthly input values for the transient historical model.

[ft, foot; NAVD 88, North American Vertical Datum of 1988; PET, potential evapotranspiration; ft/d, foot per day; ft³/s, cubic foot per second]

Input	Wet season	August	September	October
Average water levels (ft above NAVD 88)				
Tide	−0.50	−0.57	−0.29	0.02
WCA 2A	10.87	11.11	11.66	11.88
WCA 2B	8.09	8.71	9.07	9.24
WCA 3A	8.36	8.85	9.52	9.79
WCA 3B	6.25	6.30	6.64	6.82
Tail water increase over tidal levels (ft)				
G-56	0.460	0.418	0.505	0.408
S-37A	0.220	0.186	0.286	0.285
S-36	0.425	0.385	0.545	0.442
S-33	0.373	0.336	0.465	0.395
G-54	0.687	0.671	0.834	0.684
S-13	0.363	0.365	0.483	0.403
Average rainfall and PET rate (ft/d)				
Average rainfall	0.018	0.020	0.025	0.013
Average PET	0.016	0.018	0.014	0.012
Average inflows into surface-water model (ft³/s)				
Hillsboro Canal	59.1	61.5	69.8	42.4
C-9 Canal	149.3	158.7	182.3	117.7
S-39	208.5	256.8	156.3	128.7
S-38	337.4	402.8	367.3	368.6
S-34	146.3	172.2	180.7	184.9

Summary of Model Fit to Historical Conditions

Both the steady-state and transient models produce groundwater levels similar overall to measured levels. Simulated groundwater levels within the steady-state model had a mean difference of −0.028 ft when excluding site G-2395 located near production wells. The transient model produced qualitatively similar groundwater-level time-series to measured values with a mean MD of −0.29 ft, a mean RMSD of 0.90 ft, and a mean PEV of 46.0 percent. Differences in simulated mean groundwater levels and in the magnitude and timing of groundwater fluctuations can partially be attributed to the differences in simulated surface-water stages. Simulated surface-water structure operations likely deviate from actual operations, resulting in differences between simulated versus measured surface-water stages. The strong connection between the surface-water and underlying groundwater results in these differences affecting the simulated groundwater statistics.

The steady-state and transient models produce similar average wet season results for the primary structure flows and upstream stages. The steady-state model produces simulated primary structure flows and upstream stages with mean differences of −4.2 ft³/s and 0.150 ft compared to measured values, respectively. The transient model produced upstream stage and flow rate time series qualitatively similar to measured values. The simulated flow through the primary structures had a mean MD of −0.9 ft³/s and a mean RMSD of 106.6 ft³/s compared to measured values. The simulated upstream stage had a mean MD of −0.139 ft and a mean RMSD of 0.672 ft compared to measured values. The transient model shows differences in the timing and magnitude of flows through the primary structures because of differences between actual and simulated structure operation. The model was constructed using the specified operational rules, control elevations, and pumping capacities to establish invert elevations, structure widths, gate openings, and stage-discharge curves for the SWR1 structures to simulate the intended behavior and purpose of the drainage system, and simulation results inevitably differ from actual

measurements. The same parameters used to simulate historical conditions were used to simulate various future scenarios (chapter C).

References Cited

Decker, J.D., 2022, MODFLOW-NWT datasets for the simulation of drainage infrastructure and groundwater system response to changes in sea-level and precipitation, Broward County, Florida: U.S. Geological Survey data release, https://doi.org/10.5066/P9ITQBFZ.

Decker, J.D., Hughes, J.D., and Swain, E.D., 2019, Potential for increased inundation in flood-prone regions of southeast Florida in response to climate and sea-level changes in Broward County, Florida, 2060–69: U.S. Geological Survey Scientific Investigations Report 2018–5125, 106 p., accessed November 3, 2021, at https://doi.org/10.3133/sir20185125.

Nash, J.E., and Sutcliffe, J.V., 1970, River flow forecasting through conceptual models part I—A discussion of principles: Journal of Hydrology, v. 10, no. 3, p. 282–290, accessed July 14, 2022, at https://doi.org/10.1016/0022-1694(70)90255-6.

Sepúlveda, N., 2021, Evaluation of actual evapotranspiration rates from the Operational Simplified Surface Energy Balance (SSEBop) model in Florida and parts of Alabama and Georgia, 2000–17: U.S. Geological Survey Scientific Investigations Report 2021–5072, 66 p., accessed June 8, 2022, at https://doi.org/10.3133/sir20215072.

South Florida Water Management District [SFWMD], 2016, Structure books: West Palm Beach, Fla., South Florida Water Management District, 597 p., accessed November 8, 2021, at ftp://ftppub.sfwmd.gov/outgoing/Survey_Report/AsBuilts/Other%20Reports/OCC%20Structure%20Book.pdf.

Sumner, D.M., Hinkle, C.R. and Becker, K.E., 2017, Evapotranspiration (ET) at University of Central Florida urban site, daily data, Orange County, Florida, January 29, 2009–September 27, 2012: U.S. Geological Survey data release, accessed June 15, 2022, at https://doi.org/10.5066/F7JS9NZB.

Chapter C. Simulated Effects of Increased Sea Level and Precipitation on the Hydrologic System

By Jeremy D. Decker

To evaluate the effects of increased sea level on the hydrologic system, four different scenarios of increased mean sea levels were simulated using the historical steady-state and transient models (chapters B and E). To evaluate the effects of wetter conditions under elevated sea-level conditions, an increased precipitation rate was simulated along with the highest of the simulated sea levels. Indicators of reduced drainage capacity that were evaluated include increased upstream and downstream stages at the primary coastal structures and reduced head differences at the primary coastal structures. Indicators of reduced soil storage capacity that were evaluated include increases in groundwater levels, which reduce the available unsaturated zone storage. The steady-state model can be used to produce seasonal model results quickly with limited model input requirements. The transient model simulations require more model inputs and longer run times but can be used to evaluate the response of the hydrologic system on shorter temporal scales and better evaluate the effect on the dynamic surface-water operations. Model input files, executables, and outputs described here are included in the associated U.S. Geological Survey data release (Decker, 2022).

Development of Future Sea-Level Scenarios

Except for the S-13 structure, all primary coastal structures within the study area are gravity-controlled and require a positive head difference (inland to tidal) to drain excess water to tide (fig. A1). When the downstream stage approaches the upstream control elevation, the head difference is reduced, resulting in a decreased flow rate for a particular gate opening. The reduction in flow rates over the range of gate openings, while maintaining a specified upstream stage, can be referred to as a loss of drainage capacity. The percentage of time that tidal levels are above the upstream control elevation of the coastal structure is likely an indicator of reduced drainage capacity caused by increased downstream water levels, and this analysis focused on this indicator. When high flow rates are necessary for drainage purposes, the loss of drainage capacity at the coastal structures can result in increased upstream stages, which can then increase the likelihood of inundation within inland communities. It should be noted that actual drainage capacity for the structure would likely be reduced before downstream levels reach the upstream control elevations because of tail water effects.

The future sea-level scenarios developed in this study use historical tidal observations adjusted upward to various mean tidal levels expected to affect the operations of the coastal structures. These scenarios were assigned expected arrival time ranges using the "Unified Sea Level Rise Projection for Southeast Florida" document released by the Southeast Florida Regional Climate Change Compact Sea Level Rise Work Group (2020), which uses projections developed by the Intergovernmental Panel on Climate Change (IPCC, 2014) and the National Oceanic and Atmospheric Administration (NOAA) (Sweet and others, 2017).

Coastal Structure Control Elevations

The seven primary, coastal gated structures within the study area have upstream control elevations that range from 1.6 to 7.5 feet (ft) above the National Geodetic Vertical Datum of 1929 or 0.09–5.99 ft above the North American Vertical Datum of 1988 (NAVD 88) (table C1). Gate operations are specified to occur for upstream (inland) canal levels as low as −0.11 ft above NAVD 88, and the mean tidal level measured during 2013–17 was −0.55 ft above NAVD 88, with mean tidal range of ±1.116 ft (chapter E, fig. E15) (SFWMD, 2016). Additionally, gate operations for three of the coastal structures (S-13, S-33, and G-57) call for gate closings when the difference between upstream and downstream pool elevations falls below 0.2 ft. The S-29 structure is more restrictive and is specified to close when the difference between upstream and downstream pool elevations falls below 0.3 ft. These gate closing rules help to prevent saltwater intrusion inland of the coastal structures and could further decrease drainage capacity. The S-13 structure has the lowest control elevation (0.09 ft above NAVD 88) but also has the infrastructure to pump water from the upstream side of the structure to the downstream side. Water may be pumped through the S-13 structure (1) when the downstream water levels exceed the control elevation of the structure, (2) when the head difference between the upstream and downstream stage is not sufficient in providing the desired flow rate, or (3) to prevent inland flooding during high rainfall events (table C1).

Future Sea-Level Scenarios

Increased sea-level scenarios with mean tidal levels of 0.5, 2.0, 2.5, and 3.0 ft above NAVD 88 were selected on the basis of the control elevations of the primary coastal structures (table C1). These four scenarios represent sea-level increases of 1.05, 2.55, 3.05, and 3.55 ft over the 2013–17 measured mean tidal level of −0.55 ft above NAVD 88. They also correspond closely to the S-29, S-33/S-37A, G-54, and G-57 control elevations, respectively.

Table C1. Operating parameters for primary coastal gated spillways and pump station within the study area (SFWMD, 2016).

[ft, foot; NAVD 88, North American Vertical Datum of 1988; ft³/s, cubic foot per second; N/A, not applicable]

Structure	Upstream control elevation (ft above NAVD 88)	Gate open elevation (ft above NAVD 88)	Gate close elevation (ft above NAVD 88)	Pump capacity (ft³/s)	2013–17 mean flow (ft³/s)
Primary coastal gated spillways					
S-13	0.09	0.29	−0.11	N/A	144.0
S-29	0.49	0.99	−0.01	N/A	299.5
S-33	1.99	2.49	1.49	N/A	415.2
S-37A	1.99	2.89	1.49	N/A	415.2
G-54	2.49	2.99	1.99	N/A	117.2
S-36	2.99	3.39	2.49	N/A	72.1
G-57	2.99	3.29	2.79	N/A	13.6
G-56	5.99	6.49	5.49	N/A	250.9
Coastal pump station					
S-13	0.99	N/A	N/A	540	76.5

The four time series of tidal levels used for the sea-level scenarios were created by uniformly increasing measured historical (2013–17) tidal levels to obtain mean sea levels of 0.5, 2.0, 2.5, and 3.0 ft above NAVD 88 for the simulation period. Within the transient model, the hourly tidal input values were used to specify stages within tidal reaches, and the groundwater model uses daily tidal input values to represent eastern tidal specified head boundaries (fig. A1). The drainage capacity for each structure can decrease as downstream (tidal) water levels enter the operational range of gate openings and closings. When the mean downstream water levels equal the control elevations at each structure, gate operations will be restricted to periods of lower tide. When the flow capacity of a structure at a specified upstream control elevation is reduced below drainage needs, upstream (inland) stage will necessarily increase to an elevation that provides a head difference that results in the required flow rates. To avoid this necessary increase in upstream stage associated with gravity-controlled structures, pumps or similar infrastructure would need to be installed or flows would need to be diverted away from the compromised structure.

For the historical scenario, measured hourly tidal levels were already equal to or greater than the S-29 and S-13 upstream control elevations 11.4 and 24.9 percent of the time, respectively (table C2). When the mean tidal level is increased to 0.5 ft above NAVD 88, the resulting hourly tidal levels are equal to or greater than the S-13 and S-29 upstream control elevations 49.6 and 64.9 percent of the time, respectively. For the remaining scenarios with mean tidal levels of 2.0, 2.5, and 3.0 ft above NAVD 88, the hourly tidal levels are above the S-29 and S-13 upstream control elevations nearly the entire time. For these simulations, the S-13 structure can rely on its pumping capabilities to maintain upstream water levels, whereas the S-29 structure would likely have to maintain a higher upstream water level to maintain the required flow rates to meet drainage needs.

For the 2.0-ft scenario, the hourly tidal water level is above or equal to the S-37A and S-33 upstream control elevations 49.6 percent of the time and above the G-57 and G-54 upstream control elevations 12.4 and 30.3 percent of the time, respectively (table C2). For the 2.5-ft scenario, the hourly tidal water level is above the upstream control elevations of the G-57, G-54, and S-37A/S-33 structures 30.3, 49.6, and 68.8 percent of the simulation time, respectively. When mean tidal level is increased to 3.0 ft above NAVD 88, the hourly tidal water level is above the upstream control elevations of the G-57, G-54, and S-37A/S-33 structures 49.6, 68.8, and 87.8 percent of the simulation time, respectively. The hourly tidal level is above the upstream control elevation of the G-56 structure 0.0 percent of the time for all simulations because of its relatively high control elevation of 5.99 ft above NAVD 88.

The percentage of time that mean tide level is above the control elevation of a structure was used here to indicate a general reduction in drainage capacity for the four sea-level scenarios. For the transient model, wetter periods occasionally coincide with periods of higher tidal levels throughout a scenario, resulting in increased drainage volumes, reduced drainage capacity, and increased upstream stages. Conversely, during drier periods, higher downstream water levels may have little effect on upstream water levels because of decreased drainage volumes. Increases in seasonal rainfall or frequency and (or) intensity of storm events would increase the likelihood of elevated upstream stages at the coastal structure resulting from sea-level rise because of the higher

Table C2. Percentage of simulation time that hourly tidal level input is above each coastal structure's control elevation for the historical, 0.5-, 2.0-, 2.5-, and 3.0-ft sea-level scenarios.

[ft, foot; NAVD 88, North American Vertical Datum of 1988]

Scenario	Primary coastal structures (control elevation, ft above NAVD 88)					
	G-56 (5.99 ft)	G-57 (2.99 ft)	G-54 (2.49 ft)	S-37A/S-33 (1.99 ft)	S-29 (0.49 ft)	S-13 (0.09 ft)
Historical	0.0	0.0	0.0	0.0	11.4	24.9
0.5 ft	0.0	0.1	0.5	3.1	49.6	64.9
2.0 ft	0.0	12.4	30.3	49.6	98.8	100.0
2.5 ft	0.0	30.3	49.6	68.8	100.0	100.0
3.0 ft	0.0	49.6	68.8	87.8	100.0	100.0

drainage volumes. It should also be noted that this analysis focused primarily on comparing tidal levels to control elevations as an indicator of a possible reduction in drainage capacity, whereas actual downstream stages at these structures are typically higher, on average, than tidal levels because of the coastal flow direction and the associated hydraulic gradient. However, because of dampening, downstream stages at the coastal structures tend to have a reduced daily range compared to measured tidal stages.

Expected Arrival Times for Future Sea-Level Scenarios

The "Unified Sea Level Rise Projection for Southeast Florida" document by the Southeast Florida Regional Climate Change Compact Sea Level Rise Work Group (2020) was used to assign ranges of expected arrival times to the sea-level scenarios. The document is intended to be used as guidance when considering sea-level rise for both short and long-term projects in the southeast Florida region. In increasing order of sea-level rise, the three projections adopted by the working group are the IPCC median, NOAA Intermediate-High, and the NOAA High curves. The IPCC median curve is recommended for application to most projects within a short-term planning horizon (less than 50 years). The NOAA Intermediate-High curve is recommended for noncritical infrastructure expected to be in service beyond 50 years. The NOAA High curve is recommended for critical, high-risk projects expected to be in service beyond 50 years. The NOAA High curve is also recommended for projects that are not easily replaced or upgraded, such as roadways, bridges, and utilities. The projections begin in the year 2000 and continue to 2120. The projected mean sea levels for 2070 range from 0.94 to 3.71 ft above NAVD 88, and projected mean sea levels for 2120 range from 2.51 to 10.54 ft above NAVD 88 (table C3, fig. A5). These projections assume a growing greenhouse gas emission concentration consistent with the IPCC Fifth Assessment Report's Representative Concentration Pathways (RCP 8.5) (Southeast Florida Regional Climate Change Compact Sea Level Rise Work Group, 2020). Differences in projections occur because of variations in potential thermal expansion, ice melt, and other factors contributing to increased sea level.

Table C3. Projected mean sea level using the Intergovernmental Panel on Climate Change median (IPCC Med), the National Oceanic and Atmospheric Administration (NOAA) Intermediate-High (NOAA IH), and the NOAA High (NOAA H) sea-level projection curves (Southeast Florida Regional Climate Change Compact Sea Level Rise Work Group, 2020).

[ft, foot; NAVD 88, North American Vertical Datum of 1988]

Year	Projected mean sea level (ft above NAVD 88)		
	IPCC Med	NOAA IH	NOAA H
2000	−0.78	−0.78	−0.78
2010	−0.59	−0.48	−0.45
2020	−0.39	−0.22	−0.09
2030	−0.15	0.20	0.40
2040	0.06	0.60	0.96
2050	0.35	1.16	1.68
2060	0.62	1.78	2.60
2070	0.94	2.53	3.71
2080	1.25	3.39	4.96
2090	1.62	4.34	6.31
2100	1.94	5.36	7.78
2120	2.51	6.86	10.54

Expected arrival times for each sea-level scenario were linearly interpolated from the IPCC median, NOAA Intermediate-High, and NOAA High sea-level projection curves (table C3). The resulting arrival years for each scenario represent a range of expected arrival times (table C4). Using this method, the 0.5-ft mean sea-level scenario has a range of expected arrival time of 2032–56. The 2.0-ft mean sea-level scenario has a range of expected arrival time of 2053–2102. The 2.5-ft mean sea-level scenario has a range of expected arrival time of 2059–2120. Lastly, the 3.0-ft mean sea-level scenario has a range of expected arrival time of 2064 to beyond 2120, which is the last year of the published projections.

Simulation of Steady-State Wet Season Conditions Under Future Sea Level and Increased Precipitation Scenarios

The steady-state model developed using average wet season conditions for 2013–17 was used to simulate changes in groundwater levels, surface-water stages, and structure flows under increased sea-level scenarios. Measured, mean wet season recharge and potential evapotranspiration rates from the historical period (2013–17) were used as inputs for the future sea-level scenarios. The 2013–17 measured mean wet season tidal level was −0.50 ft above NAVD 88 compared to a yearly mean tidal level of −0.55 ft above NAVD 88. To simulate the yearly mean sea-level scenarios of 0.5, 2.0, 2.5, and 3.0 ft above NAVD 88, sea-level increases of 1.05, 2.55, 3.05, and 3.55 ft were applied to the mean wet season tidal level. The eastern groundwater specified-head and surface-water specified-stage boundaries representing tide were increased to the new sea-level values. An additional scenario was simulated with a 15-percent increase in rainfall recharge, representing an increase in precipitation, in conjunction with the 3.0-ft mean sea-level scenario to understand the effects of possible changes in average rainfall. The increase in recharge does not necessarily represent an equal increase in precipitation given the complex relationship between precipitation and recharge. The model inputs for tail water and downstream stage values for the coastal structures were increased by 1.05, 2.55, 3.05 and 3.55 ft for the corresponding mean sea-level scenario.

The 23 monitoring stations were divided into three groups on the basis of location: stations west of the coastal water-control structures, stations near the coastal water-control structures, and stations east of the coastal water-control structures (table C5, fig. B1). The mean differences in groundwater levels for the eight monitoring stations west of the coastal structures were 0.004, 0.031, 0.047, and 0.069 ft for the 0.5-, 2.0-, 2.5-, 3.0-ft sea-level scenarios when compared to the historical simulation, respectively (table C5). The mean differences in groundwater levels for the six monitoring stations near the coastal structures were 0.176, 0.430, 0.520, and 0.615 ft for the 0.5-, 2.0-, 2.5-, and 3.0-ft sea-level scenarios when compared to the historical simulation, respectively (table C5). The mean differences in groundwater levels for the nine monitoring stations near the coastal structures were 0.790, 1.909, 2.288, and 2.654 ft for the 0.5-, 2.0-, 2.5-, 3.0-ft sea-level scenarios when compared to the historical simulation, respectively (table C5). The contrast between the simulated groundwater level differences at monitoring locations west of the coastal structures and those east of the coastal structures demonstrates the ability of the active surface-water system to mitigate against increases in coastal water levels and also illustrates the vulnerability of areas east of these structures to changes in sea level. Increased groundwater levels result in reduced soil storage capacity, which increases the likelihood of inundation during precipitation events. The simulated groundwater levels within the active model area ranged from 0.802 to 9.330 ft above NAVD 88 for the 3.0-ft sea-level scenario (fig. C1).

Table C4. Interpolated arrival times for the 0.5-, 2.0-, 2.5-, and 3.0-foot sea-level rise scenarios using the Intergovernmental Panel on Climate Change median (IPCC Med), the National Oceanic Atmospheric Administration (NOAA) Intermediate-High (NOAA IH), and the NOAA High (NOAA H) sea-level projection curves (Southeast Florida Regional Climate Change Compact Sea Level Rise Work Group, 2020).

[ft, foot; NAVD 88, North American Vertical Datum of 1988]

Mean sea level (ft above NAVD 88)	Sea-level rise from 2017 (ft)	Future sea-level scenario arrival times, in years, interpolated from future projections			
		NOAA H	NOAA IH	IPCC Med	Expected range
0.5	1.05	2032	2038	2056	2032–2056
2.0	2.55	2053	2063	2102	2053–2102
2.5	3.05	2059	2070	2120	2059–2120
3.0	3.55	2064	2075	2120+	2064–2120+

Table C5. Simulated steady-state wet season groundwater levels at groundwater monitoring locations for future sea-level scenarios and differences compared to historical simulation.

[foot, ft; NAVD 88, North American Vertical Datum of 1988; N/A, not applicable]

Station name	Groundwater levels for historical and future sea-level scenarios (ft above NAVD 88)					Differences in groundwater levels for future sea-level scenarios (ft)			
	Historical scenario	0.5-ft scenario	2.0-ft scenario	2.5-ft scenario	3.0-ft scenario	0.5-ft scenario	2.0-ft scenario	2.5-ft scenario	3.0-ft scenario
Groundwater monitoring stations west of coastal structures									
G-2739	7.042	7.043	7.043	7.043	7.020	0.000	0.000	0.001	−0.022
G-1213	9.090	9.097	9.106	9.109	9.111	0.007	0.015	0.018	0.020
G-2031	5.761	5.761	5.761	5.761	5.761	0.000	0.000	0.000	0.000
G-2033	5.167	5.169	5.172	5.174	5.189	0.002	0.005	0.007	0.022
G-2032	2.752	2.760	2.793	2.852	2.958	0.008	0.041	0.100	0.206
G-617	2.072	2.079	2.093	2.115	2.144	0.007	0.021	0.043	0.072
G-2034	2.316	2.316	2.320	2.322	2.323	0.000	0.004	0.006	0.007
G-1636	2.024	2.036	2.183	2.228	2.268	0.012	0.159	0.204	0.244
Mean	N/A	N/A	N/A	N/A	N/A	0.004	0.031	0.047	0.069
Groundwater monitoring stations near coastal structures									
G-1315	8.556	8.579	8.611	8.622	8.633	0.023	0.055	0.066	0.076
G-1316	7.370	7.382	7.399	7.407	7.414	0.012	0.029	0.037	0.044
G-2395	0.048	0.313	0.685	0.800	0.956	0.266	0.637	0.752	0.909
G-1221	0.771	1.102	1.463	1.572	1.689	0.331	0.692	0.801	0.918
G-1223	1.030	1.266	1.574	1.680	1.780	0.236	0.544	0.650	0.750
G-1225	1.199	1.390	1.821	2.012	2.196	0.191	0.622	0.813	0.997
Mean	N/A	N/A	N/A	N/A	N/A	0.176	0.430	0.520	0.615
Groundwater monitoring stations east of coastal structures									
G-1260	4.435	4.903	5.573	5.796	6.019	0.468	1.138	1.361	1.584
G-2866	5.566	6.026	6.682	6.896	7.107	0.460	1.116	1.330	1.541
G-2147	2.019	2.875	4.060	4.437	4.808	0.856	2.041	2.419	2.789
G-1220	0.930	1.906	3.246	3.647	4.020	0.977	2.316	2.718	3.090
G-561	1.010	2.016	3.400	3.841	4.271	1.005	2.389	2.831	3.261
G-2900	0.008	1.015	2.448	2.929	3.409	1.008	2.440	2.921	3.401
G-1226	0.765	1.507	2.604	3.022	3.418	0.742	1.839	2.257	2.653
G-2035	0.769	1.515	2.610	3.032	3.431	0.746	1.841	2.263	2.662
F-291	0.639	1.482	2.696	3.131	3.541	0.843	2.057	2.492	2.902
Mean	N/A	N/A	N/A	N/A	N/A	0.790	1.909	2.288	2.654

The effects of increased sea level on groundwater levels within the eastern, coastal areas are evident in the percentage of sea-level rise reflected in the increased average wet season groundwater levels (fig. C2). Much of the area east of the coastal control structures show groundwater level increases nearly equivalent to the sea-level increases, indicated by a value close to 100 percent. Much of the area west of the coastal structures show minimal groundwater-level increases, indicated by values close to 0 percent, illustrating the capability of coastal structures to maintain historical upstream stages. The exception is in the southern part of the county where the S-29 structure's low control elevation of 0.49 ft above NAVD 88 cannot be maintained when sea levels are increased for the 2.0-, 2.5-, and 3.0-ft sea-level scenarios. Such increases result in increased stage and groundwater levels along the C-9 Canal, as evidenced by the inland movement of the 50 percent of sea-level rise contour for the 3.0-ft sea-level scenario. The S-13 coastal structure can nearly always maintain its lower control elevation of 0.09 ft above NAVD 88, but the structure flow is entirely reliant on the stage-discharge curve

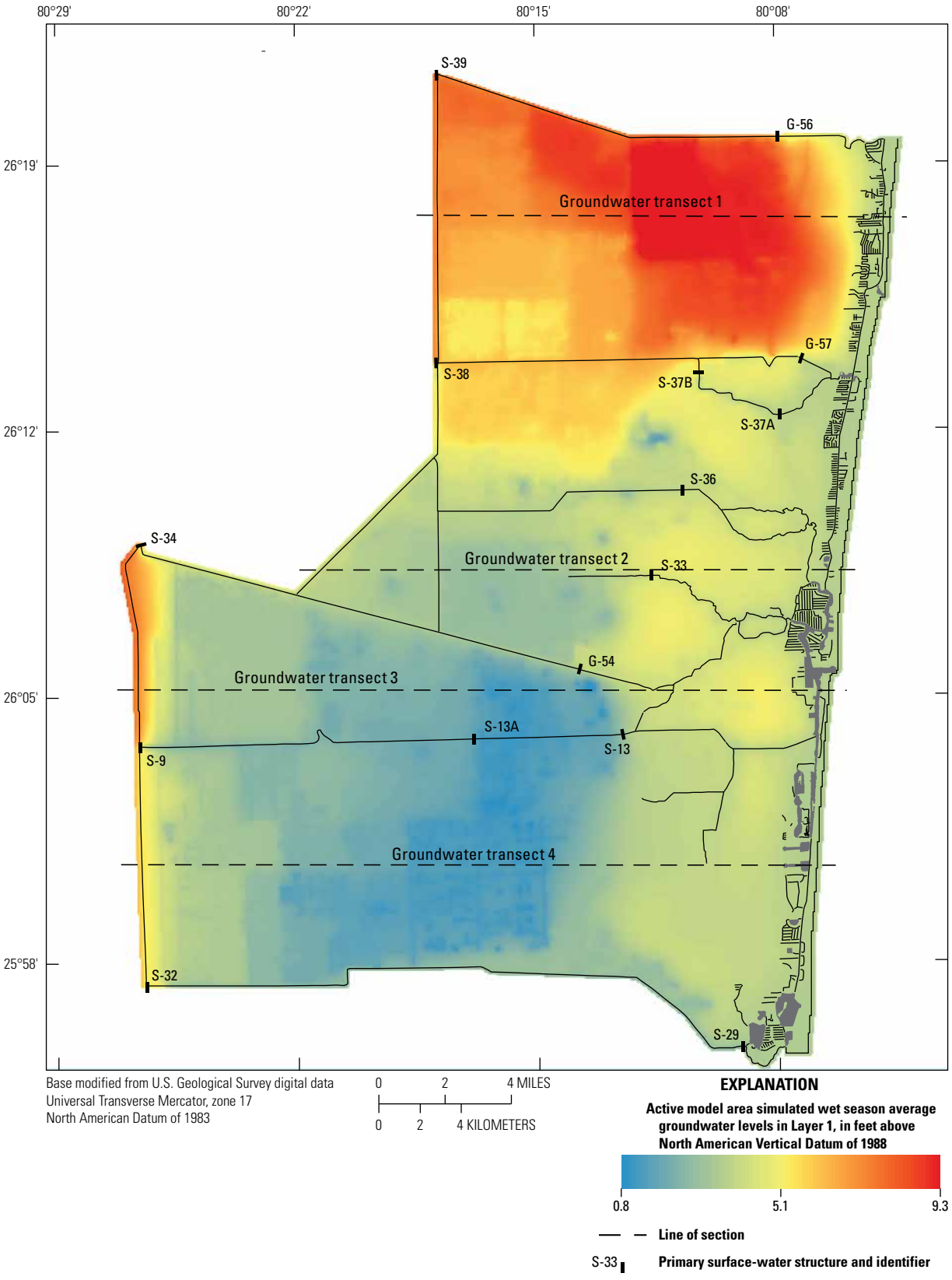

Figure C1. Simulated steady-state wet season groundwater levels in feet above the North American Vertical Datum of 1988 (NAVD 88) for the 3.0-foot future sea-level scenario.

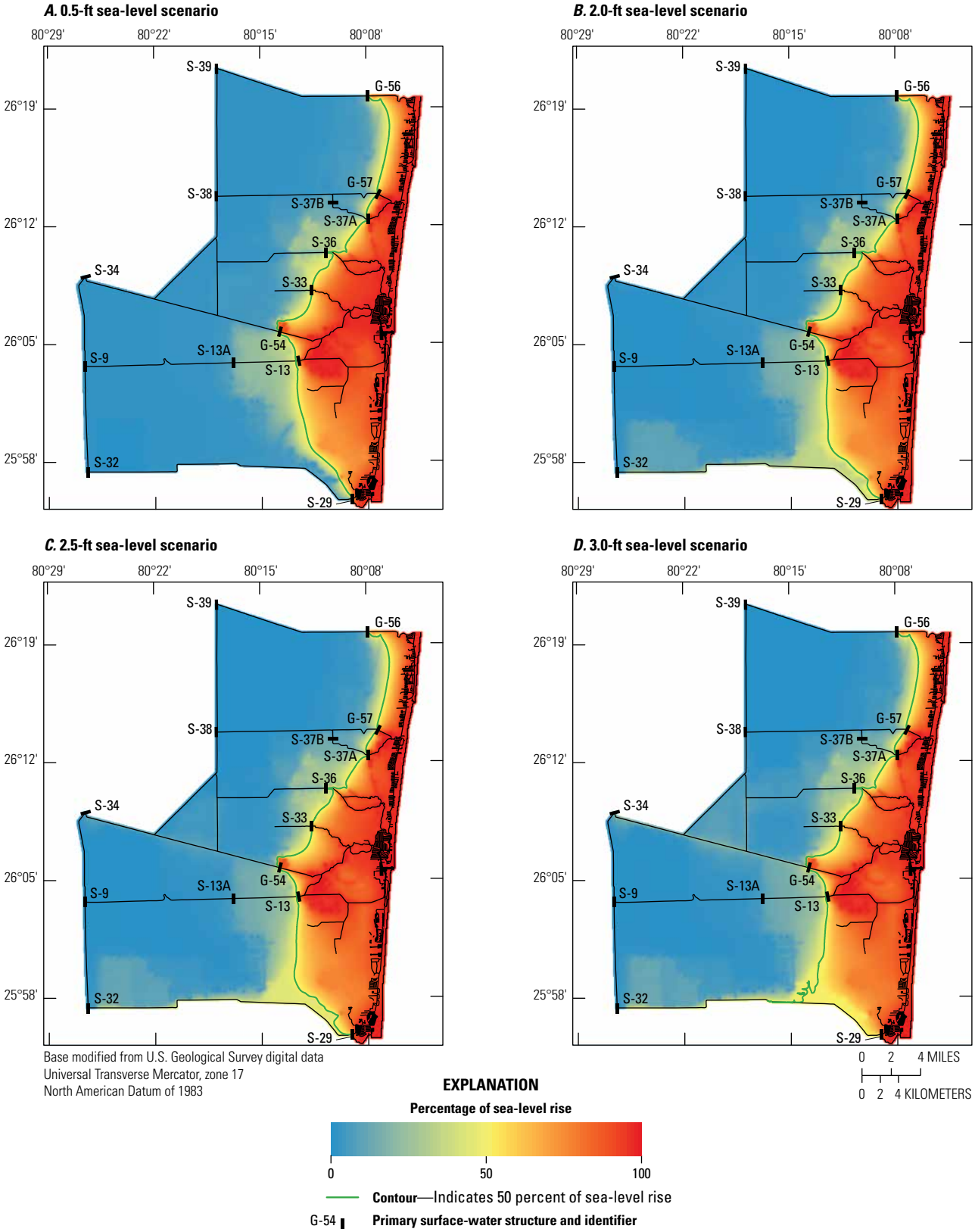

Figure C2. Percentage of sea-level rise reflected in increased steady-state average wet season groundwater levels for *A*, 0.5-foot (ft), *B*, 2.0-ft, *C*, 2.5-ft, and *D*, 3.0-ft future sea-level scenarios.

representing the pumps. A slight increase in the upstream stage at the S-13 structure is attributable to an increase in discharge corresponding to a higher stage on the linear stage-discharge curve and is a byproduct of the representation of pumps in the surface-water model (table C6).

The four historical groundwater level transects show a general west-to-east downward gradient and lower groundwater levels in the southern part of the county (fig. B3). The groundwater transects for the increased sea-level scenarios show little differences from historical groundwater levels in the western part of the county and increasing deviations from historical levels in the eastern part (figs. C3, C4, C5, and C6). The historical trend of downward gradient groundwater levels from west to east is not evident in groundwater transects 2, 3, and 4 for the 2.0-, 2.5-, and 3.0-ft sea-level scenarios. Additionally, central parts of the transect show lower groundwater levels than the western and eastern parts, which is due to the pump operations within the water control/drainage districts and the representation of the coastal structures discharging during periods of lower tide. The implication of the higher groundwater levels to the east and west is that gravity-controlled structures are no longer effective to move water out of the area. Additionally, groundwater will be flowing into these areas downgradient and will have to be removed to maintain the centralized control elevations. The western groundwater levels and coastal structure control elevations in transect 1 are sufficiently high to maintain the historical west-to-east downward gradient and show groundwater level increases only in areas east of the coastal structure, G-56.

The simulated upstream stages for most of the primary control structures increased with the increases in tide, tail water, and downstream stages associated with the increased sea-level scenarios, particularly the 2.5- and 3.0-ft scenarios (table C6). As downstream stages approach or surpass the structure's control elevation, upstream stages necessarily must rise to maintain a head difference to produce a given flow rate. The 0.5-ft sea-level scenario exhibited a small increase in upstream stages at all primary structures except S-13, which increased 0.259 ft above the historical value and has a control elevation of 0.09-ft above NAVD 88 (table C6). The 2.0-ft sea-level scenario caused an increase in upstream stage of 0.865 ft above the historical value at S-29, which has a control elevation of 0.49 ft above NAVD 88. This scenario resulted in a further increase in upstream stage at S-13 to 0.457 ft above the historical value. The upstream stage at S-13 did not increase substantially over this value for the remaining two scenarios, because the pumps became the only source of flow from the structure, and the stage-discharge rating for the pumps provided adequate flows. The remaining upstream stage values for the 2.0-ft sea-level scenario did not change substantially. The 2.5-ft sea-level scenario resulted in increased upstream stage at three additional structures, namely S-37A, S-33, and G-54, which had increased upstream stages 0.336, 0.477, and 0.431 ft above historical stage values, respectively. These structures have control elevations of 1.99, 1.99, and 2.49 ft above NAVD 88, respectively (table C1). The maximum change in upstream stage occurred at S-29, which had an increase of 1.338 ft above the historical stage value. The 3.0-ft sea-level scenario resulted in increased upstream stage for all structures except G-56, G-57, and S-9. G-56 and G-57 have control elevations of 2.99 and 5.99 ft above NAVD 88, respectively, and S-9 is a pump structure near the western boundary of the model that moves water from the C-11 Canal west into the water conservation areas. The S-9 structure is represented by a stage-discharge curve and had a small change in upstream stage for all scenarios. The maximum increase in upstream stage for the 3.0-ft sea-level scenario occurred at S-29, which had an increase of 1.831 ft above the historical stage value (table C6).

Table C6. Simulated upstream stage at the primary water-control structures for steady-state future sea-level scenarios and differences compared to historical simulation.

[Stage values are in feet above the North American Vertical Datum of 1988. Differences are in feet. foot, ft]

Structure name	Historical stage	Future sea-level scenario							
		0.5 ft		2.0 ft		2.5 ft		3.0 ft	
		Stage	Difference	Stage	Difference	Stage	Difference	Stage	Difference
G-56	5.102	5.105	0.003	5.109	0.007	5.111	0.008	5.111	0.009
G-57	3.065	3.072	0.007	3.083	0.018	3.087	0.022	3.092	0.027
S-37A	2.414	2.424	0.010	2.516	0.103	2.749	0.336	3.059	0.645
S-36	2.810	2.817	0.007	2.828	0.018	2.837	0.027	3.043	0.233
S-33	1.899	1.928	0.029	1.988	0.089	2.376	0.477	2.866	0.967
G-54	2.293	2.303	0.010	2.384	0.091	2.724	0.431	3.187	0.894
S-9	1.774	1.774	0.000	1.775	0.001	1.775	0.002	1.776	0.003
S-13	0.094	0.353	0.259	0.550	0.457	0.574	0.480	0.599	0.506
S-29	0.681	0.698	0.018	1.545	0.865	2.019	1.338	2.511	1.831

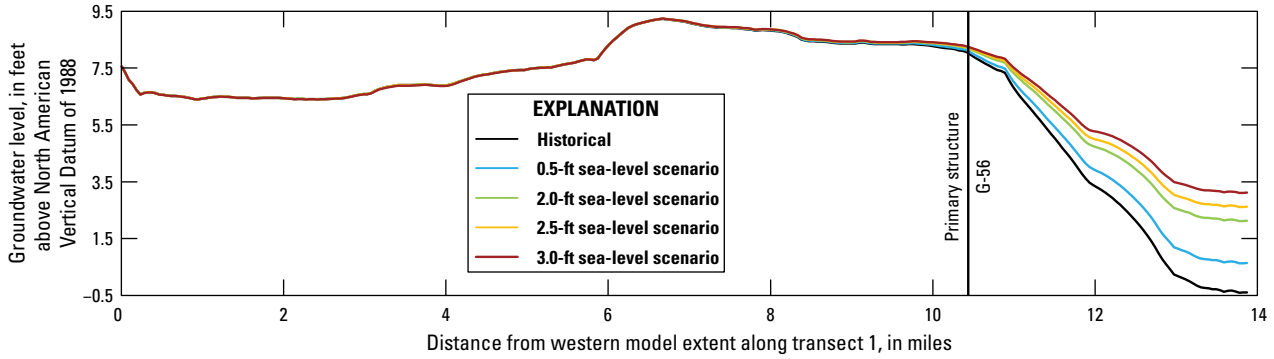

Figure C3. Simulated groundwater levels in feet above the North American Vertical Datum of 1988 for historical and future sea-level scenarios across groundwater transect 1 (fig. C1).

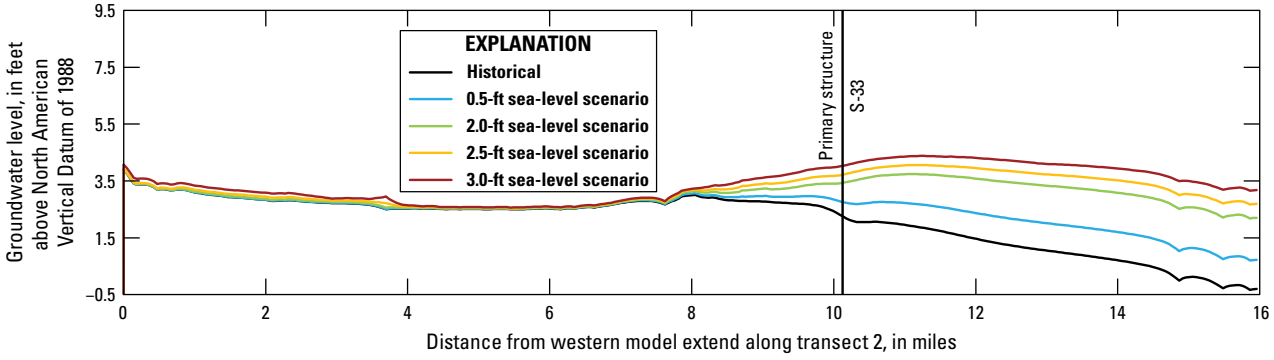

Figure C4. Simulated groundwater levels in feet above the North American Vertical Datum of 1988 for historical and future sea-level scenarios across groundwater transect 2 (fig. C1).

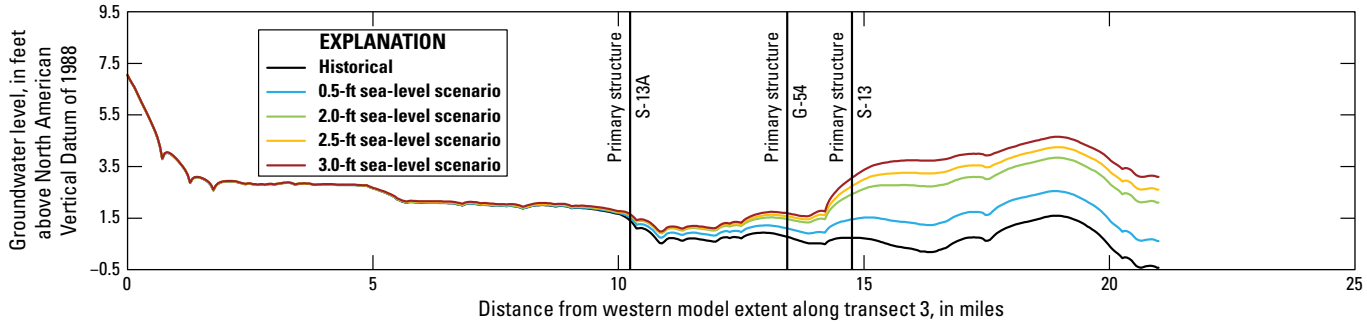

Figure C5. Simulated groundwater levels in feet above the North American Vertical Datum of 1988 for historical and future sea-level scenarios across groundwater transect 3 (fig. C1).

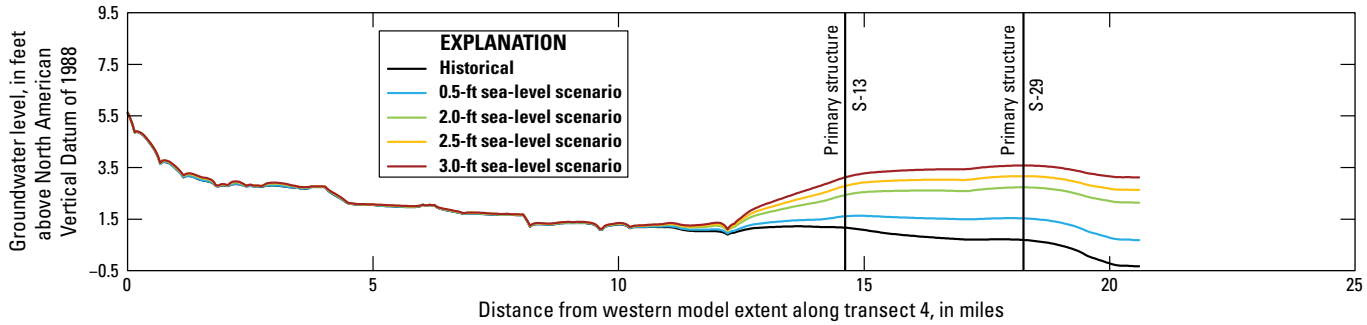

Figure C6. Simulated groundwater levels in feet above the North American Vertical Datum of 1988 for historical and future sea-level scenarios across groundwater transect 4 (fig. C1).

The simulated steady-state flow rate for the increased sea-level scenarios shows a general trend of increased flows out of the primary structures as tidal levels increase. The total flow through the primary structures increased by 57.9, 119.8, 131.4, and 127.0 cubic feet per second (ft^3/s) for the 0.5-, 2.0-, 2.5-, and 3.0-ft sea-level scenarios (table C7). These increases correspond to increases of 3.0, 6.2, 6.8, and 6.6 percent in flow rates for the four scenarios, respectively. The increase in flow rates out of the primary structures is likely due to the increased groundwater levels in the eastern part of the county causing increased groundwater leakage to surface water, thereby reducing the west-to-east groundwater gradients and flows. The general trend of increased flow for each scenario is exhibited by all the primary structures except for G-54 and S-29. Simulated flows at these two structures increase for the 0.5- and 2.0-ft sea-level scenarios but begin to decline for the 2.5- and 3.0-ft sea-level scenarios. The simulated flow at G-54 is 10.5 ft^3/s lower for the 3.0-ft sea-level scenario than for the historical simulation (table C7). The decrease in the flow rate through G-54 for the higher sea-level scenario is likely due to groundwater flow being diverted to adjacent drainage areas that use pump-equipped structures with lower control elevations.

An additional simulation was run using the 3.0-ft sea-level scenario with a recharge rate increased by 15 percent for each of the rainfall zones. Estimated surface-water inflows into the Hillsboro and C-9 Canals representing rainfall contributions from outside of the active model extents were also increased by 15 percent. The resulting groundwater levels show a maximum increase of 0.45 ft compared to the 3.0-ft sea-level scenario using the historical recharge rate (fig. C7). The increases mostly appear in areas where simulated surface-water stages were below the drainage area's control elevation in the 3.0-ft sea-level scenario or in areas having a lower density of surface-water features. Groundwater levels in the Pine Tree Water Control District (area of interest A, fig. C7), Cocomar Water Control District (area of interest B, fig. C7), and Broward Water Control District #4 (area of interest C, fig. C7) increased as a result of increased surface-water stage in drainage areas that had previously simulated surface-water stages below the control elevations. Upstream stage at the coastal structures exhibited a small change with the increased recharge rate. The 15-percent increase in recharge resulted in a 16.4-percent increase in the flows through the primary structures (table C8).

Table C7. Simulated structure flow rates through the primary water-control structures for the steady-state future sea-level scenarios and differences compared to historical simulation.

[Flow rates and differences are in cubic feet per second. ft, foot]

Structure name	Historical flow rate	Future sea-level scenario							
		0.5 ft		2.0 ft		2.5 ft		3.0 ft	
		Flow rate	Difference	Flow rate	Difference	Flow rate	Difference	Flow rate	Difference
G-56	346.8	351.2	4.3	357.3	10.5	359.4	12.6	360.3	13.4
G-57	16.0	18.5	2.5	22.1	6.1	23.6	7.6	25.2	9.2
S-37A	461.2	468.7	7.5	478.8	17.6	480.3	19.1	481.5	20.3
S-36	143.9	148.6	4.7	155.9	12.1	162.2	18.4	160.0	16.2
S-33	8.9	13.2	4.3	19.4	10.5	20.8	11.9	23.2	14.3
G-54	163.4	171.6	8.1	178.7	15.3	167.3	3.9	153.0	−10.5
S-9	90.5	91.3	0.8	94.2	3.7	97.0	6.5	100.7	10.2
S-13	283.7	284.1	0.5	297.3	13.6	309.8	26.1	323.7	40.0
S-29	403.6	428.8	25.2	434.1	30.5	428.9	25.3	417.4	13.8
Total	1,918.0	1,975.9	57.9	2,037.8	119.8	2,049.3	131.4	2,045.0	127.0

Simulation of Transient Conditions Under Future Sea Level and Increased Precipitation Scenarios

The transient model developed to simulate the 2013–17 historical period was used to simulate changes in groundwater levels, surface-water stages, and structure flows under increased sea-level scenarios. The historical, measured time series of rainfall and potential evapotranspiration rates were used. Future mean sea-level scenarios of 0.5, 2.0, 2.5, and 3.0 ft above NAVD 88 were simulated, which corresponded to sea-level increases of 1.05, 2.55, 3.05, and 3.55 ft, respectively. The hourly time series representing the eastern groundwater specified head boundary and the surface-water specified stage boundaries representing tide and structure tail waters were each increased by the corresponding sea-level increases for each scenario. An additional 3.0-ft mean sea-level scenario was run with the historical time series for rainfall input increased 15 percent above measured values to understand the effects of possible changes in rainfall.

Simulated Groundwater Levels

Average wet season (May 1–October 31) groundwater levels for the 23 monitoring stations were calculated and the stations were divided into three groups: stations west of the coastal water-control structures, stations near the coastal water-control structures, and stations east of the coastal water-control structures (table C9, fig. B1). The mean differences in average wet season groundwater levels for the eight monitoring stations west of the coastal water structures were 0.020, 0.083, 0.116, and 0.151 ft for the 0.5-, 2.0-, 2.5-, and 3.0-ft sea-level scenarios when compared to the historical scenario, respectively (table C9). The mean differences in average wet season groundwater levels for the six monitoring stations near the coastal water-control structures were 0.182, 0.468, 0.563, and 0.665 ft for the 0.5-, 2.0-, 2.5-, and 3.0-ft sea-level scenarios compared to the historical scenario, respectively. The mean differences in average wet season groundwater levels for the nine monitoring stations east of the coastal water-control structures were 0.827, 2.010, 2.403, and 2.791 ft for the 0.5-, 2.0-, 2.5-, and 3.0-ft sea-level scenarios compared to the historical scenario, respectively. Like the results of the steady-state model simulations, the contrast between the simulated groundwater level differences at monitoring locations west of the coastal water-control structures and those east of the coastal water-control structures demonstrate the active surface-water system's capability to mitigate against increases in coastal water levels and also illustrate the vulnerability of areas east of these structures to changes in sea level. The contrast in the effects of increased sea level between coastal and inland areas is further evidenced by the percentage of sea-level rise reflected in the increased average wet season groundwater levels (fig. C8). Much of the area east of the coastal water-control structures show groundwater increases nearly equivalent to the sea-level rise, indicated by 100 percent. Much of the areas west of the coastal control structures show minimal groundwater level increases. Similar to results seen in the steady-state model simulations, the only exception to this are the areas surrounding the C-9 Canal, which is controlled by the S-29 structure that has a low control elevation of 0.09 ft above NAVD 88. The simulated average wet season groundwater levels within the active model area ranged from 0.706 to 9.326 ft above NAVD 88 for the 3.0-ft sea-level scenario (fig. C9).

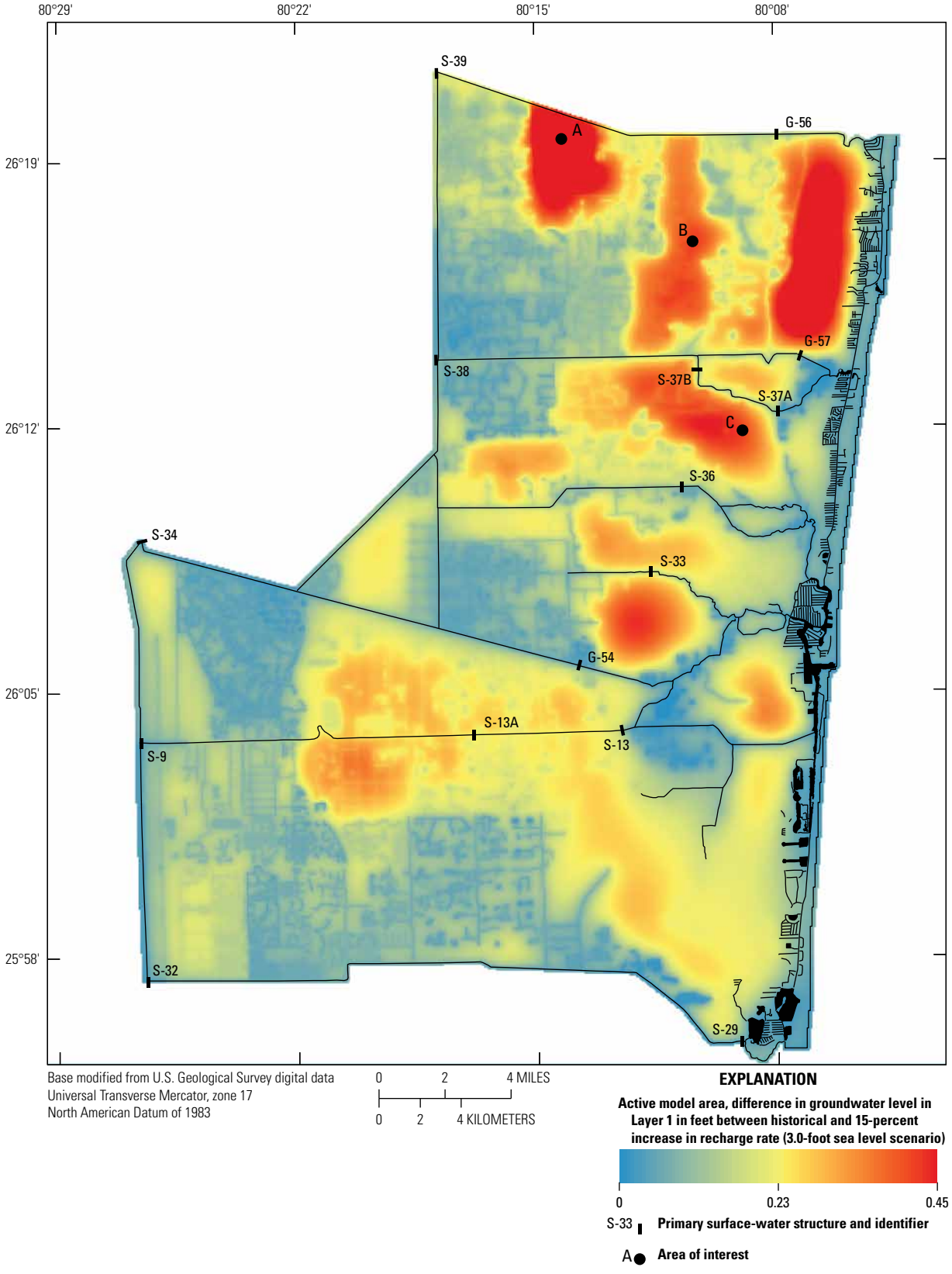

Figure C7. Difference in simulated groundwater levels in feet between 3.0-foot future sea-level scenario with historical and 15-percent increase in historical recharge rate.

Table C8. Simulated upstream stage and flow at the primary structures for the 3.0-foot future sea-level scenario with historical and 15-percent increase in historical recharge.

[ft, foot; NAVD 88, North American Vertical Datum of 1988; ft³/s, cubic foot per second; N/A, not applicable]

Structure name	Simulated upstream stage (ft above NAVD 88)		Difference (ft)	Simulated structure flow (ft³/s)		Difference (ft³/s)	Difference (percent)
	Historical recharge	15-percent increase in recharge		Historical recharge	15-percent increase in recharge		
G-56	5.111	5.141	0.030	360.3	405.9	45.6	12.7
G-57	3.092	3.098	0.006	25.2	27.6	2.4	9.4
S-37A	3.059	3.113	0.054	481.5	535.4	53.9	11.2
S-36	3.043	3.079	0.036	160.0	192.4	32.4	20.2
S-33	2.866	2.871	0.005	23.2	31.5	8.3	35.9
G-54	3.187	3.194	0.007	153.0	182.1	29.2	19.1
S-9	1.776	1.785	0.008	100.7	132.7	32.1	31.8
S-13	0.599	0.678	0.079	323.7	366.1	42.4	13.1
S-29	2.511	2.521	0.010	417.4	506.0	88.7	21.2
Total	N/A	N/A	N/A	2,045.0	2,379.8	334.8	16.4

The average wet season groundwater level transects produced by the transient model for the increased sea-level scenarios show similar trends compared to the steady-state model. Only small changes to groundwater levels occur west of the coastal water-control structures, and deviations from the historical groundwater levels begin to increase near the coastal water-control structures and toward the coast. The historical west-to-east downward trend in groundwater levels is no longer evident in groundwater transects 2, 3, and 4 for the 3.0-ft sea-level scenario. The central parts of the transects show lower groundwater levels than in the western and eastern parts of the county as water is being pumped out of water control/drainage districts and into the primary canals (fig. C10).

The likelihood of parts of Broward County becoming inundated during moderate or extreme precipitation events is increased in areas having a shallow depth to groundwater because of the corresponding decrease in soil storage capacity. The increase in area where the depth to groundwater is less than 2 ft, particularly in the eastern part of the county, is an indication of the increased risk of inundation for these vulnerable areas. In the 3.0-ft sea-level scenario, there was an additional 22.97 square miles (mi²) of inundated area and an additional 37.43 mi² of area where the depth to groundwater was less than 2 ft over the historical simulation (fig. C11).

Simulated Stages and Flows at Primary Surface-Water Control Structures

Time series of simulated upstream stages and flows through the primary structures for the historical and future sea-level scenarios were compared, and differences in wet season average results were calculated. The simulated wet season average upstream stage for most of the primary structures increased with the increased tide and tail water stages associated with the future sea-level scenarios (table C10). The S-13, S-33, and S-29 structures were the only ones affected during the 0.5-ft sea-level scenario, with increased wet season averaged upstream stages of 0.166, 0.171, and 0.204 ft above the historical values, respectively. The 2.0-ft sea-level scenario resulted in an increase in wet season average upstream stages of 0.483, 0.196, and 0.394 ft above the historical value at the S-37A, S-36, and G-54 structures and further increases in wet season average upstream stage at the S-13, S-33, and S-29 structures to 0.371, 0.575, and 0.989 ft above the historical values. The 2.5-ft sea-level scenario resulted in increased wet season average upstream stage values at all structures except S-9, which is a pump structure in the western part of the county, and G-56, which has a control elevation of 5.99 ft above NAVD 88. The increases in upstream stage at the other structures for the 2.5-ft sea-level scenario ranged from 0.133 to 1.394 ft above the historical values. The 3.0-ft sea-level scenario caused increased upstream stage at all primary structures except S-9. The maximum increase in wet season average upstream stage for the 3.0-ft sea-level scenario occurred at the S-29 structure, where stage increased 1.831 ft above the historical value. The time series of upstream stage for the S-29, S-13, S-37A, S-36, S-33, and G-54 structures show that the increased values of upstream stage resulting from the 3.0-ft sea-level scenario are consistently evident throughout the simulation period (figs. C12, C13, and C14).

Table C9. Simulated transient wet season average groundwater levels at groundwater monitoring locations for future sea-level scenarios and differences compared to the historical simulation.

[ft, foot; NAVD 88, North American Vertical Datum of 1988; N/A, not applicable]

Station name	Groundwater levels for historical and future sea-level scenarios (ft above NAVD 88)					Differences in groundwater levels for future sea-level scenarios (ft)			
	Historical simulation	0.5-ft scenario	2.0-ft scenario	2.5-ft scenario	3.0-ft scenario	0.5-ft scenario	2.0-ft scenario	2.5-ft scenario	3.0-ft scenario
Groundwater monitoring stations west of coastal structures									
G-2739	6.741	6.750	6.763	6.768	6.772	0.009	0.022	0.027	0.031
G-1213	8.903	8.917	8.938	8.944	8.951	0.015	0.035	0.041	0.048
G-2031	5.660	5.662	5.666	5.667	5.668	0.002	0.006	0.007	0.008
G-2033	4.810	4.826	4.864	4.886	4.916	0.016	0.054	0.076	0.105
G-2032	2.423	2.458	2.580	2.651	2.747	0.035	0.157	0.228	0.324
G-617	1.883	1.896	1.939	1.960	1.988	0.013	0.055	0.077	0.104
G-2034	2.194	2.201	2.231	2.245	2.258	0.008	0.037	0.051	0.064
G-1636	1.697	1.762	2.999	2.115	2.217	0.064	0.302	0.418	0.520
Mean	N/A	N/A	N/A	N/A	N/A	0.020	0.083	0.116	0.151
Groundwater monitoring stations near coastal structures									
G-1315	8.336	8.376	8.431	8.449	8.467	0.041	0.095	0.113	0.129
G-1316	6.997	7.021	7.058	7.070	7.084	0.024	0.060	0.073	0.075
G-2395	−0.505	−0.227	0.177	0.326	0.496	0.278	0.682	0.831	0.952
G-1221	0.599	0.877	1.276	1.383	1.495	0.278	0.676	0.783	0.891
G-1223	0.702	0.929	1.280	1.384	1.491	0.227	0.577	0.682	0.780
G-1225	0.851	1.099	1.566	1.747	1.935	0.248	0.715	0.896	1.068
Mean	N/A	N/A	N/A	N/A	N/A	0.182	0.468	0.563	0.665
Groundwater monitoring stations east of coastal structures									
G-1260	4.065	4.559	5.263	5.497	5.732	0.494	1.198	1.432	1.667
G-2866	4.686	5.183	5.890	6.125	6.359	0.497	1.204	1.439	1.673
G-2147	1.410	2.294	3.541	3.949	4.351	0.884	2.131	2.539	2.941
G-1220	0.597	1.596	3.014	3.462	3.883	0.999	2.417	2.865	3.286
G-561	0.609	1.641	3.090	3.556	4.010	1.032	2.481	2.947	3.401
G-2900	−0.038	0.979	2.430	2.914	3.397	1.018	2.468	2.952	3.435
G-1226	0.361	1.170	2.361	2.770	3.186	0.809	2.000	2.409	2.824
G-2035	0.362	1.177	2.373	2.785	3.204	0.815	2.012	2.423	2.842
F-291	0.286	1.183	2.469	2.902	3.338	0.897	2.183	2.617	3.052
Mean	N/A	N/A	N/A	N/A	N/A	0.827	2.010	2.403	2.791

The simulated wet season average flow rate generally increased with increases in mean tidal levels (table C11). The total flow through the primary structures increased 57.8, 119.2, 130.9, and 138.6 ft^3/s above the historical values for the 0.5-, 2.0-, 2.5-, and 3.0-ft sea-level scenarios, respectively. These values correspond to increases of 3.1, 6.5, 7.1, and 7.5 percent in flow rates for the four scenarios, respectively. The increased flow through the coastal structures is due to the increased groundwater levels, resulting in decreased west-to-east groundwater gradients and corresponding coastward groundwater flow. The time series of flow through the S-13 and S-33 structures show the increased flow resulting from the 3.0-ft sea-level scenario while the increased flow through the S-29, S-37A, and S-36 structures are not evident within the time series. Parts of time with decreased flow through the G-54 structure can be seen and increases in the peak flows through the S-36 and S-33 are evident within the time series of flow from the 3.0-ft sea-level scenario (figs. C12, C13, and C14).

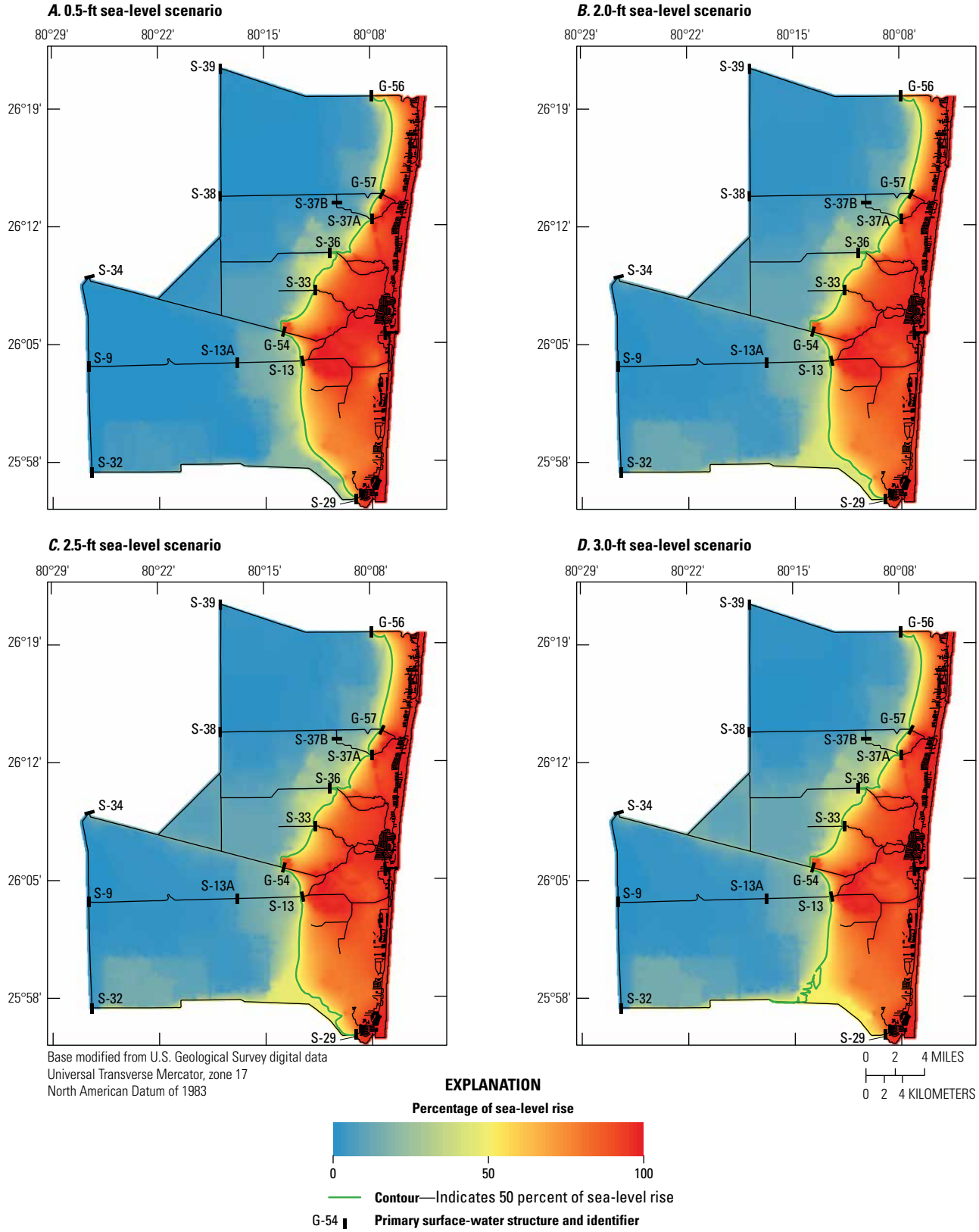

Figure C8. Percentage of sea-level rise reflected in increased wet season average groundwater levels from the transient model for *A*, 0.5-foot (ft), *B*, 2.0-ft, *C*, 2.5-ft, and *D*, 3.0-ft future sea-level scenarios.

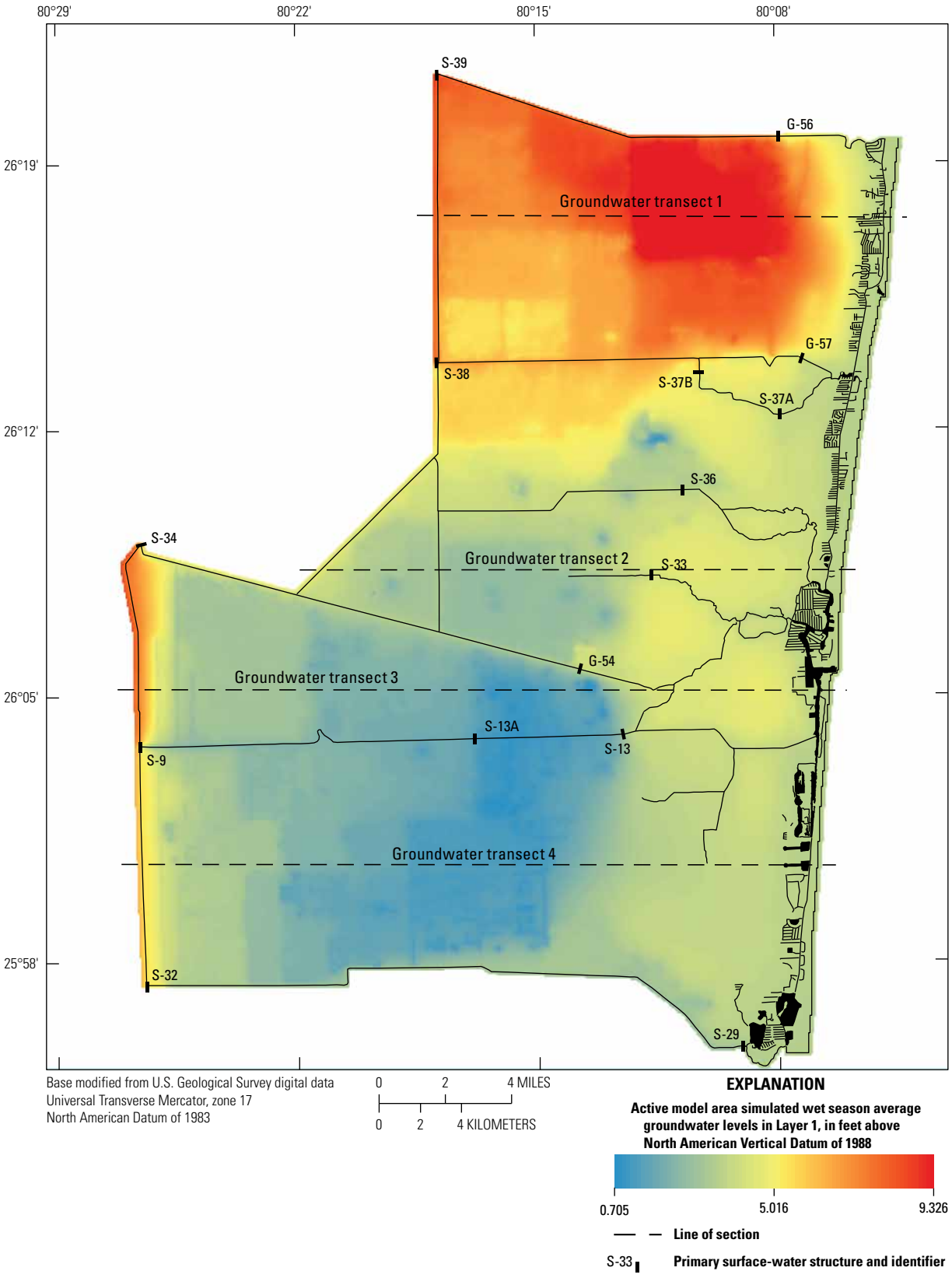

Figure C9. Simulated transient wet season average groundwater levels in feet above the North American Vertical Datum of 1988 for the 3.0-foot future sea-level scenario.

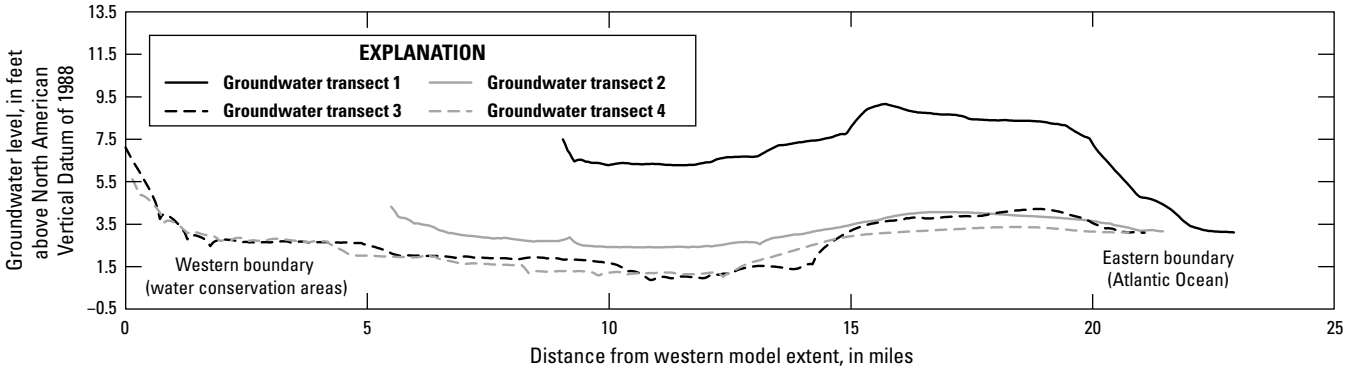

Figure C10. Simulated wet season average groundwater levels in feet above the North American Vertical Datum of 1988 for the 3.0-foot future sea-level scenario across groundwater transects for the transient model.

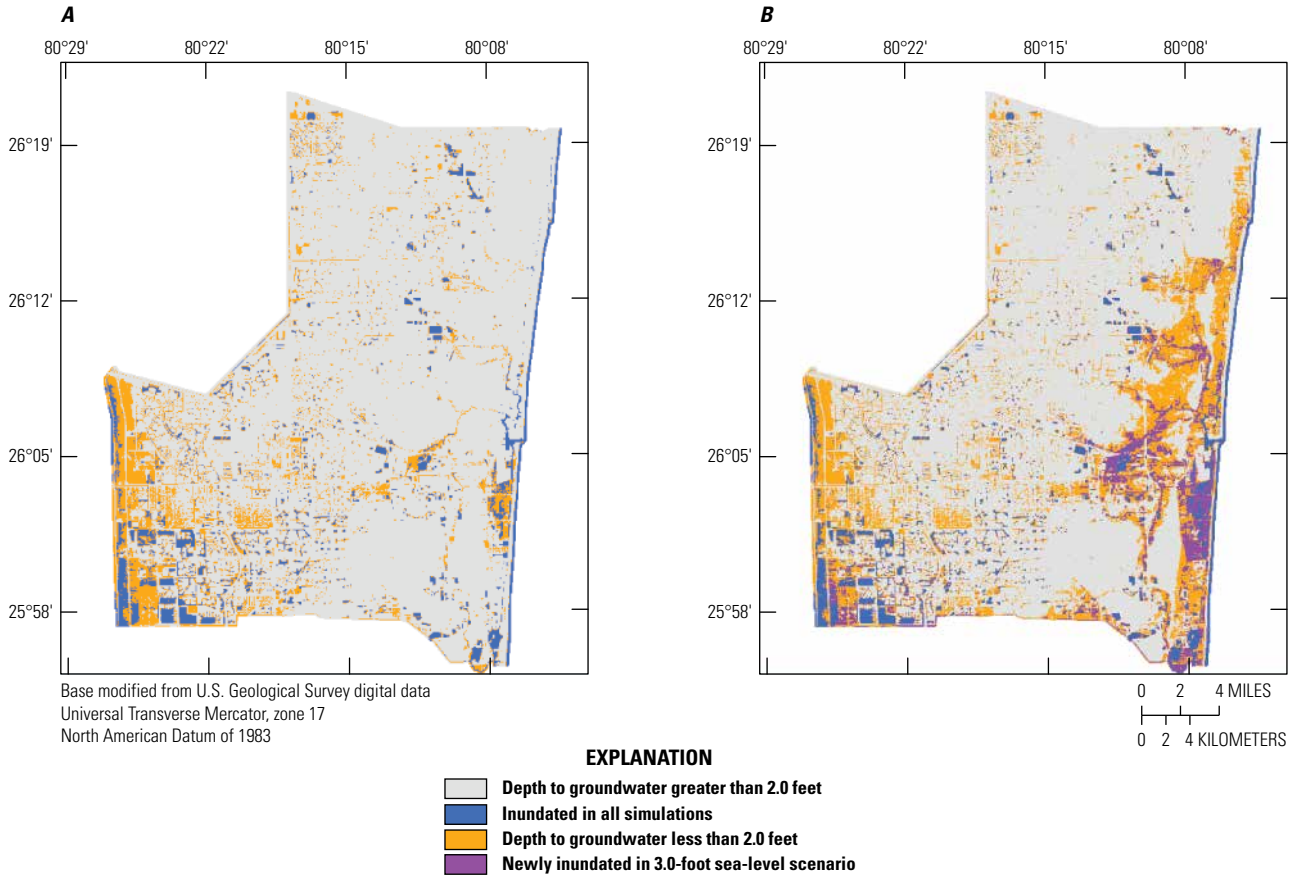

Figure C11. Wet season average depth to groundwater for, *A*, historical and, *B*, 3.0-foot future sea-level scenarios for the transient model.

Table C10. Simulated wet season average upstream stage at the primary water-control structures for future sea-level scenarios and differences compared to the historical simulation for the transient model.

[Stage values are in feet above the North American Vertical Datum of 1988. Differences are in feet. ft, foot]

Structure name	Historical stage	Future sea-level scenario							
		0.5 ft		2.0 ft		2.5 ft		3.0 ft	
		Stage	Difference	Stage	Difference	Stage	Difference	Stage	Difference
G-56	4.893	4.927	0.034	4.975	0.081	4.991	0.098	5.012	0.120
G-57	3.048	3.060	0.013	3.113	0.066	3.179	0.133	3.290	0.243
S-37A	2.366	2.417	0.051	2.848	0.483	3.134	0.768	3.491	1.125
S-36	2.784	2.806	0.022	2.978	0.196	3.117	0.335	3.317	0.536
S-33	1.628	1.799	0.171	2.201	0.575	2.467	0.841	2.860	1.234
G-54	2.258	2.312	0.054	2.656	0.394	2.886	0.624	3.204	0.940
S-9	1.782	1.783	0.000	1.784	0.002	1.784	0.003	1.785	0.004
S-13	0.156	0.322	0.166	0.522	0.371	0.546	0.395	0.570	0.420
S-29	0.656	0.860	0.204	1.673	0.989	2.086	1.394	2.563	1.831

An additional simulation was run using the 3.0-ft sea-level scenario with the time series of rainfall rates increased by 15 percent for each of the rainfall zones. The estimated inflows into the Hillsboro and C-9 Canals representing rainfall influxes from the parts of those drainage areas outside of the active model extents were also increased by 15 percent. The wet season average upstream stage at the primary structures showed little increase, whereas the total flow through those structures increased by 13.2 percent (table C12).

Summary of Simulated Effects of Future Sea Level on the Hydrologic System

The simulated effects of increased future sea level on wet season groundwater levels, upstream stage at the primary structures, and flow through the primary structures were similar when evaluated using a steady-state or transient model. In response to various increases in sea level, the simulated results at 23 groundwater monitoring locations indicate little change in groundwater levels west of the coastal water-control structures and the highest changes in groundwater levels east of the coastal water-control structures. In agreement with this, the percentage of sea-level rise reflected in increased average wet season groundwater levels is nearly 100 percent in the easternmost, coastal parts of the simulated area and nearly 0 percent in those areas west of the coastal water-control structures. The areas along the C-9 canal are the exception as increases in sea level cause increases in upstream stage for the S-29 coastal structure, particularly for the 3.0-ft sea-level scenario. For the 3.0-ft sea-level scenario, the total area where depth to groundwater is less than 2 ft increased by 37.43 mi^2, indicating an increased risk of inundation for these areas. The total area inundated during the mean wet season increased by 22.97 mi^2.

Simulated historical groundwater-level transects show a general west-to-east downslope gradient with higher groundwater levels in the northern part of the county. In comparison to simulated historical groundwater-level transects, only small differences are indicated in the simulated groundwater-level transects west of the coastal control structures for the future sea-level scenarios. In contrast, east of the coastal control structures, simulated groundwater-level transects show increasing differences from the historical simulation with increasing sea levels. Furthermore, in contrast to the trend of west-to-east downward gradient groundwater levels in the simulated historical transects, a flat or reverse east-to-west gradient toward the center of the simulated area is measured in the three most southern simulated groundwater-level transects for the 2.0-, 2.5-, and 3.0-ft sea-level scenarios. The implications for these results are that the hydrologic controls can still be effective at maintaining wet season groundwater levels near to historical levels for areas west of the control structures. However, the peaks in groundwater levels and canal stages caused by short-term events can be affected. Areas east of the control structures will experience increases in groundwater levels nearly equivalent to the rise in sea level.

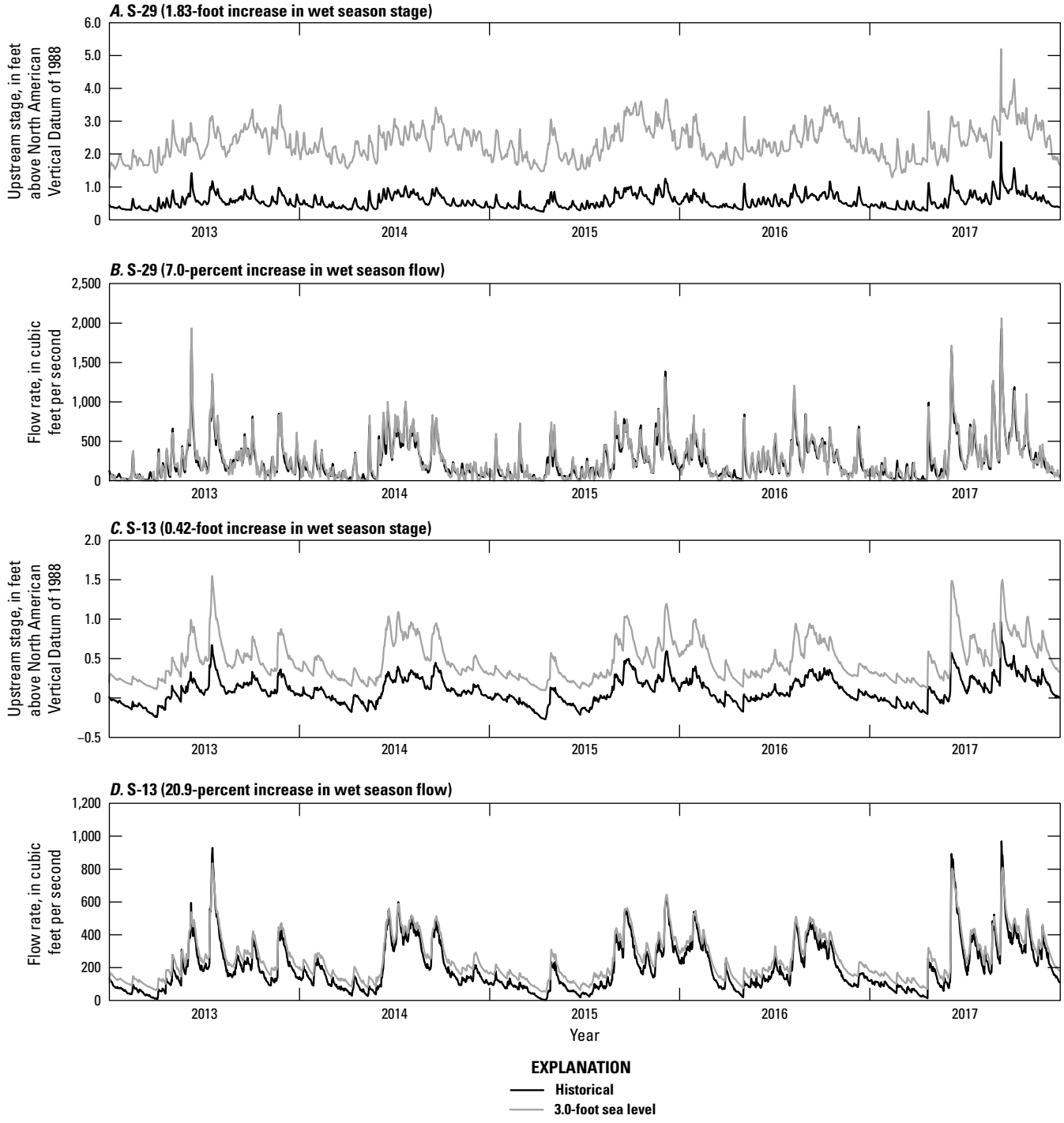

Figure C12. Simulated upstream stage and flow through S-29 and S-13 structures for the historical and 3.0-foot sea-level scenarios.

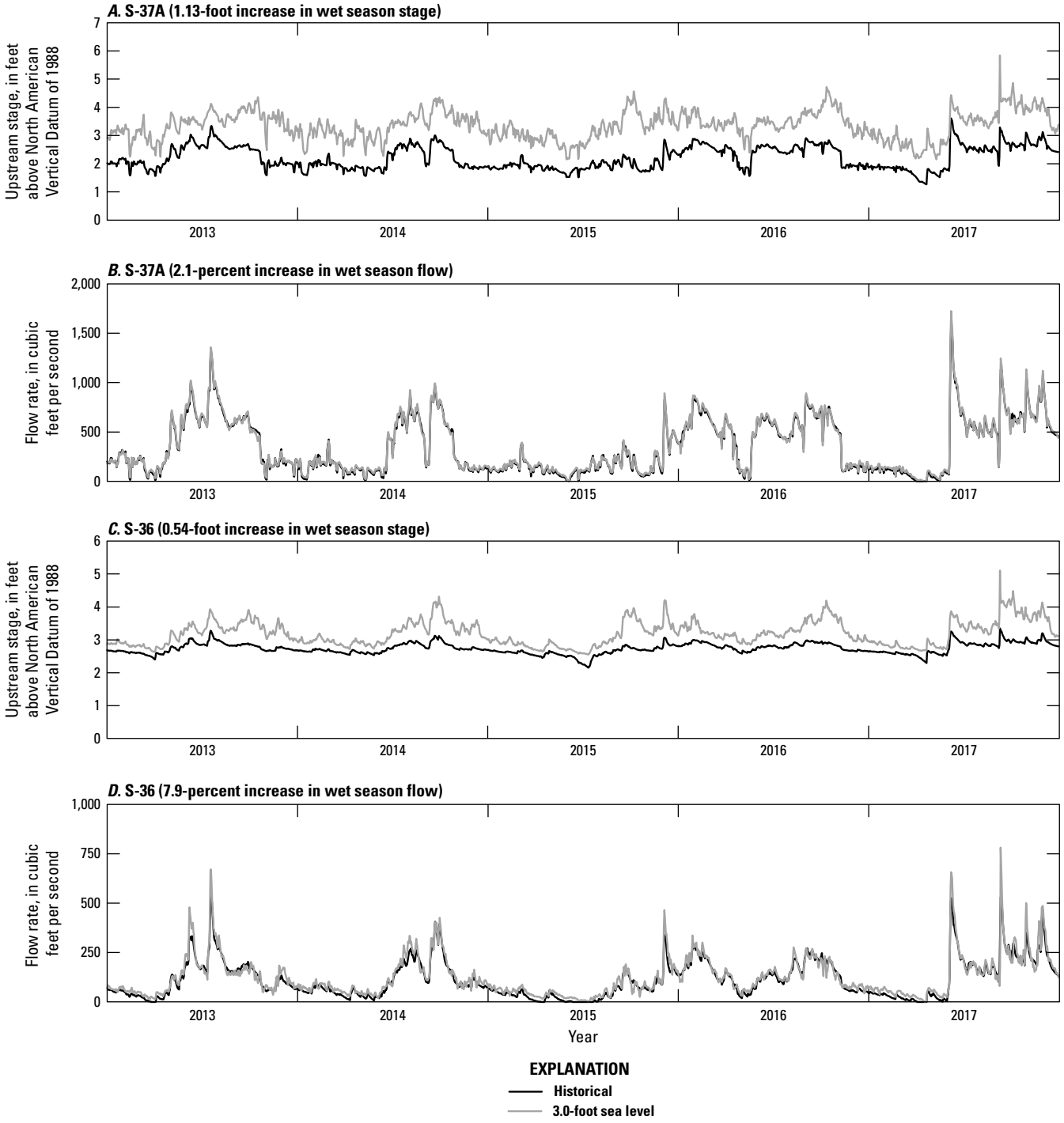

Figure C13. Simulated upstream stage and flow through S-29 and S-13 structures for the historical and 3.0-foot sea-level scenarios.

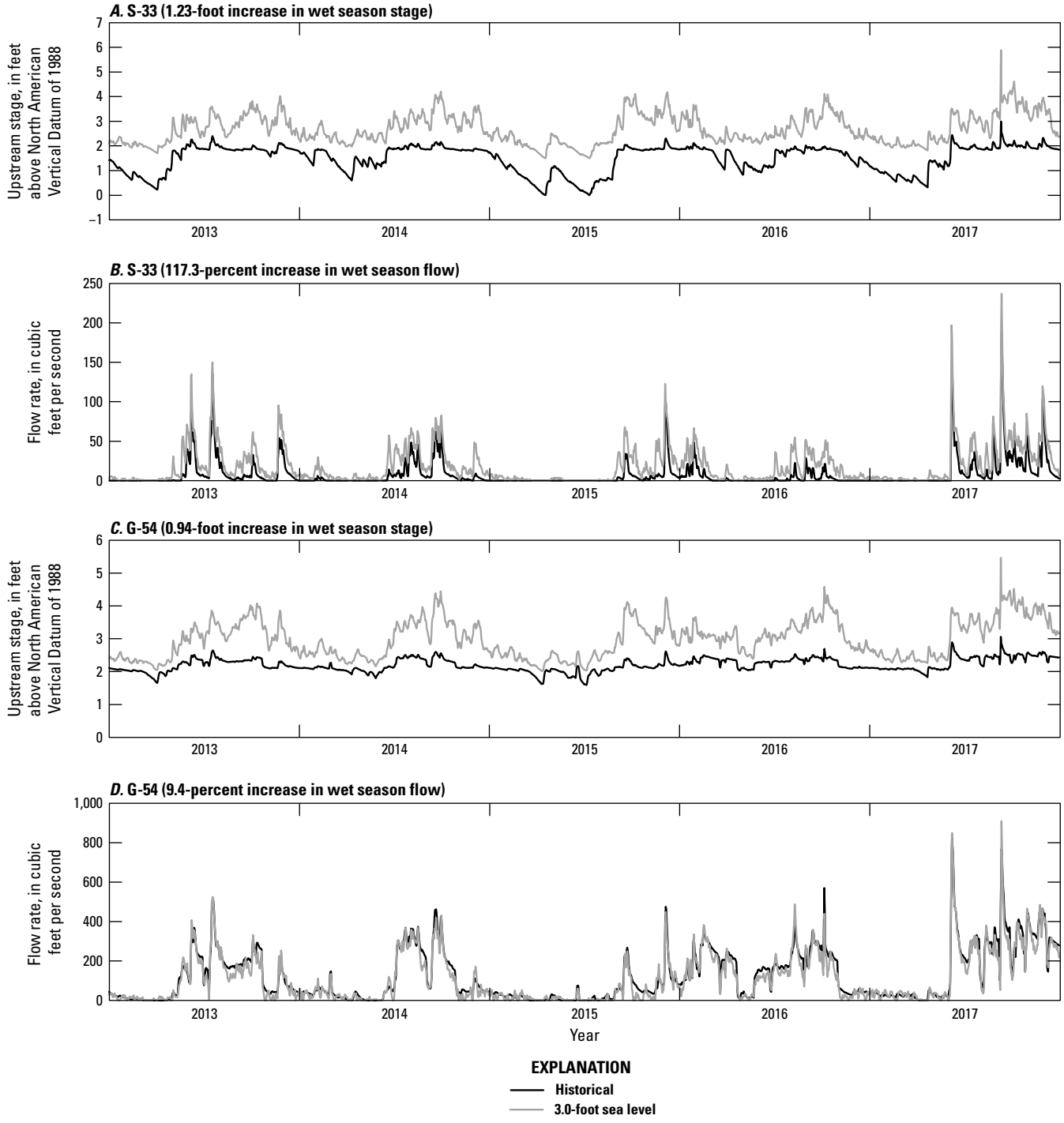

Figure C14. Simulated upstream stage and flow through S-29 and S-13 structures for the historical and 3.0-foot sea-level scenarios.

Table C11. Simulated wet season average flow through the primary structures at the primary water-control structures for future sea-level scenarios and differences compared to historical simulation for the transient model.

[All flow rates and differences are in cubic feet per second. foot, ft]

Structure name	Historical flow rate	Future sea-level scenario							
		0.5 ft		2.0 ft		2.5 ft		3.0 ft	
		Flow rate	Difference	Flow rate	Difference	Flow rate	Difference	Flow rate	Difference
G-56	314.5	319.5	5.0	326.6	12.1	328.9	14.4	331.1	16.6
G-57	11.7	14.3	2.6	18.6	6.9	20.2	8.5	22.7	11.0
S-37A	461.9	469.0	7.1	475.5	13.6	474.8	12.9	471.7	9.8
S-36	145.2	153.0	7.8	160.0	14.9	159.4	14.2	156.7	11.5
S-33	11.5	14.7	3.2	19.9	8.4	21.8	10.4	25.0	13.5
G-54	168.8	174.1	5.3	168.1	−0.8	161.4	−7.4	152.9	−15.9
S-9	116.1	117.5	1.4	123.4	7.3	126.3	10.2	129.7	13.6
S-13	257.2	265.2	8.0	284.7	28.8	297.7	40.5	311.0	53.8
S-29	349.9	368.4	17.4	378.9	27.9	378.1	27.1	375.6	24.7
Total	1,837.9	1,895.7	57.8	1,957.1	119.2	1,968.8	130.9	1,976.5	138.6

Table C12. Simulated wet season average upstream stage and flow at primary structures for the 3.0-foot future sea-level scenario with historical and 15-percent increase in historical rainfall.

[ft, foot; NAVD 88, North American Vertical Datum of 1988; ft^3/s, cubic foot per second; N/A, not applicable]

Structure name	Simulated upstream stage (ft above NAVD 88)		Difference (ft)	Simulated structure flow (ft^3/s)		Difference (ft^3/s)	Difference (percent)
	Historical recharge	115 percent rainfall		Historical recharge	115 percent rainfall		
G-56	5.012	5.060	0.047	331.1	367.8	36.7	11.1
G-57	3.290	3.309	0.019	22.7	25.3	2.6	11.4
S-37A	3.491	3.537	0.046	471.7	514.5	42.8	9.1
S-36	3.317	3.368	0.051	156.7	174.8	23.8	15.2
S-33	2.860	2.947	0.087	25.0	30.8	5.8	23.2
G-54	3.204	3.261	0.057	152.9	174.8	21.9	14.3
S-9	1.785	1.791	0.005	129.7	150.9	21.2	16.3
S-13	0.570	0.641	0.071	311.0	358.9	37.8	12.2
S-29	2.563	2.579	0.016	375.6	444.0	68.4	18.2
Total	N/A	N/A	N/A	1,976.5	2,237.4	260.9	13.2

The simulated wet season average upstream stage for most of the primary structures increased with the increased tide, tail water, and groundwater levels associated with the future sea-level scenarios. Results from the steady-state model show that the 0.5- and 2.0-ft sea-level scenarios resulted in increased upstream stage values for the structures having the lowest control elevations, S-13 and S-29, and results from the transient model indicated increased stages at the S-37A, S-36, S-33, and G-54 structures as well. Steady-state simulation results for the 2.5-ft sea-level scenario indicated an increase in upstream stage values for the S-37A, S-33, and G-54 structures and further increases in upstream stage values for structures S-13 and S-29. The transient model results indicated increased upstream stages at all structures except G-56 and S-9 for the 2.5-ft sea-level scenario. The 3.0-ft sea-level scenario resulted in increased upstream stage for all primary structures except S-9, G-56, and G-57 using the steady-state model, whereas only the S-9 structure was mostly unaffected within the transient model results. Although the S-13 structure has the lowest control elevation, the S-29 structure had the greatest increase of all structures in upstream stage values for the future sea-level scenarios. This occurs because the S-13 structure can operate pumps to maintain flow at increased sea level without increasing upstream stage. Simulated flow through the primary structures increases as sea-level increases. This is partially due to the increased leakage into the surface-water network as groundwater levels increase near the coast and reduce groundwater gradients and eastward groundwater flows.

Additional simulations were run with a 15-percent increase in recharge or rainfall rates for the 3.0-ft sea-level scenario. The results show that there were only small increases in the upstream stage values at the primary structures for the steady-state and transient models. The wet season flow rates for the primary structures increased by 16.0 percent for the steady-state model and by 13.2 percent for the transient model. Simulated steady-state average wet season groundwater levels indicate increases in groundwater levels of up to 0.45 ft. The increases mostly occurred in areas where simulated historical groundwater levels and surface-water stages are below the control elevations for the drainage area. The remaining areas with increased simulated groundwater levels tended to be in coastal areas or areas having a lower density of surface-water features.

References Cited

Decker, J.D., 2022, MODFLOW-NWT datasets for the simulation of drainage infrastructure and groundwater system response to changes in sea-level and precipitation, Broward County, Florida: U.S. Geological Survey data release, https://doi.org/10.5066/P9ITQBFZ.

Intergovernmental Panel on Climate Change [IPCC], 2014, Climate change 2014 *in* Pachauri, R.K., and Meyer, L.A., eds., Fifth assessment report of the Intergovernmental Panel on Climate Change: Geneva, Switzerland, Intergovernmental Panel on Climate Change, Synthesis Report, Contribution of Working Groups I, II and III, 151 p.

South Florida Water Management District [SFWMD], 2016, Structure books: West Palm Beach, Fla., South Florida Water Management District, 597 p., accessed May 19, 2016, at ftp://ftp.sfwmd.gov/pub/hehmke/AsBuilts/Other%20Reports/OCC%20Structure%20Book.pdf.

Southeast Florida Regional Climate Change Compact Sea Level Rise Work Group, 2020, Unified sea level rise projection southeast Florida: Southeast Florida Regional Climate Change Compact Climate Leadership Committee, 36 p., accessed November 3, 2021, at https://southeastfloridaclimatecompact.org/unified-sea-level-rise-projections/.

Sweet, W.V., Kopp, R.E., Weaver, C.P., Obeysekera, J., Horton, R.M., Thieler, E.R., and Zervas, C., 2017, Global and regional sea level rise scenarios for the United States: Silver Spring, Md., National Oceanic and Atmospheric Administration technical report NOS CO–OPS 083, 75 p.

Chapter D. Summary of Historical and Increased Sea-Level Scenario Simulation Results and Model Limitations

By Jeremy D. Decker

Summary

A groundwater/surface-water model was developed for the urbanized areas of Broward County, Florida, to simulate the possible effects of changes in sea level and climate. Transient model inputs were developed to simulate the 2013–17 historical period, and steady-state model inputs were developed to simulate the average wet season conditions for the same 2013–17 period. Four future mean sea-level scenarios were developed referencing current, specified primary structure operations. These four sea-level scenarios were assigned a range of expected arrival times using the sea-level rise projections for southeast Florida (Southeast Florida Regional Climate Change Compact Sea Level Rise Work Group, 2020). Additional scenarios were developed to simulate the effects of additional rainfall on groundwater levels and primary structure stage and flow.

Model Description

The primary data source used to develop the groundwater/surface-water model was the existing inundation and saltwater intrusion model of the same area (Decker and others, 2019). The calibrated groundwater parameters and layering from the saltwater intrusion model were interpolated to obtain the groundwater layering and hydraulic parameters for the current model. The extensive canal system was dynamically simulated as a series of level pools representing drainage areas, basins, and subbasins interconnected through surface-water structures. The steady-state model used the Modular Finite-Difference Groundwater Flow Model (MODFLOW) recharge and evapotranspiration packages. The transient model used the MODFLOW Urban Runoff (URO) process to simulate rainfall, evapotranspiration, infiltration, and recharge. A select set of model parameters were estimated to improve the model fit to historical average wet season conditions.

Simulations were run using measured rainfall, potential evapotranspiration, water conservation area (WCA) groundwater levels, and tidal stages from 2013–17 to establish the model's capability to reproduce the historical behavior of the hydrologic system. Model-fit statistics were calculated, and time-series data were analyzed for 23 groundwater monitoring locations and 9 primary canal structures. Four future sea-level scenarios were simulated with mean sea levels of 0.5, 2.0, 2.5, and 3.0 feet (ft) above the North American Vertical Datum of 1988 (NAVD 88), corresponding to 1.05, 2.55, 3.05, and 3.55 ft of sea-level rise relative to the 2013–17 historical period. Scenarios were run with a 15-percent increase in recharge and a mean sea level of 3.0 ft above NAVD 88 using the steady-state and transient models to assess the effects on groundwater levels and primary structure flows.

Estimation of Selected Model Parameters

A limited set of model parameters was estimated to improve model fit to steady-state historical average wet season conditions using the automated Parameter ESTimation software (PEST) (Doherty, 2010). The parameters adjusted include canal leakance, general-head boundary conductances, and evapotranspiration extinction depths. The observations used to quantify model fit were flows through nine primary structures: G-56, G-57, S-37B, S-36, S-33, G-54, S-9, S-13, and S-29 (fig. B1).

Twelve canal leakance values were assigned on the basis of drainage area and drainage through the primary structures and adjusted by PEST software to improve model fit. The resulting values of canal leakance ranged from 0.50 to 9.983 day^{-1} with a mean of 2.60 day^{-1}. Leakage between the Surface-Water Routing (SWR1) process reach and underlying groundwater cell is calculated by multiplying this leakance value by the reach length, reach width, and the difference between the reach stage and corresponding groundwater level. General head-boundary conductance values were calculated using existing model input data for the four WCAs and were scaled independently to improve model fit. The resulting boundary conductance scaling factors ranged from 0.583 to 3.169. Additionally, existing spatially variable extinction depth values were scaled independently for 18 rain zones. The resulting scale factors ranged from 0.28 to 1.902.

The mean difference between simulated and measured flow through the nine primary structures included as observations was −5.5 cubic feet per second with a total difference in flows of −49.5 cubic feet per second (−2.6 percent). The largest differences occurred at the S-29 structure, which is adjacent to the southern boundary. Parts of the associated drainage area for this structure are not actively simulated and the missing flows were estimated, which partially explains the differences between simulated and measured flows. Additional information describing the completed parameter estimation is included in chapter E.

Simulated Results

When analyzing simulated results, comparative modeling is often more meaningful than focusing on the quantitative results of a single model. The uncertainties in predicted changes caused by uncertainties in model construction are reduced when comparisons are made between model

simulations. When analyzing and comparing the results of hypothetical future conditions and historical simulations, it is also more beneficial to focus on the qualitative effects rather than exact quantitative results. When using a physically based simulation tool, it is easier to capture the generalized behavior of the system than the exact magnitude of changes. The direction and range in magnitude of results are useful for understanding the response of the hydrologic system to changes in stresses and determining the primary causes for the response. From the results of the steady-state average wet season and transient models, the following observations were made:

- The steady-state model was able to produce similar responses to the changes in sea level as the transient model while having a reduced simulation run time. This version of the model offers a faster, although less detailed, analysis of hypothetical future scenarios.
- The effects of increased future sea level are far more evident in the easternmost, coastal areas of the county where increases in groundwater levels are nearly equivalent to sea-level rise. Areas west of the coastal water-control structures exhibit only small changes in average wet season groundwater levels. As sea levels further increase above coastal structures' control elevations, increases in groundwater levels can begin to propagate past coastal structures and into areas surrounding the corresponding primary canals because of increased simulated upstream stage values.
- The 0.5-ft sea-level scenario, corresponding to 1.05 ft of sea-level rise, resulted in mean increases in the easternmost groundwater measurement locations of 0.790 ft in the steady-state average wet season model and 0.827 ft in the wet season average from the transient model.
- The 2.0-ft sea-level scenario, corresponding to 2.55 ft of sea-level rise, resulted in mean increases in the easternmost groundwater measurement locations of 1.911 ft in the steady-state average wet season model and 2.010 ft in the wet season average from the transient model.
- The 2.5-ft sea-level scenario, corresponding to 3.05 ft of sea-level rise, resulted in mean increases in the easternmost groundwater measurement locations of 2.291 ft in the steady-state average wet season model and 2.403 ft in the wet season average from the transient model.
- The 3.0-ft sea-level scenario, corresponding to 3.55 ft of sea-level rise, resulted in mean increases in the easternmost groundwater measurement locations of 2.665 ft in the steady-state average wet season model and 2.791 ft in the wet season average from the transient model.
- The westernmost groundwater measurement locations exhibited little change in groundwater level caused by increases in sea level. The 3.0-ft sea-level rise scenario, corresponding to 3.55 ft of sea-level rise, resulted in mean increases of 0.084 and 0.151 ft in the steady-state average wet season model and the wet season average from the transient model, respectively.
- The historical groundwater transects show a general west-to-east downward gradient with higher groundwater levels in the northern part of the county. Increased sea-level scenarios resulted in very small changes to groundwater transects west of the coastal water-control structures. Increasing differences from the historical simulation are shown in areas east of the coastal water-control structures with increased sea level. Higher sea-level scenarios result in central parts of the county exhibiting groundwater levels relatively lower than areas to the east and west.
- Results from the steady-state model indicate that the simulated wet season average upstream stage for most of the primary structures increased because of the increased tide and tail water levels associated with the future sea-level scenarios. The structures having the lowest control elevations, S-13 and S-29, were affected by the 0.5- and 2.0-ft sea-level scenarios. The 3.0-ft sea-level scenario resulted in increased upstream stage for all the primary coastal structures except for those with the highest control elevations, G-56 and G-57.
- Results from the transient model indicate an increased effect on the wet season average upstream stage values for the primary structures caused by increased sea level when compared to the steady-state model. The 2.0-ft sea-level scenarios result in increases in upstream stages for the S-37A, S-36, S-33, G-54, S-13, and S-29 structures. The 3.0-ft sea-level scenario resulted in increased upstream stage at all primary coastal structures.
- The simulated flow through the primary structures increased because of increased sea level. The steady-state average wet season model exhibited increases in total flow out of the primary structures of 3.0, 6.2, 6.9, and 7.2 percent compared to the historical simulation for the 0.5-, 2.0-, 2.5-, and 3.0-ft sea-level scenarios, respectively. The transient model's wet season average total flow out of the primary structures increased by 3.1, 6.4, 7.1, and 7.5 percent compared to the historical simulation for the 0.5-, 2.0-, 2.5-, and 3.0-ft sea-level scenarios, respectively.
- Transient model results from the 3.0-ft sea-level scenario show an increase of 37.43 square miles in areas having a wet season average depth to groundwater of less than 2 ft and an increase of 22.97 square miles in newly inundated areas compared to historical simulation results.

- A 15-percent increase either in recharge or in the time series for rainfall rate produced small increases in upstream stage values at the primary structures and 16.0- and 13.2-percent increases in wet season flow rates for the primary structures for the steady-state and transient model, respectively. Simulated steady-state average wet season groundwater levels indicate increases in groundwater levels of up to 0.45 ft in some areas where historical simulation results show groundwater levels and surface-water stages below the control elevations for the drainage area. Other areas having increased groundwater levels tended to be in coastal areas or areas having a low density of surface-water drainage features.

Model Limitations

The general limitations of numerical models include the following:

- A hydrologic model's ability to reproduce historical conditions and behaviors does not guarantee its capability to predict future conditions.
- Models are limited by their spatial and temporal scales. Processes occurring on shorter temporal and spatial scales may not be simulated accurately by the model. The current analysis does not consider inundation from short-term events such as high intensity rainfall, storm surge, or king tides and instead focuses on longer term impacts of an increase in sea level.
- The conceptualized flow model of the hydrologic system necessarily uses simplifications of the natural processes and represents an approximation of the natural system.
- Steady-state simulations do not account for changes in storage which would occur during seasonal transitions.
- Data availability and reliability affect the calibration of model parameters and comparison to historical conditions.

Additional, more specific limitations of the model are listed in the following sections and should be considered when analyzing the results.

Groundwater-Model Properties

- The groundwater properties for the model were derived from the southern and central Broward County saltwater intrusion model, which was calibrated with a primary focus on matching historical salinity concentrations (Hughes and others, 2016). Uncertainties and errors contained within these datasets are propagated into the current model. A limited number of parameters were adjusted to improve model fit, but most inputs were used directly from existing models.

Western Groundwater Head Boundaries

- The general-head boundaries composing the western boundaries of the model represent connections to the WCAs. The groundwater level input for each WCA uses data from a single representative monitoring location. Actual groundwater levels along the perimeter of the WCAs most likely deviate along the boundary.
- Groundwater flow conductance at boundaries simulated along each WCA were initially calculated as an averaged value for each layer using the groundwater properties of the saltwater intrusion model and an estimated connection distance. These estimated values were scaled using the PEST software to obtain a better fit to steady-state wet season average conditions; however, actual conductance likely varies along the entire boundary.
- Future groundwater levels along the western boundaries are uncertain but will likely differ from historical levels. For this study, historical general-head boundary input values were used for future scenarios. Higher groundwater levels in the WCA would likely result in increased groundwater levels along the western boundary of the urban areas, increased leakage into the surface-water system, and increased flow through the primary structures. These effects, in turn, could result in increased canal stages in areas managed by gravity-controlled structures and having reduced future drainage capacity.

Tidal Boundaries and Tail Waters

- The specified-head boundary representing the Atlantic Ocean was created using data from the National Oceanic and Atmospheric Administration's Virginia Key tidal station, which is outside of the model's geographic domain. No attempt was made to correct for the tidal stage or timing differences caused by the change in geographic location. Simulated groundwater levels and coastal structure operations would likely be affected by changes to any tidal inputs.
- The surface-water stages representing the Intracoastal Waterway within the SWR1 process are approximated by using the same tidal data series as the coastal boundary. The measured coastal tidal data likely differ in mean stage, tidal range, and the timing of high and low tides from the actual stage within the Intracoastal Waterway, resulting in possible changes to simulated groundwater levels.

- For each structure, daily tail water measurements were used to calculate the representative difference between tail water stage and tidal stage for a given month. The hourly tail water stage specified in SWR1 associated with each structure was calculated by adding that structure's calculated tail water difference for the current month to the hourly measured tidal value. Actual, hourly tail water stage likely differs from the calculated values. Changes to the downstream stage values at a structure would affect the simulated flow rate and upstream stage, resulting in changes to the surrounding groundwater levels.
- The representation of sea-level rise involved adding the projected rise for each sea-level scenario to the historical time series without considering shifts in daily time series or any imbedded natural cycles. The same method was used to estimate future changes in tail water stages for the primary coastal structures, where the rise in sea level was added to the estimated historical tail water.

Drainage Network

- Active canal segments are represented as a series of connected level pools rather than sloped water surfaces. With the typically low surface-water gradients observed west of the coastal control structures, this assumption is not likely to affect model accuracy substantially.
- The surface-water system was created with the intent to capture the system's behavior and may deviate from actual systems and operations. Examples include the representation of pumps as stage-discharge curves, movable gates as fixed underflow gates or fixed weirs, and culverts as fixed weirs. Additionally, the parameters of these simulated structures were specified using operational rules, control elevations, and pumping capacities. Actual structure operations are often ad hoc and deviate from the stated operational specifications. The resulting simulated structure flows and stages do differ from measured values.
- The canal network was created using measured or estimated canal top widths and rectangular cross sections that likely result in canal cross-sectional areas that differ from those they represent. Differences in top width and shape would result in stage-volume curves for a given level pool that deviate from actual curves, resulting in different stages for a given volume flux.
- Frictional values for the Manning's flow connected level pools were specified using a standard value and may deviate from actual characteristics. An overestimated frictional resistance value would reduce flow and increase stage differences between level pool groups. An underestimated frictional resistance value would increase flow and decrease stage differences between level pool groups. Additionally, frictional resistance may be temporally variable and change as more or less debris or vegetation is present within a canal.

Rainfall and Evapotranspiration

- Eighteen rainfall zones were used to apply measured rainfall from 18 measurement locations to the model. Calculated potential evapotranspiration data from the Geostationary Operational Environmental Satellite were applied to the model using these same zones. Evapotranspiration (ET), infiltration, and recharge are calculated by the URO process using simplified methodologies and estimated parameters. Calculated recharge accounts for 78 percent of the groundwater model inflows and calculated ET accounts for 31 percent of the model outflows for the transient historical model. Published values of estimated actual ET for the study area would indicate a greater percent of ET in the hydrologic budget. Precipitation and ET may also vary on a finer resolution and could cause differences in simulated output. Variations in the spatial distribution of rainfall data between measurement locations were not considered in the model.
- Future sea-level scenarios were simulated using historical potential ET. If future projections of potential ET were considered, the amount of ET calculated and removed by the URO process would also change. The future sea-level scenarios were simulated using historical rainfall values. Additional scenarios were simulated with a 15 percent increase in rainfall within the transient model and a 15 percent increase in recharge in the steady-state model. The change in recharge associated with a 15 percent increase in rainfall would likely not translate into a 15 percent increase in recharge. Changes in precipitation and resulting recharge would result in changes in surface-water flows and stages and groundwater levels.
- The primary objective for this study was to develop a model capable of simulating historical hydrologic conditions (that is, groundwater levels, surface-water stages, surface-water flows) that can then be used to simulate hypothetical future conditions using projected hydrologic forcings. During the calibration process, the ability of the model to match historical conditions was evaluated on the basis of the simulated groundwater levels and surface-water stages and flows. Scaling factors for previously calibrated ET extinction depths were used as parameters for 18 rainfall zones. The resulting effects of these parameters during model calibration were changes to the calculated net recharge to the

groundwater flow model. The calculated ET volumes during the simulation were not directly evaluated as part of the process, nor were published estimated values of actual ET used to constrain model results.

- The yearly averaged, simulated ET of 26.2 inches per year is lower than some estimates of actual ET within south Florida. Limited data exists to quantify and compare actual ET rates within urban areas. An increase in simulated ET would likely lead to reduced flows through the primary structures and to the boundaries representing tide/tidal areas. An increase in simulated ET could lead to lower groundwater levels east of the primary control structures but would likely not result in substantial decreases to the groundwater and surface-water levels west of these structures.

Future Sea-Level Scenario

- Future sea-level projections generally have a high uncertainty. These projections are attempts to capture the outcome of highly complex systems that have complicated interactions. The range of expected arrival times for mean sea-level stages represent the current best knowledge, but still retain a high level of uncertainty. Both more conservative and more extreme sea-level projections exist but typically have a lower chance of occurrence and were not considered during this analysis.

References Cited

Decker, J.D., Hughes, J.D., and Swain, E.D., 2019, Potential for increased inundation in flood-prone regions of southeast Florida in response to climate and sea-level changes in Broward County, Florida, 2060–69: U.S. Geological Survey Scientific Investigations Report 2018–5125, 106 p., accessed November 3, 2021, at https://doi.org/10.3133/sir20185125.

Doherty, J.E., 2010, PEST, model-independent parameter estimation—User manual (5th ed.): Brisbane, Australia, Watermark Numerical Computing, 336 p.

Hughes, J.D., Sifuentes, D.F., and White, J.T., 2016, Potential effects of alterations to the hydrologic system on the distribution of salinity in the Biscayne aquifer in Broward County, Florida: U.S. Geological Survey Scientific Investigations Report 2016–5022, 114 p., accessed November 3, 2021, at https://doi.org/10.3133/sir20165022.

Southeast Florida Regional Climate Change Compact Sea Level Rise Work Group, 2020, Unified sea level rise projection southeast Florida: Southeast Florida Regional Climate Change Compact Climate Leadership Committee, 36 p., accessed November 3, 2021, at https://southeastfloridaclimatecompact.org/unified-sea-level-rise-projections/.

Chapter E. Numerical Model Construction

By Jeremy D. Decker

This section describes the construction of the numerical groundwater/surface-water model used for this study. The model was constructed using a modified version of Modular Finite-Difference Groundwater Flow Model Newton formulation (MODFLOW-NWT) (Niswonger and others, 2011) that includes the Urban Runoff (URO) process (Decker and Hughes, 2013). The model uses the Basic, Layer-Property Flow, Well, General-Head Boundary (GHB), Evapotranspiration (EVT), Recharge, and Specified Head (CHD) Modular Finite-Difference Groundwater Flow Model (MODFLOW) packages (Harbaugh, 2005) and the Surface-Water Routing (SWR1) process (Hughes and others, 2012). The information provided in these model processes includes model extent and discretization, land-surface elevations, aquifer layering information, aquifer flow properties, groundwater boundaries, groundwater pumpage, representation of the surface-water system, surface-water system boundaries, rainfall and evapotranspiration (ET), and information on how selected model parameters were estimated using automated parameter estimation software. Model input files, executables, and outputs described here are included in the associated U.S. Geological Survey data release (Decker, 2022).

Extent and Discretization

The active flow model area is approximately 456 square miles (mi^2) in the eastern, urbanized part of Broward County and the northeastern most part of Miami-Dade County (fig. A1). The extent represents the approximate combined active flow model areas of the central, southern, and northern Broward County saltwater intrusion models (Langevin and Zygnerski, 2013; Hughes and others, 2016). The active flow model is generally bounded on the east by the Atlantic Ocean and on the west by the Everglades and Water Conservation Areas (WCAs) 2A, 2B, 3A, and 3B. The model is bounded to the north by the Hillsboro Canal and on the south by the C-9 Canal. The major canals along the north, south, and west boundaries are included in the surface-water model and the underlying, active groundwater model extends a few additional grid cells beyond them.

The model consists of 822 rows and 1,002 columns with a spatial discretization of 250 by 250 feet (ft). By comparison, the previous related studies used a spatial discretization of 500 by 500 ft for the countywide model and a spatial discretization of 166.7 by 166.7 ft for a higher resolution submodel (Hughes and others, 2016; Decker and others, 2019). Within the central and southern saltwater intrusion model, the surficial aquifer was discretized into 12 vertical layers with the 3 designations of upper (UPR), production (PRD), and lower (LWR) zones. These zone designations were used to create three vertical layers for this model, which combine layers 1–2, 3–10, and 11–12 of the saltwater intrusion model. This same methodology was used for the previous county-scale flow model (Decker and others, 2019). The simulated area has a total of 610,344 active groundwater cells that cover 1,368 mi^2.

The 5-year historical simulation period used for this study begins on January 1, 2013, and ends on December 31, 2017. The simulation uses a daily MODFLOW stress period and 25 time steps per stress period. Approximately 50 time steps per day are used by the SWR1 process and 100 time steps per day are used by URO processes. The short MODFLOW time steps reduce the number of outer MODFLOW iterations and overall run times, because the SWR1 and URO processes are implicitly coupled and rely on updated groundwater levels for leakage, infiltration, and recharge calculations. The increased sea-level simulations also use a 5-year simulation period and the same time step/stress period discretization used for the historical simulation. No specific years are assigned to the increased sea-level period, but a potential range of years is presented based on projections of future mean sea level.

Land Surface and Layer-Bottom Elevations

The top of layer 1 of the groundwater model corresponds to land surface. The average land-surface elevation was 7.03 ft above the North American Vertical Datum of 1988 (NAVD 88) within the active model area, with minimum and maximum elevations of −4.21 and 214.79 ft above NAVD 88 (fig. E1). The highest elevations are not from the natural landscape and occur in very small areas that are anthropogenic. The land-surface elevations were created from the 2007–08 Florida Division of Emergency Management light detection and ranging (lidar) data prepared by the South Florida Water Management District (SFWMD, 2007). The elevation of each 250- by 250-ft grid cell was calculated as the mean of the 10-ft resolution lidar values contained within that cell. The layer bottom elevations were calculated through the bilinear interpolation of the corresponding bottom elevations used within the model of the previous study (Decker and others, 2019). These elevations correspond to the bottom of the three surficial aquifer zones developed as part of the central and southern saltwater intrusion model (Hughes and others, 2016). The elevations of the bottom of layer 1 of the active model area ranged from −71.77 to −23.52 ft above NAVD 88 (fig. E2). The elevations of the bottom of layer 2 of the active model area ranged from −137.95 to −50.44 ft above NAVD 88 (fig. E3). The elevations of the bottom of layer 3 of the active model area ranged from −319.22 to −181.24 ft above NAVD 88 (fig. E4).

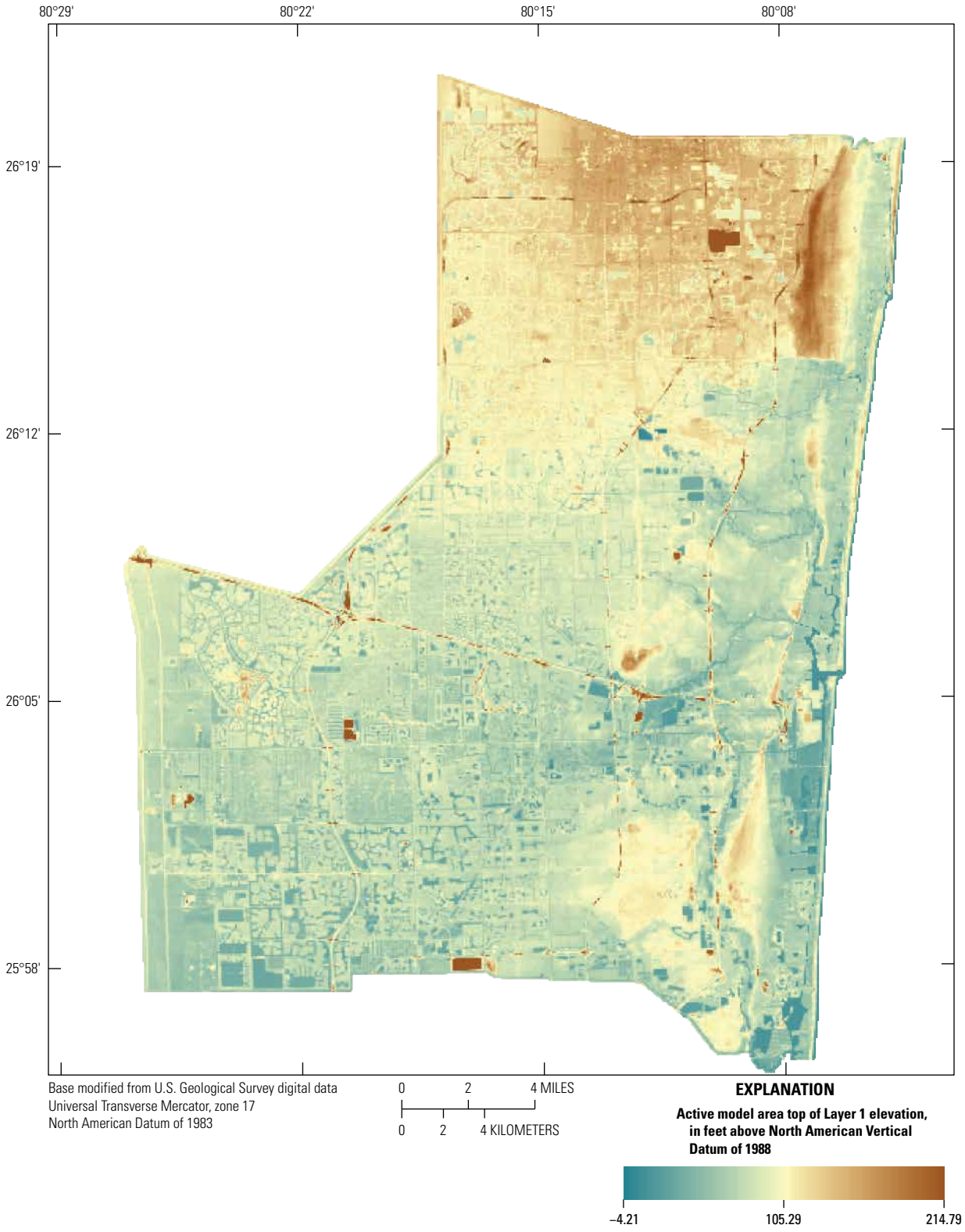

Figure E1. Top of layer 1 of groundwater model corresponding to land surface.

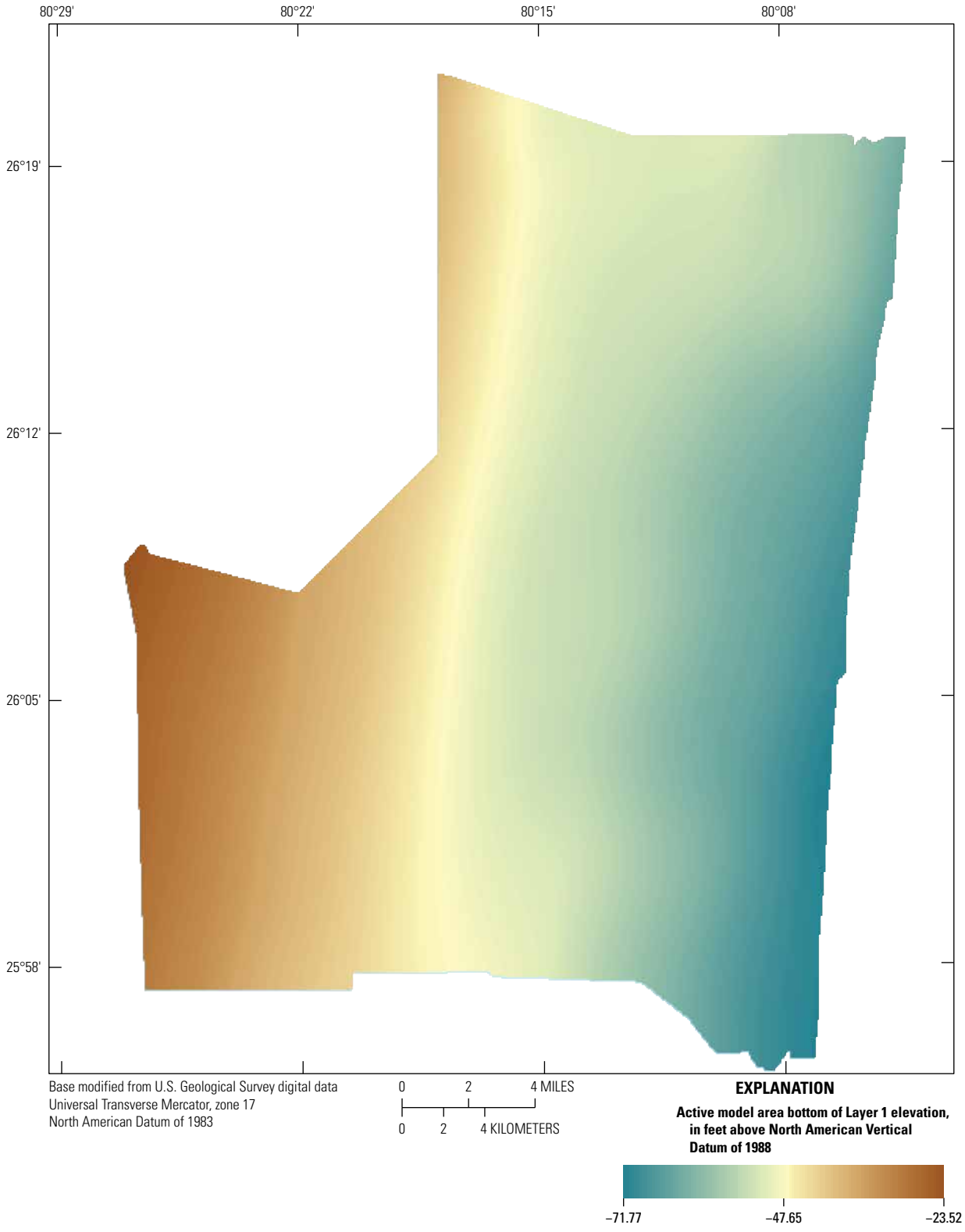

Figure E2. Bottom of layer 1 of groundwater model.

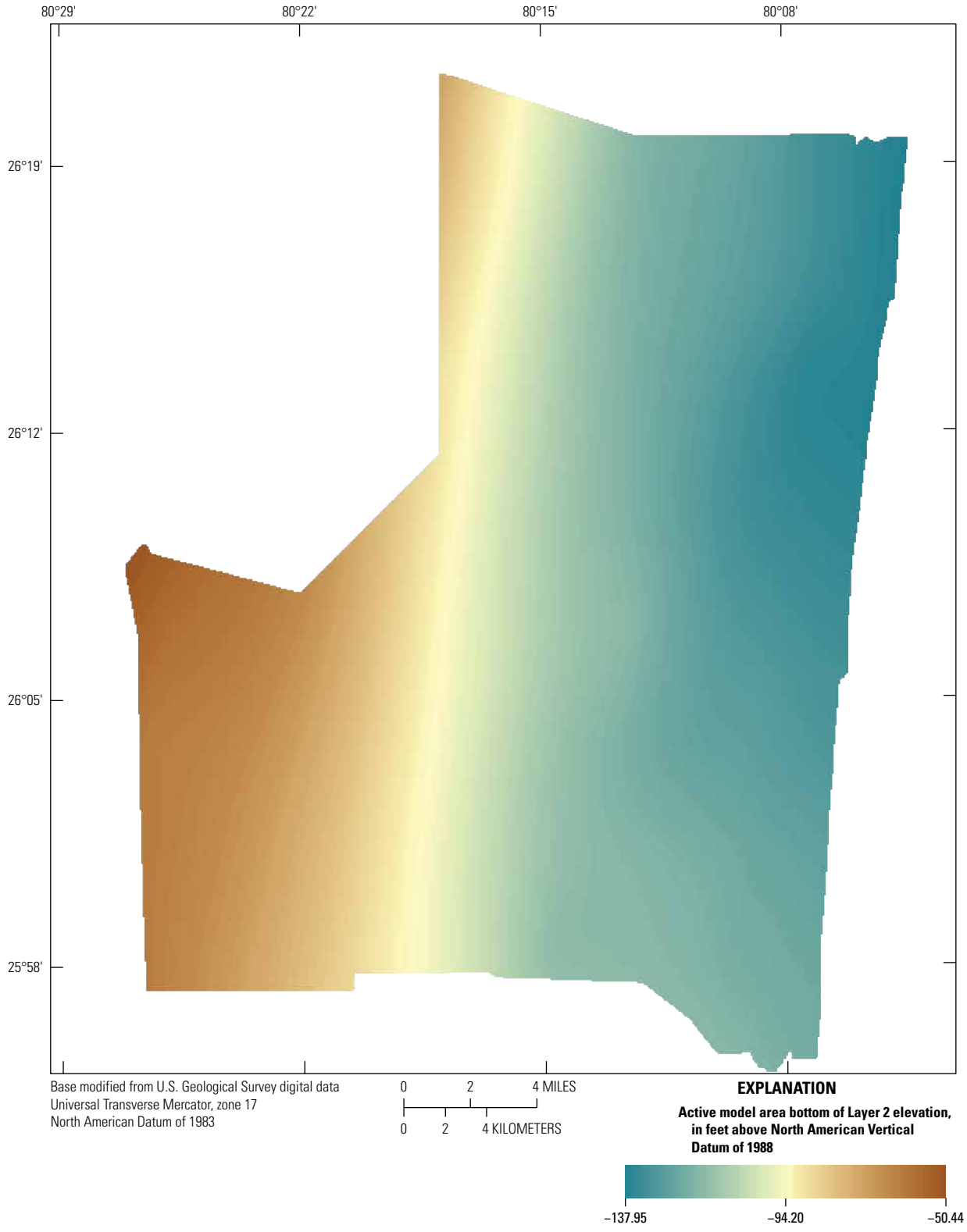

Figure E3. Bottom of layer 2 of groundwater model.

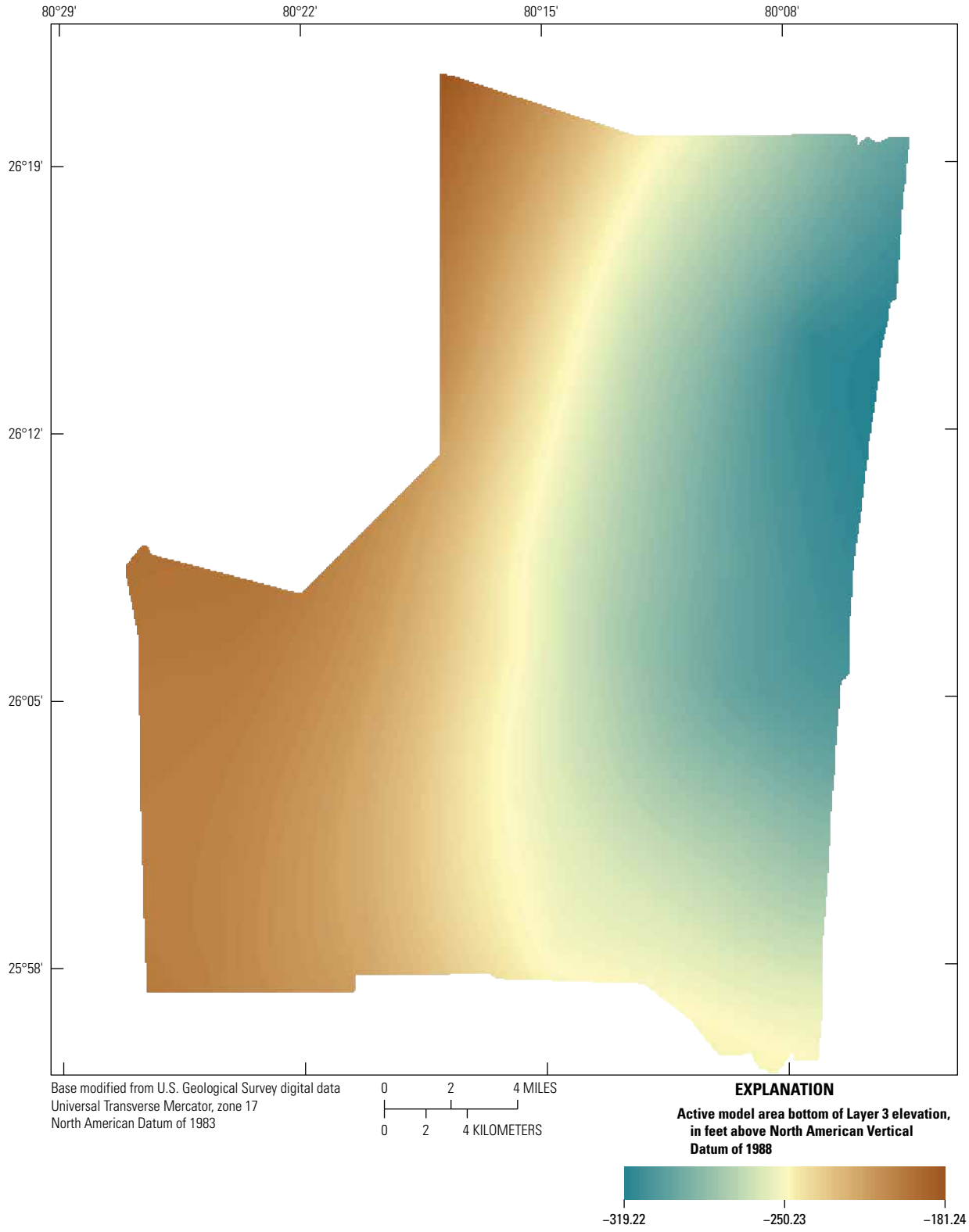

Figure E4. Bottom of layer 3 of groundwater model.

Hydraulic Parameters

The hydraulic parameters were calculated using the calibrated parameter values from the central and southern saltwater intrusion model (Hughes and others, 2016). The northern part of the county was not included as an active part of the central and southern saltwater intrusion model but was included in the dataset and constructed using calibrated hydraulic parameters from the northern saltwater intrusion model previously developed by Langevin and Zygnerski (2013). During calibration of the central and southern saltwater intrusion model, layers 1–2 were designated as the upper zone and were composed of the Q3, Q4, and Q5 marine units designated by Perkins (1977). Layers 3–10 were designated as the production zone and were composed of the Q1 and Q2 marine units. The bottom two layers, 11 and 12, were designated as the lower zone and represent an upper semiconfining unit and gray limestone aquifer (Hughes and others, 2016).

The properties for layers 1–2 (UPR zone), 3–10 (PRD zone), and 11–12 (LWR zone) of the saltwater intrusion models were averaged to produce the parameter fields for layers 1, 2, and 3, respectively. This methodology was used to calculate the hydraulic parameters used in the previous flow model developed for the area by Decker and others (2019). This resulted in 500- by 500-ft parameter fields that were bilinearly interpolated to produce the 250- by 250-ft final parameter fields used in the groundwater flow model.

Horizontal and Vertical Hydraulic Conductivity

The horizontal hydraulic conductivity (K_h) for each layer was calculated from the 12-layer saltwater intrusion model by using the layer-thickness weighted arithmetic mean. The K_h of layer 1 ranged from 236.5 to 32,000 feet per day (ft/d), with an average of 1,836.2 ft/d (fig. E5). The K_h of layer 2 ranged from 246.4 to 29,392.1 ft/d, with an average of 2,958.3 ft/d (fig. E6). The K_h of layer 3 ranged from 186.1 to 25,437.3 ft/d, with an average of 720.8 ft/d (fig. E7).

The vertical hydraulic conductivity (K_v) for each layer was calculated from the 12-layer saltwater intrusion model by using the layer-thickness weighted harmonic mean. The K_v of layer 1 ranged from 1.11 to 38.92 ft/d, with an average of 6.73 ft/d (fig. E8). The K_v of layer 2 ranged from 2.00 to 21.03 ft/d, with an average of 10.07 ft/d (fig. E9). The K_v of layer 3 ranged from 2.80 to 9.07 ft/d, with an average of 5.18 ft/d (fig. E10).

Specific Yield and Specific Storage

The specific yield of layer 1, which was specified as convertible, and the specific storage of layers 2 and 3 were all calculated using the calibrated parameters from the 12-layer saltwater intrusion model. The UPR, PRD, and LWR zone designations were used to calculate the layer-thickness weighted arithmetic means for 500- by 500-ft parameter fields that were bilinearly interpolated to obtain the final 250- by 250-ft parameter fields. The calculated specific yield (S_y) of layer 1 ranged from 0.03 to 0.40, with an average of 0.23 (fig. E11). The specific storage (S_s) of layer 1 was specified as a uniform value of 1.00×10^{-3} (1/foot [1/ft]). The calculated specific storage of layer 2 ranged from 8.18×10^{-6} to 1.21×10^{-5} 1/ft, with an average of 1.03×10^{-5} 1/ft (fig. E12). The calculated specific storage of layer 3 ranged from 8.85×10^{-6} to 1.18×10^{-5} 1/ft, with an average of 1.02×10^{-5} 1/ft (fig. E13).

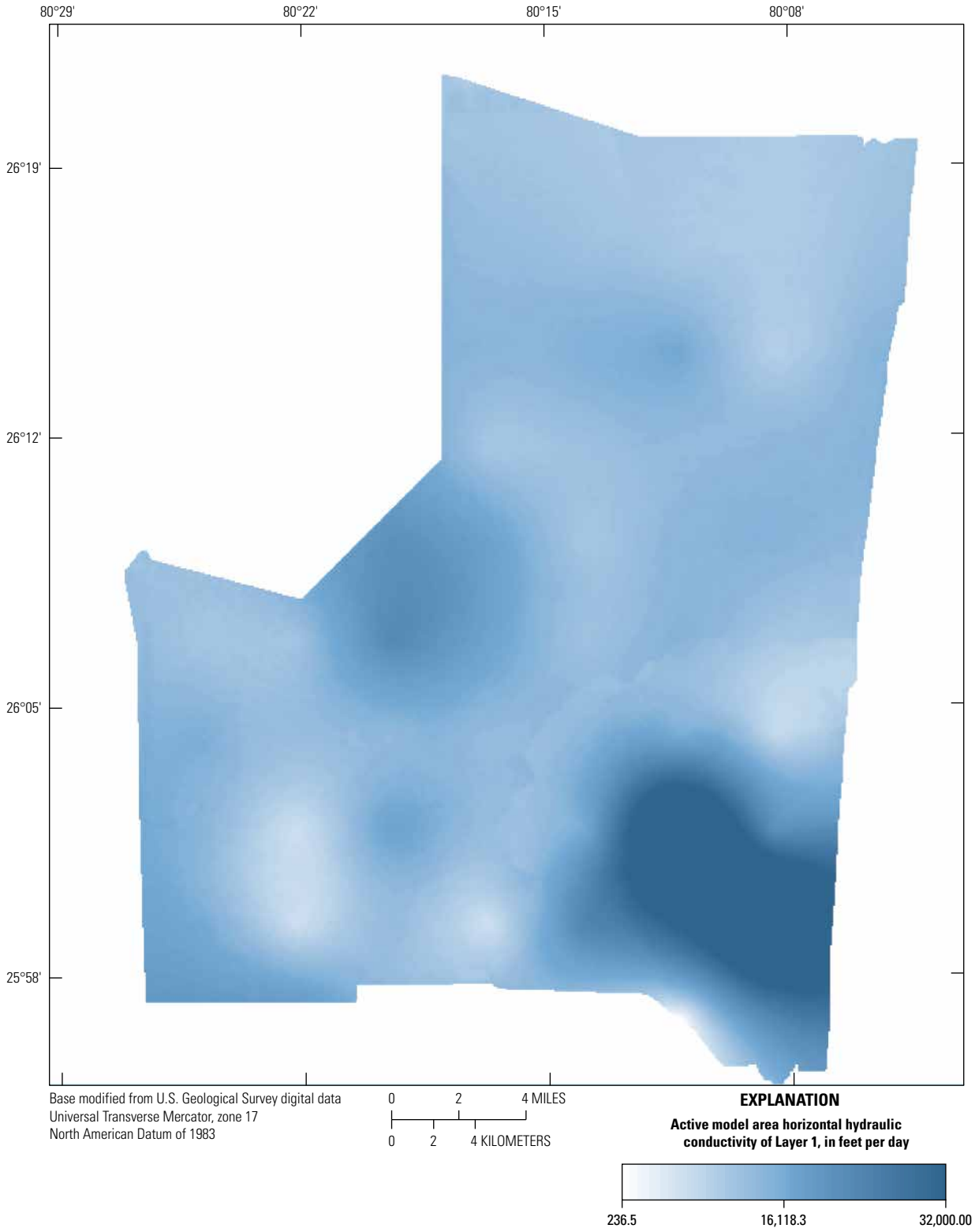

Figure E5. The calculated horizontal hydraulic conductivity (K_h) of layer 1.

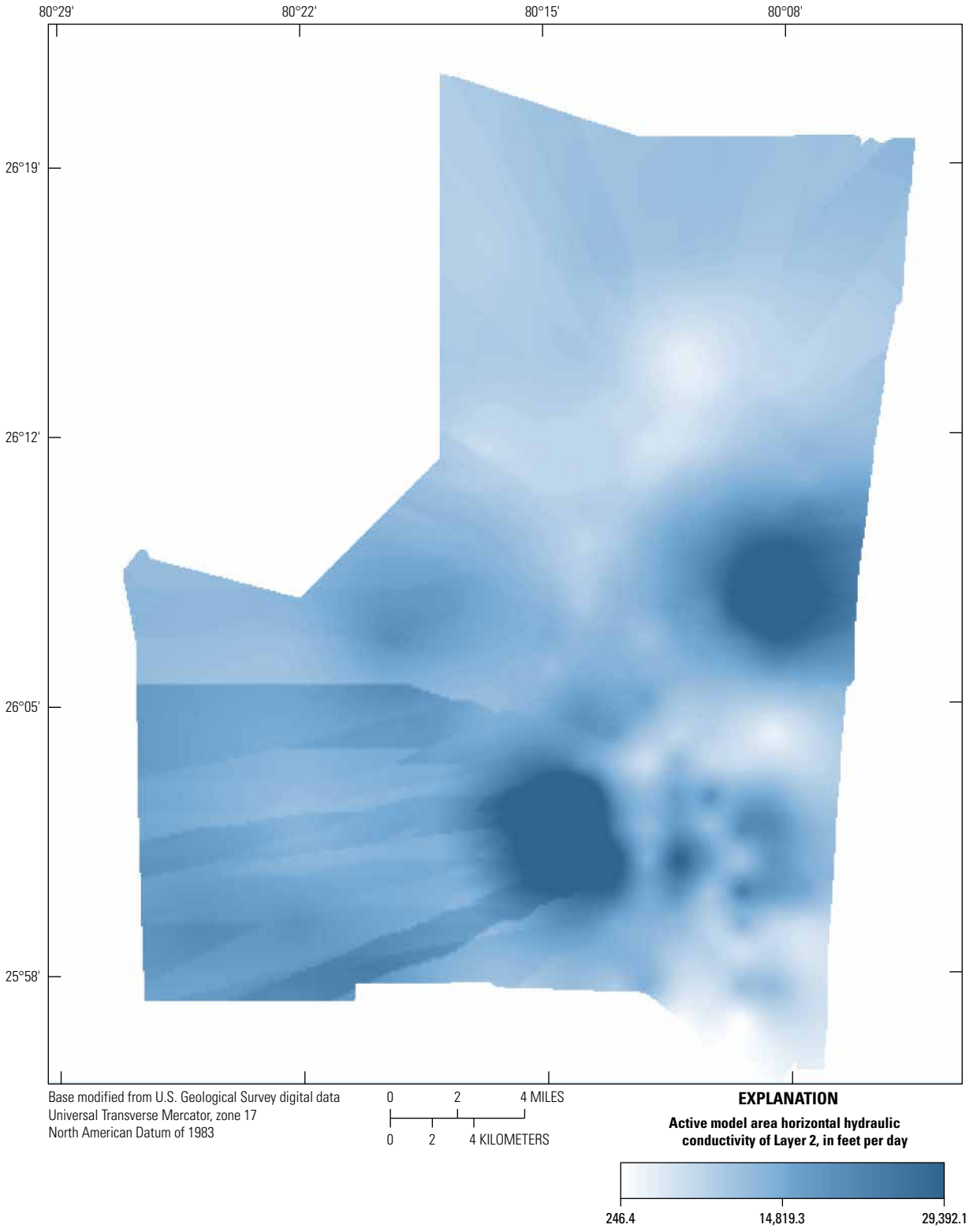

Figure E6. The calculated horizontal hydraulic conductivity (K_h) of layer 2.

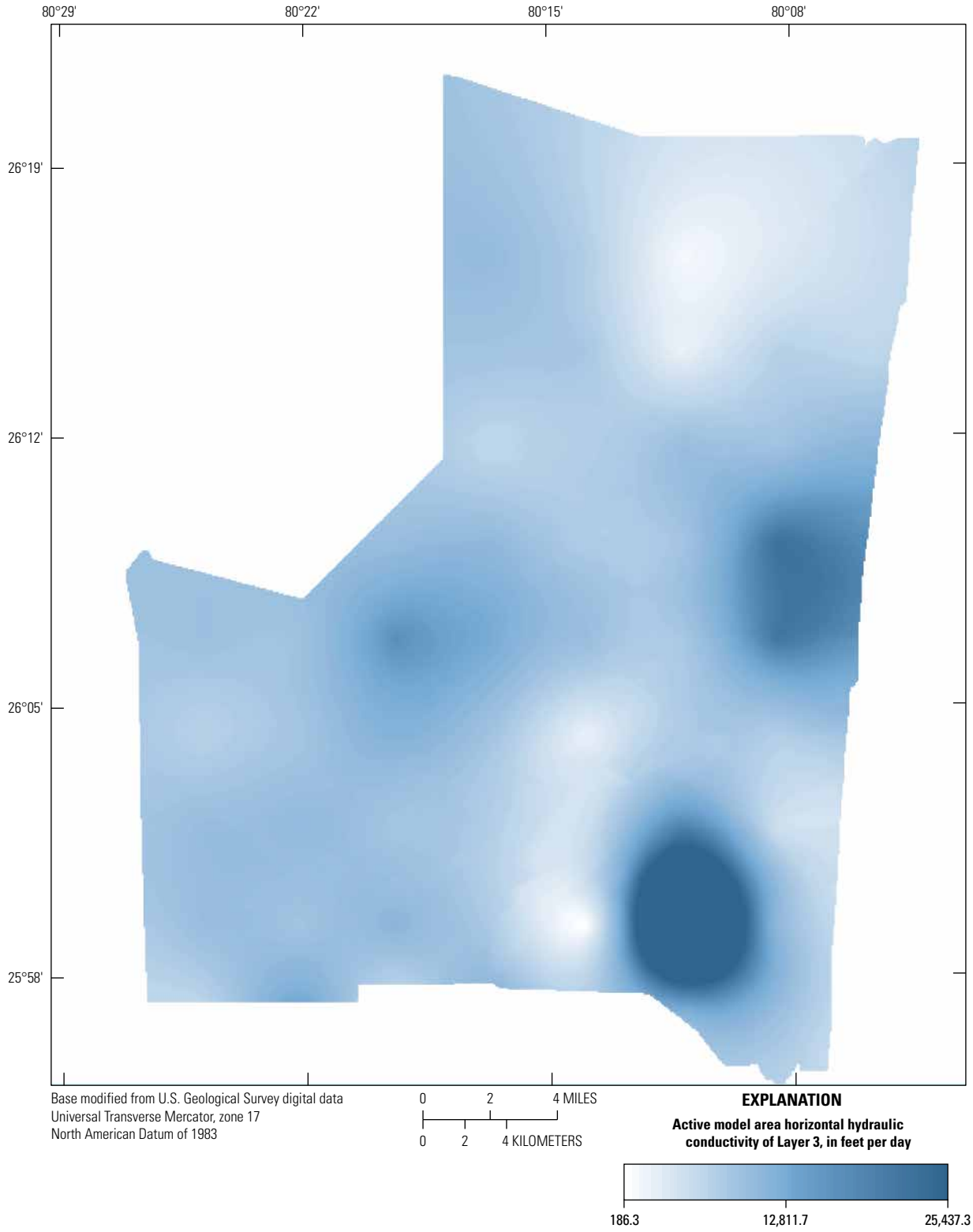

Figure E7. The calculated horizontal hydraulic conductivity (K_h) of layer 3.

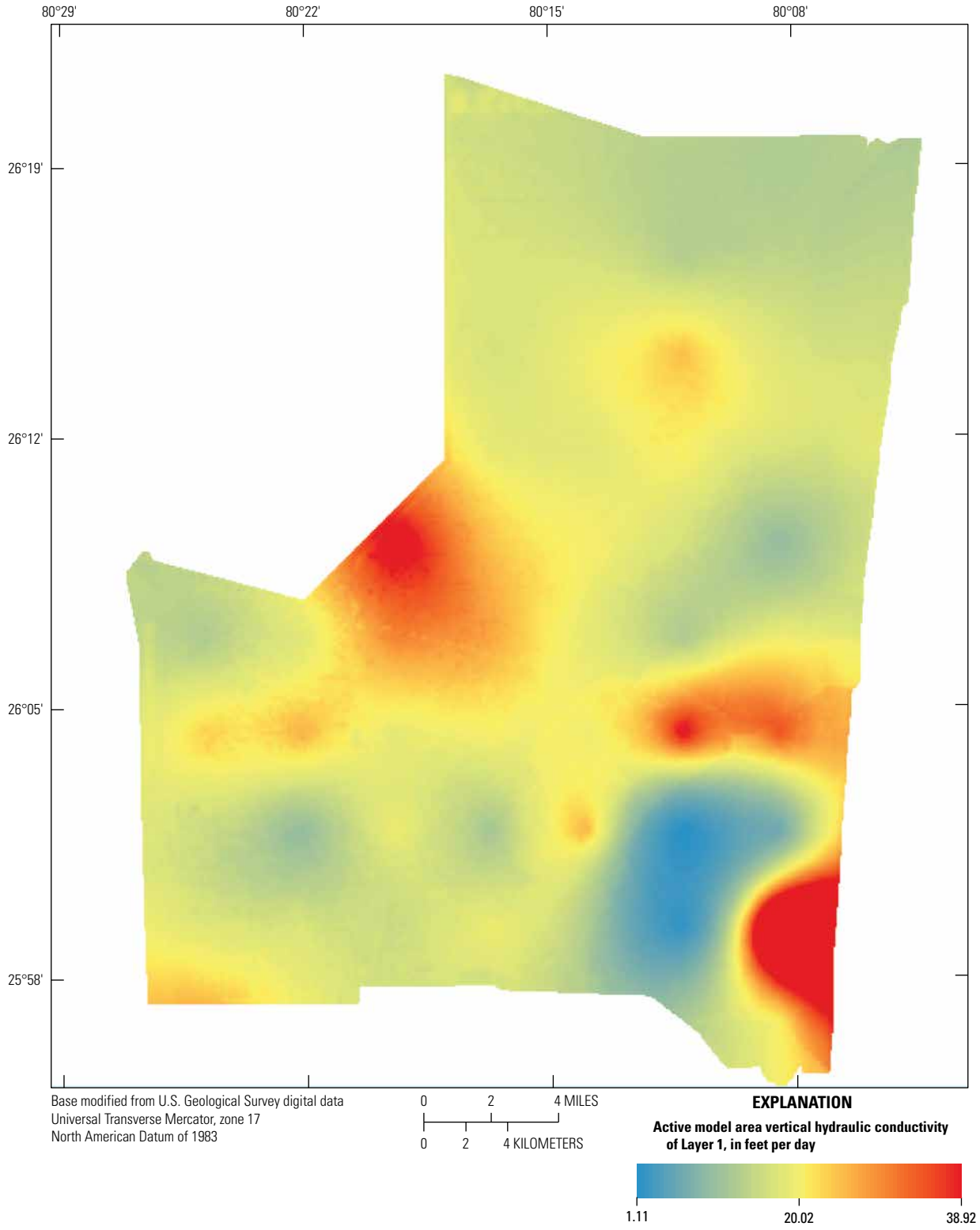

Figure E8. The calculated vertical hydraulic conductivity (K_v) of layer 1.

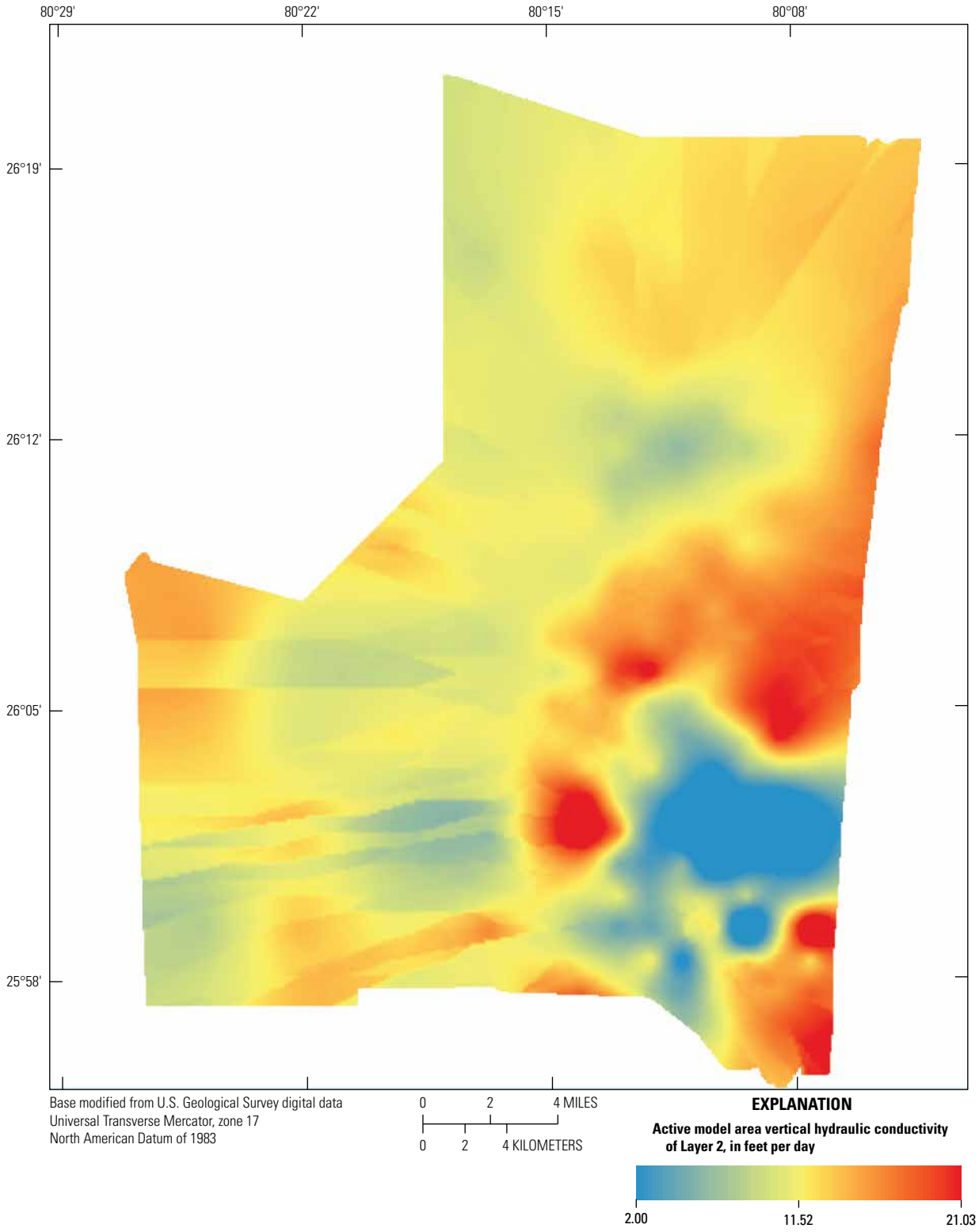

Figure E9. The calculated vertical hydraulic conductivity (K_v) of layer 2.

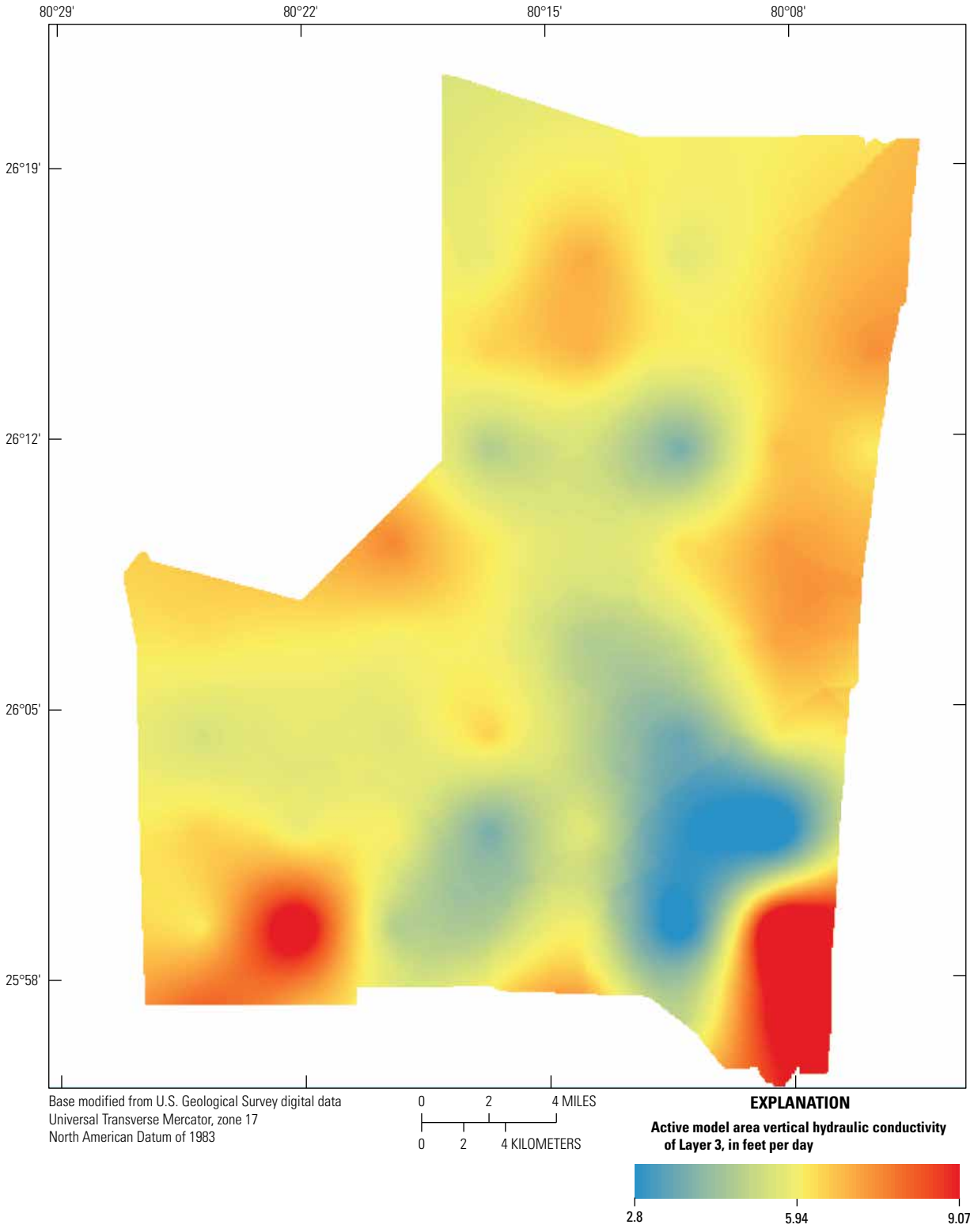

Figure E10. The calculated vertical hydraulic conductivity (K_v) of layer 3.

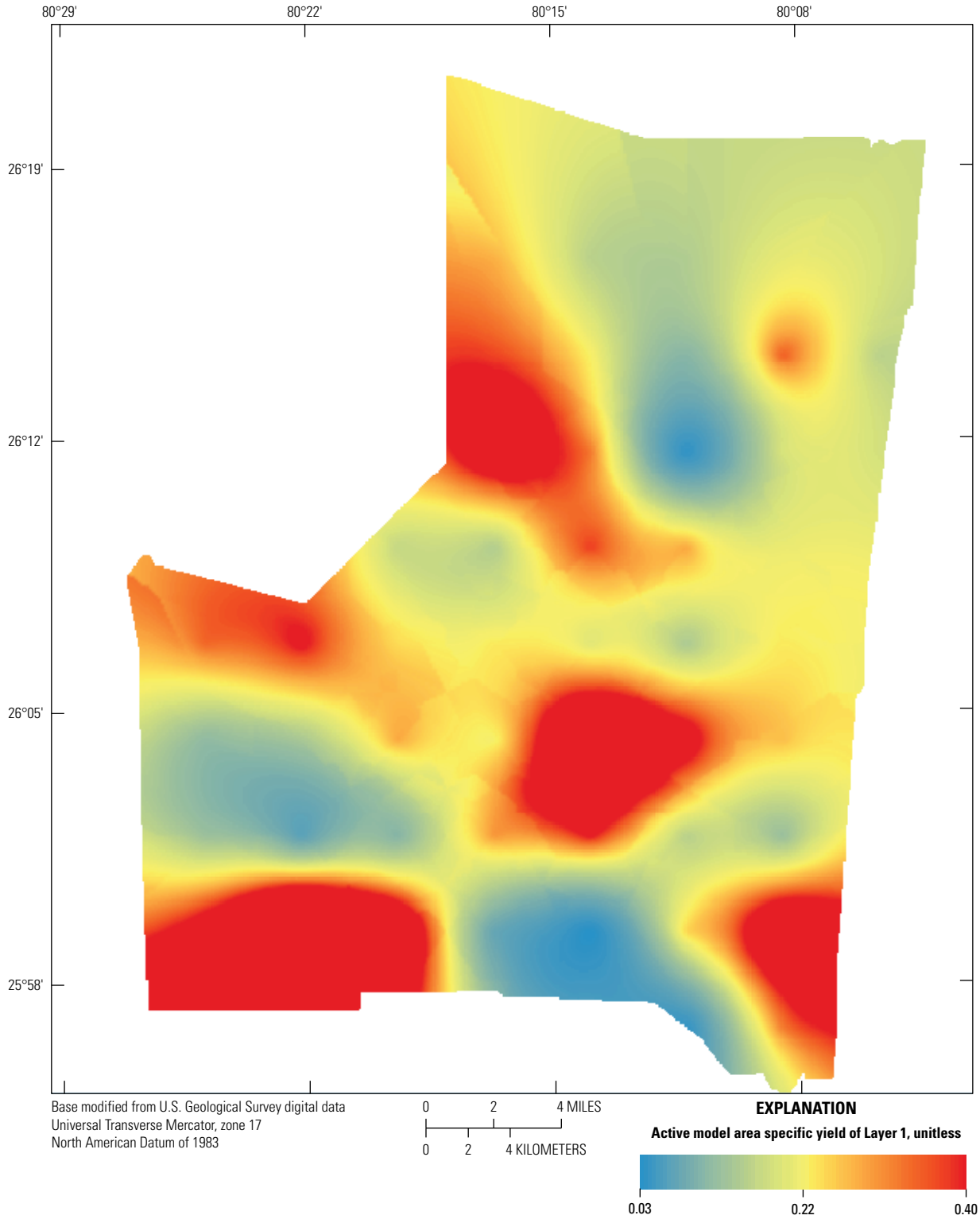

Figure E11. The calculated specific yield of layer 1.

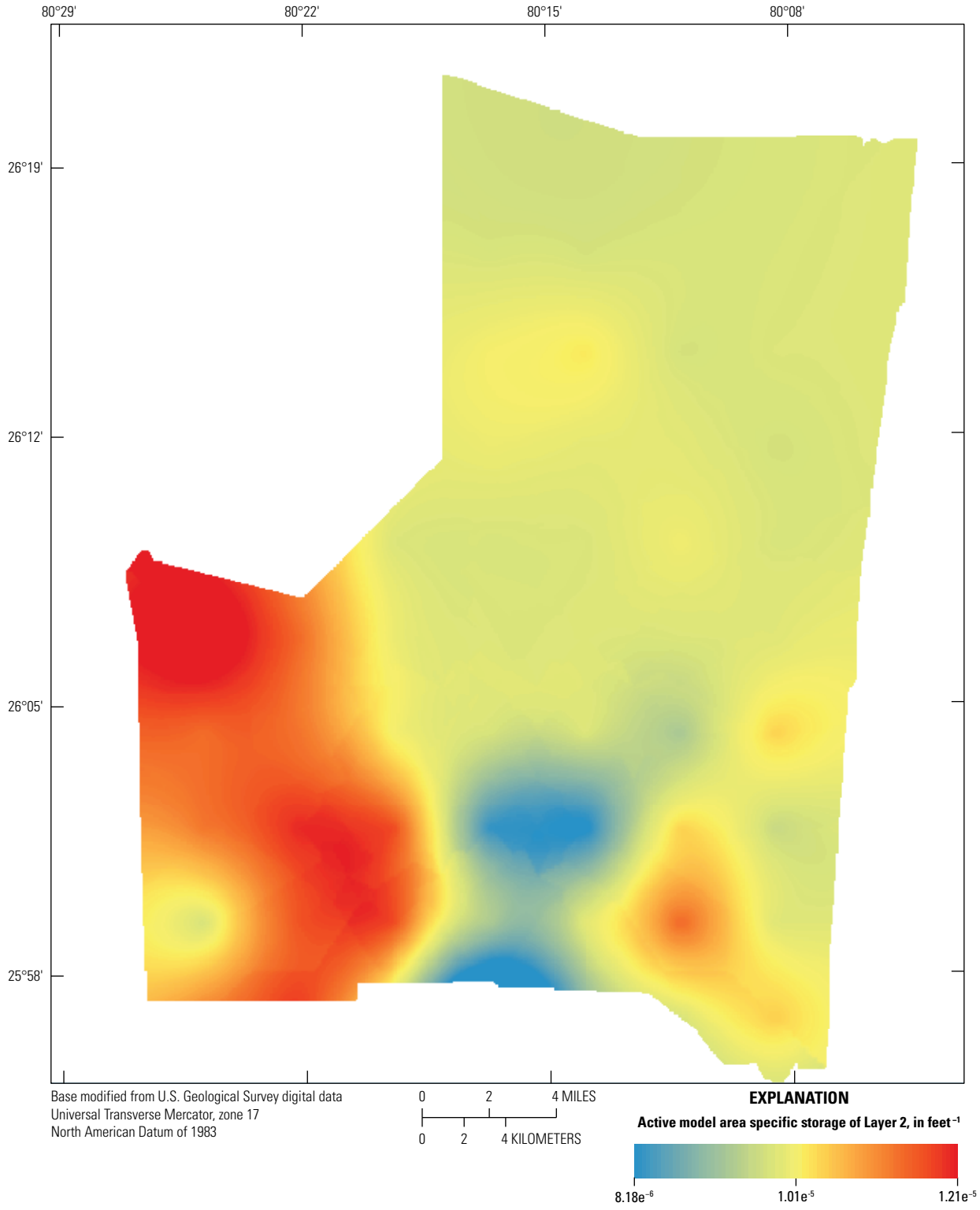

Figure E12. The calculated specific storage of layer 2.

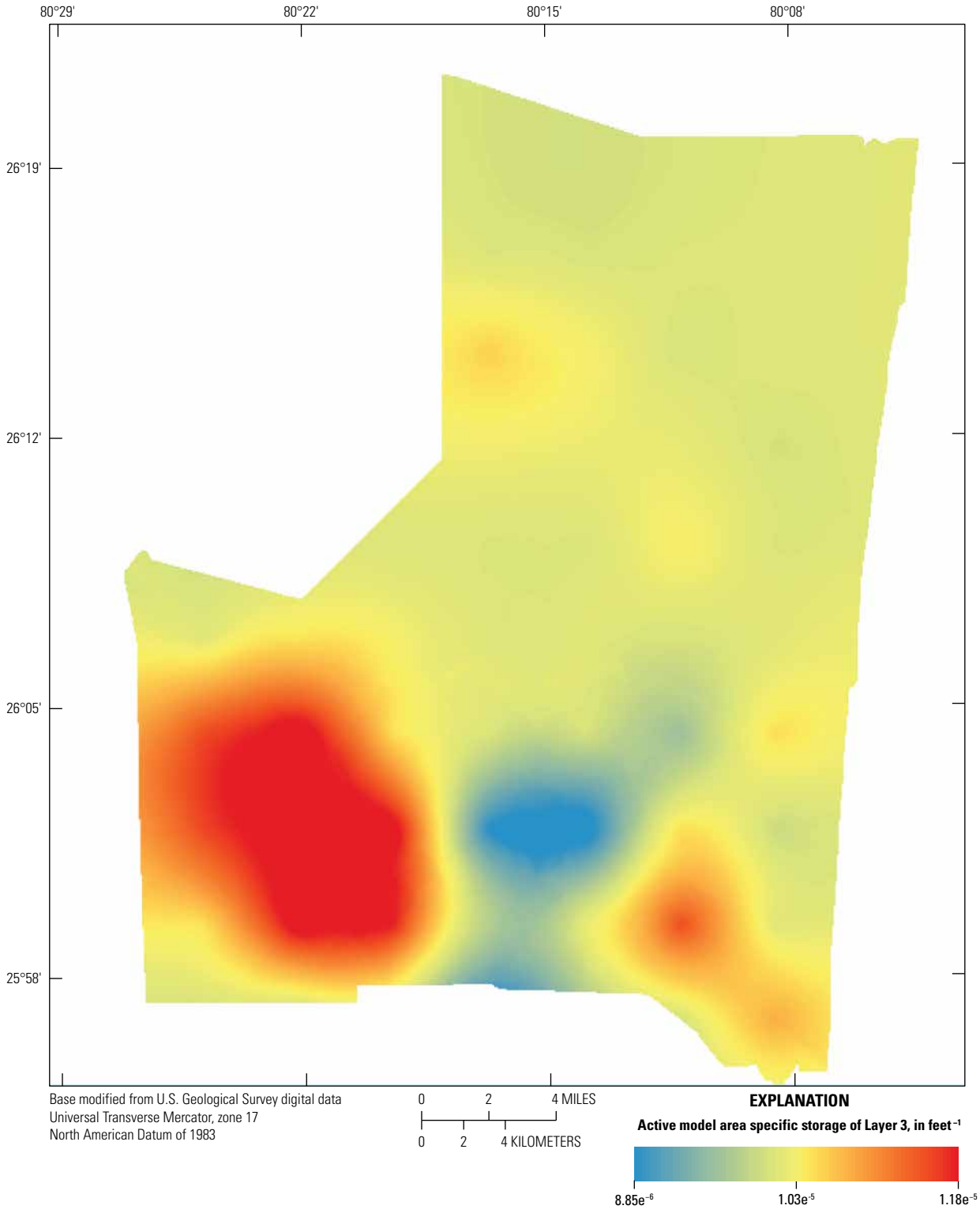

Figure E13. The calculated specific storage of layer 3.

Head-Dependent Boundaries at the Model Extents

MODFLOW GHBs are used to represent groundwater levels at the western extent of the model area. MODFLOW CHDs are used to specify the groundwater levels at the eastern extent. The active model is bounded to the west by the WCAs 2A, 2B, 3A, and 3B and bounded to the east by the Atlantic Ocean (fig. A1). Both WCA and eastern tidal boundary head values are updated daily at each MODFLOW stress period.

Western Boundaries at Water Conservation Areas

The western boundary head values were generated by using data from the Everglades Depth Estimation Network (EDEN) (Patino and others, 2017). A representative value for each WCA was used for all GHBs connected to cells along that boundary. EDEN Site_19 was used for WCA 2A, EDEN_13 was used for WCA 2B, EDEN_4 was used for WCA 3A, and EDEN Site_76 was used for WCA 3B (table E1). The average water levels during the historical period (2013–17) for these sites were 10.75, 8.63, 8.63, and 6.28 ft above NAVD 88 for Site_19, EDEN_13, EDEN_4, and Site_76, respectively (fig. E14). The GHB conductance values were calculated for each layer using

$$C = \frac{K_h A}{x}, \quad (1)$$

where

C is the conductance,
A is the perpendicular flow area, and
x is the distance from the head measurement to the grid cell.

The flow distance, x, was assumed to be 10 times the cell width, or 2,500 ft. The resulting conductance ranged from 2,460.7 to 12,095.9 square feet per day (ft²/d), with an average of 5,968.1 ft²/d. These values were then scaled as part of the steady-state model calibration. The resulting scale factor for each WCA boundary was 0.583, 0.675, 1.660, and 3.169 for WCA 2A, 2B, 3A, and 3B, respectively, making the calibrated conductance along these four sites range from 2,160.5 to 38,332.3 ft²/d (table E1).

Eastern Tidal Boundaries

The eastern tidal boundary head values were generated by using data from the National Oceanic and Atmospheric Administration tidal gage located on Virginia Key, Florida (table E2). MODFLOW CHDs were applied within layer 3 along the entire length of the coastline several grid cells east of the easternmost shoreline (fig. A1). The mean tidal level during the historical period was −0.55 ft above NAVD 88 (fig. E15). For future conditions, sea level was increased to obtain a mean value corresponding to that of several coastal structure control elevations. Uniform increments of 1.05, 2.55, 3.05, and 3.55 were added to the mean daily historical tidal level to obtain mean tidal levels of 0.5, 2.0, 2.5, and 3.0 ft above NAVD 88 (fig. E15).

Groundwater Pumpage

Groundwater pumpage within the model was represented by using the Well package. The locations and pumping rates were taken from SFWMD monthly well-field withdrawal data and permit information. Data for the historical time period included withdrawals from 408 wells located throughout the active model area (fig. E16). The average daily pumping rate for the historical period was 215.9 million gallons per day (fig. A3).

Table E1. Locations, designations, and average historical period water levels (2013–17) for the Everglades Depth Estimation Network (EDEN) stations used to generate Modular Finite-Difference Groundwater Flow Model (MODFLOW) general head boundary (GHB) input datasets.

[ft, foot; NAVD 88, North American Vertical Datum of 1988; ft²/d, square foot per day]

Water conservation area	EDEN designation	Station location, Florida State Plane (ft)		Average water level (ft above NAVD 88)		GHB conductance (ft²/d)			
		Easting	Northing	Annual	Wet season	Scaling factor	Layer 1	Layer 2	Layer 3
2A	Site_19	883361.0	708605.3	10.75	10.87	0.583	2,160.5	2,182.2	4,131.6
2B	EDEN_13	862329.1	670301.1	8.63	8.09	0.675	2,784.4	3,668.8	5,160.1
3A	EDEN_4	817985.6	639920.8	8.63	8.36	1.660	4,084.9	12,504.1	13,052.1
3B	Site_76	826112.2	608887.0	6.28	6.25	3.169	12,033.4	38,332.3	22,910.2

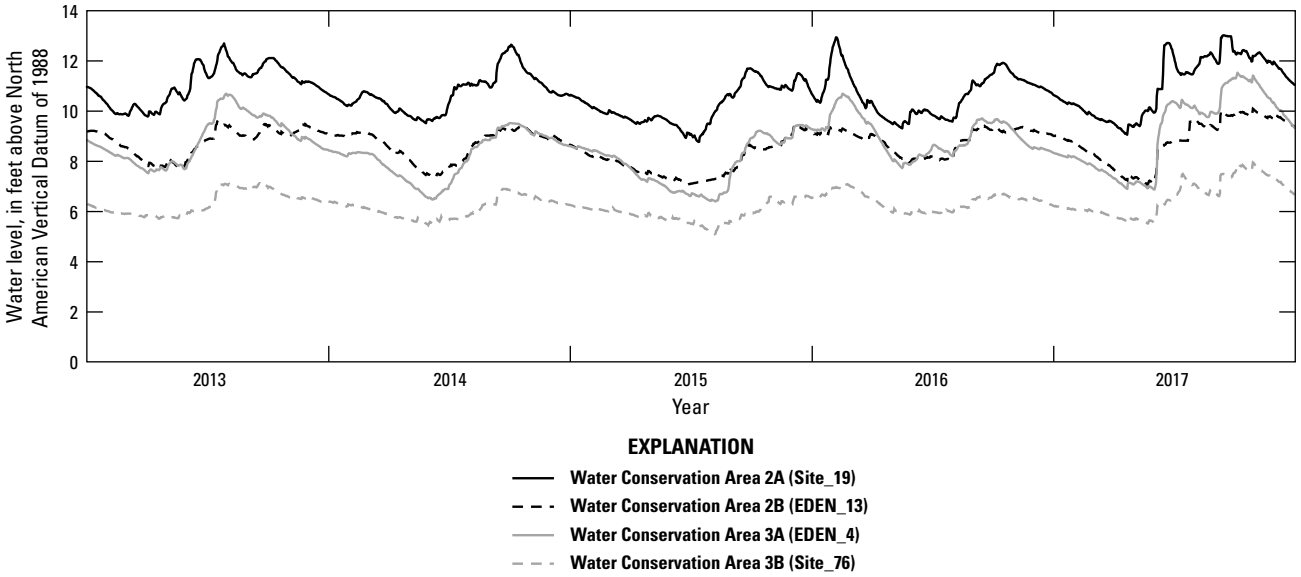

Figure E14. Daily water levels from the Everglades Depth Estimation Network (EDEN) used to represent groundwater boundaries along the western extent of the model representing the water conservation areas (WCAs).

Table E2. Locations, designations, and average historical period water levels (2013–17) for the National Oceanic and Atmospheric Administration (NOAA) tidal gage used to generate Modular Finite-Difference Groundwater Flow Model (MODFLOW) input datasets.

[ft, foot; NAVD 88, North American Vertical Datum of 1988; ID, identification]

NOAA site location	NOAA station ID	Station location, Florida State Plane (ft)		Average water level (ft above NAVD 88)	
		Easting	Northing	Annual	Wet season
Virginia Key, Florida	8723214	932146.1	509041.7	−0.55	−0.50

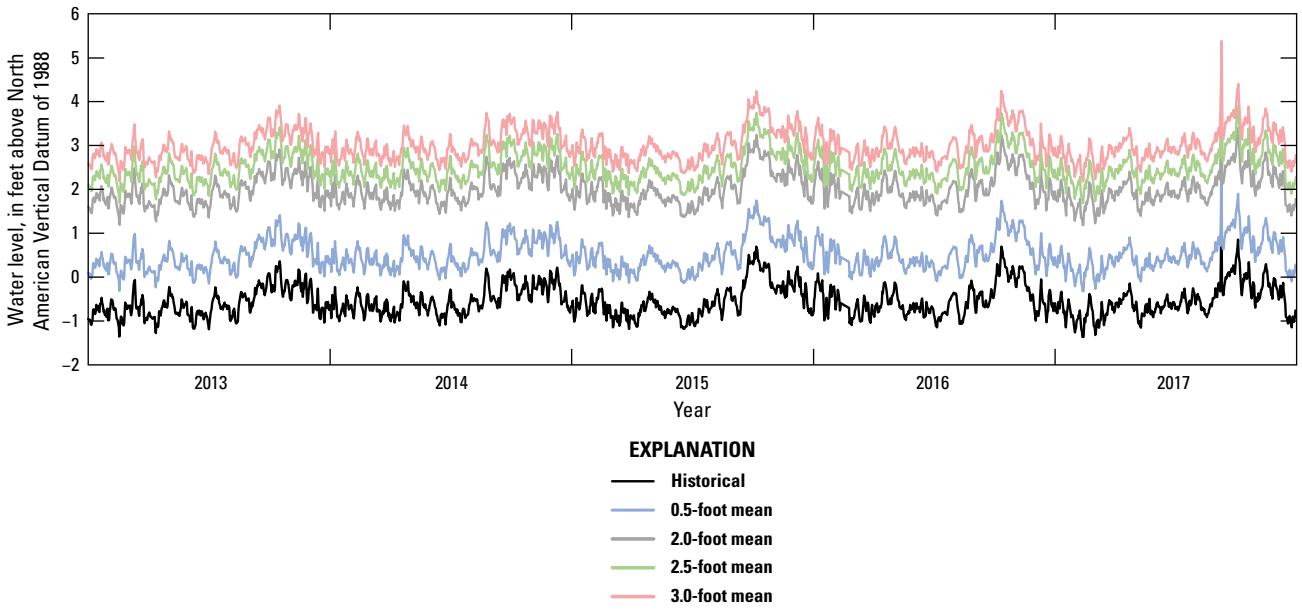

Figure E15. Daily water levels from the National Oceanic and Atmospheric Administration tidal gage on Virginia Key, Florida, used to represent groundwater boundaries along the eastern extent of the model for historical and future conditions.

Canal Representation Using Surface-Water Routing Process

The extensive canal system within the urbanized area of Broward County is represented by the SWR1 process. All primary and secondary features and some tertiary features are included. The locations and geometries used for these features are based on information from the MIKE SHE Mike 11 model, a dataset produced by Florida Atlantic University (Hindle and Restrepo, 1999), and lidar data (SFWMD, 2007). There are 103 SWR1 reach groups within the transient model connected through 124 SWR1 structures. Surface-water stages within the reaches having the same reach group number are modeled as a level pool with flow occurring through the SWR1 flow structures. The reach group assignments are based on locations within primary canals, tidal areas, and water control/drainage districts, improvement districts, development districts, and cities that have drainage plans within the county (fig. A4). Level pools within drainage areas are based on drainage infrastructure and operations, with several areas composed of more than one level pool. Weirs, culverts, and most gates included in the model are simulated as fixed-crest weirs with invert elevations that are set on the basis of drainage area control elevations or specified gate operations. Primary coastal structures (table E3) are simulated as fixed-opening underflow gates with invert elevations that are set on the basis of gate operations with opening values specified to limit maximum flow areas. Pumps within the model are simulated using linear stage-discharge curves with elevations that are set on the basis of drainage area control elevations. There are 9 fixed-opening gates, 41 fixed weirs, 34 stage-discharge curves, and 40 remaining connections that use the Manning's flow formulation within the model. Three additional structures (S-39, S-38, and S-34) that connect the WCAs to the primary drainage network are simulated as specified inflows (fig. A1).

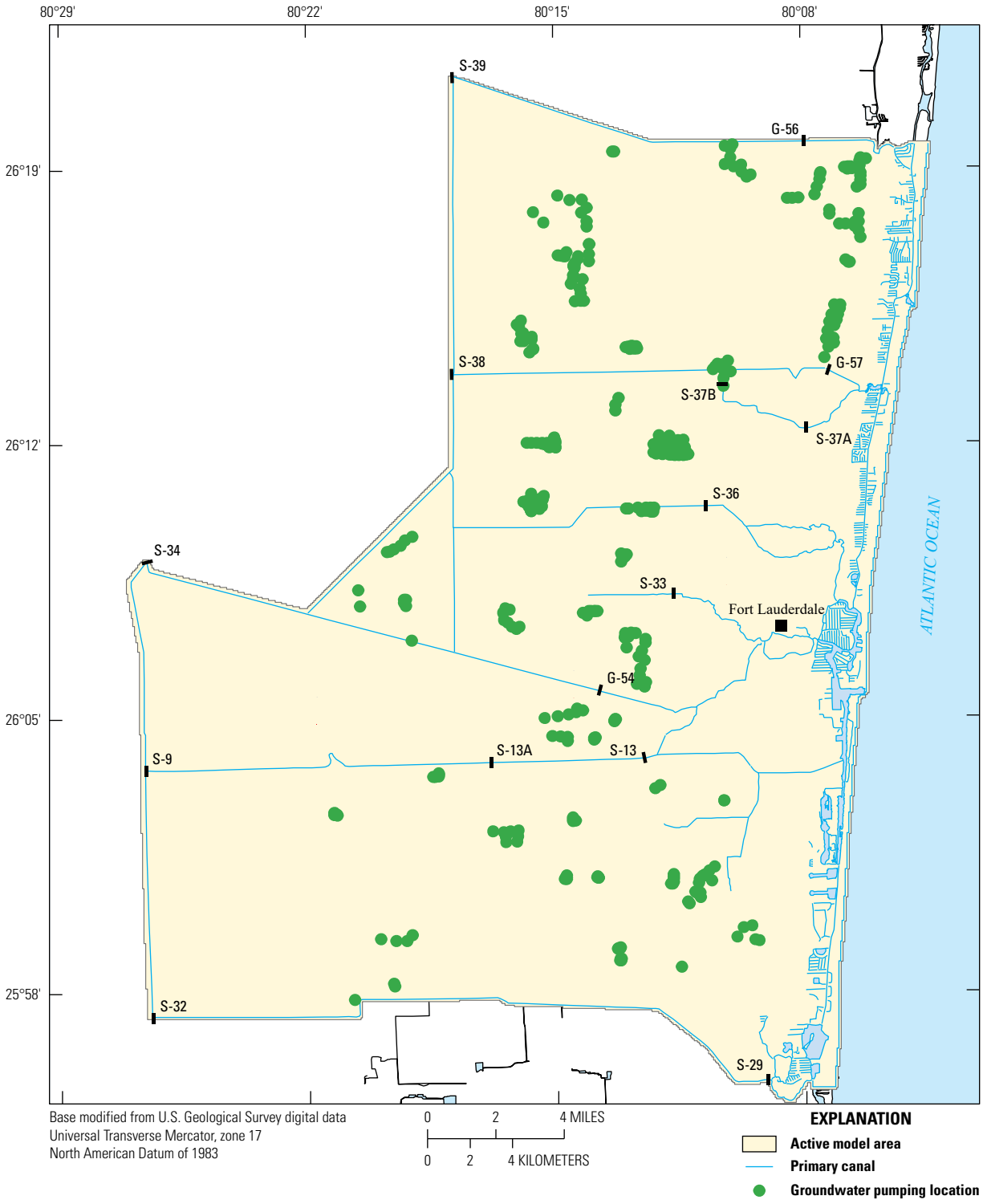

Figure E16. Location of pumping wells included in the groundwater model.

Table E3. Coastal structure physical properties, specified operations, and associated Surface-Water Routing (SWR1) process fixed gate structure parameters.

[ft, foot; NAVD 88, North American Vertical Datum of 1988; ft², square foot]

Structure name	Physical properties and specified operations of primary coastal structures						SWR1 gate parameters	
	Invert (ft above NAVD 88)	Gate open (ft above NAVD 88)	Gate close (ft above NAVD 88)	Range (ft)	Width (ft)	Flow area (ft²)	Invert (ft above NAVD 88)	Length (ft)
G-56	−5.00	6.49	5.49	1.00	60.0	689.4	4.75	344.7
G-57	−2.50	3.29	2.79	0.50	28.0	162.1	2.99	162.1
S-37A	−9.20	2.89	1.49	1.40	50.0	604.5	1.49	215.9
S-36	−8.50	3.39	2.49	0.90	25.0	297.3	2.49	165.1
S-33	−3.50	2.49	1.49	1.00	20.0	119.8	1.80	59.9
G-54	−5.50	2.99	1.99	1.00	48.0	407.5	1.99	203.8
S-13	−9.50	0.29	−0.11	0.40	16.0	156.6	−0.30	195.0
S-29	−12.50	0.99	−0.01	1.00	88.0	1,187.1	0.25	593.6

The locations and connections of the SWR1 flow structures are presented here in groups corresponding to the primary drainage canals. The Hillsboro Canal has surface-water flow connections through 16 SWR1 structures to WCA 1, the L-36 Canal, North Springs Improvement District, Pine Tree Water Control District, Cocomar Water Control District, Broward Water Control District #2, and to tide (table E4, fig. E17). The C-14 Canal has surface-water flow connections through 18 SWR1 structures to WCA 2A, the L-36 Canal, Coral Springs Improvement District, Sunshine Water Control District, City of Tamarac, North Lauderdale Water Control District, Cocomar Water Control District, Broward Water Control District #3, Broward Water Control District #4, and to tide (table E5, fig. E17). The C-13 Canal has surface-water flow connections through 16 SWR1 structures to the L-36 Canal, City of Sunrise, City of Lauderhill, City of Tamarac, and to tide (table E6, fig. E18). The C-12 Canal has surface-water flow connections through five SWR1 structures to the Old Plantation Water Control District, City of Sunrise, City of Lauderhill, and to tide (table E7, fig. E18; fig. E16 shows S-34 location). The North New River Canal has surface-water flow connections through nine SWR1 structures to the WCAs, Bonaventure Development District, City of Sunrise, Plantation Acres Improvement District, Old Plantation Water Control District, and to tide (table E8, fig. E18). The C-11 Canal passes through the East and West Central Broward County Water Control District and has surface-water flow connections through 13 SWR1 structures to the WCAs, L-37 Canal, L-33 Canal, South Broward Drainage District, Indian Trace Development District, and to tide (table E9, fig. E19). The C-9 Canal has surface-water flow connections through 11 SWR1 structures to the L-33 Canal, South Broward Drainage District, and to tide (table E10, fig. E19).

The primary coastal structures within the model were simulated as fixed-opening underflow gates with flow directions restricted to flow toward the coast/tide. Physical properties and specified operations of each structure were obtained from the SFWMD structures handbook (SFWMD, 2016). The structure inverts were initially set to heights equal to the upstream gate closing values, which would be the lower of the two values specified as the normal operational range of that structure. During calibration, inverts were adjusted to obtain upstream stages at the structures that more closely aligned with the measured wet season average during 2013–17. The resulting inverts used within the SWR1 process ranged from −0.30 to 4.75 ft above NAVD 88 (table E3). Measured upstream stages during the wet season were below the specified operational range for the S-13 and G-56 structures and resulted in SWR1 invert elevations below the specified gate closing. Structure widths were increased to allow large flow areas without large increases in upstream stages. This representation more closely mimics the behavior of an underflow gate, which can increase flow area by raising the gate structure without having a rise in upstream stage. Modified gate widths were calculated to obtain half the flow area of a gate structure using the gate width, invert, and opening values over the specified operational range of the gate. The resulting widths used within the SWR1 process ranged from 59.9 to 593.6 ft (table E3).

Table E4. Surface-Water Routing process surface-water flow connections, types, and control elevations for the Hillsboro Canal.

[ft, foot; NAVD 88, North American Vertical Datum of 1988; WCA, water conservation area; N/A, not applicable]

Model designation	Location	Connection 1	Connection 2	Control elevation (ft above NAVD 88)	Type of connection
S39	Hillsboro Canal	WCA 1	Hillsboro Canal	N/A	Specified flux
G56	Hillsboro Canal	Hillsboro Canal	Tide	5.49	Fixed gate
S39A	L-36 Canal	L36-1	Hillsboro Canal	1.69	Weir
NSID P2	North Springs Improvement District (NSID)	NSID W	L36	5.99	Pump
NSID P1	North Springs Improvement District	NSID W	L36	5.99	Pump
NSID W1	North Springs Improvement District	NSID 3	NSID W	6.99	Weir
NSID S1-2	North Springs Improvement District	NSID E	NSID W	8.49	Weir
Parkland2 W1	Parkland	Parkland	Hillsboro Canal	6.49	Weir
PTWCD W1	Pinetree Water Control District (PTWCD)	PTWCD	Hillsboro Canal	6.99	Weir
CocomarWCD W1	Cocomar Water Control District	Cocomar NW	Hillsboro Canal	9.49	Weir
CocomarWCD S46	Cocomar Water Control District	Hillsboro Canal	Cocomar NW	9.49	Pump
CocomarWCD W2	Cocomar Water Control District	Cocomar NE	Hillsboro Canal	9.49	Weir
BWCD2 S1	Broward Water Control District #2 (BWCD2)	Hillsboro Canal	BWCD2	8.49	Pump
BWCD2 W1	Broward Water Control District #2	BWCD2	Hillsboro Canal	8.49	Weir
BWCD2 S4	Broward Water Control District #2	Hillsboro Canal	BWCD2	8.49	Pump
S38B	L-36 Canal	L36-1	L36-2	6.14	Weir

The SWR1 reaches downstream from the primary coastal structures were not actively simulated but instead were assigned values corresponding to tail water stages, except for S-29 (fig. E20). The hourly values used for the tail water reaches were calculated by adding an offset value to the measured hourly tide values. The offset values were calculated as monthly averages from daily measured downstream stages for the historical period (2013–17) (table E11). The mean offset for each tail water section ranged from 0.214 to 0.600 ft. The same methodology and offset values were used to calculate the tail water stages specified for the future sea-level scenarios. The stages within the C-10 Canal were also not simulated within the SWR1 process but were specified as the hourly tidal value. The downstream side of S-29 was connected directly to tidal reaches because of its proximity to the Intracoastal Waterway.

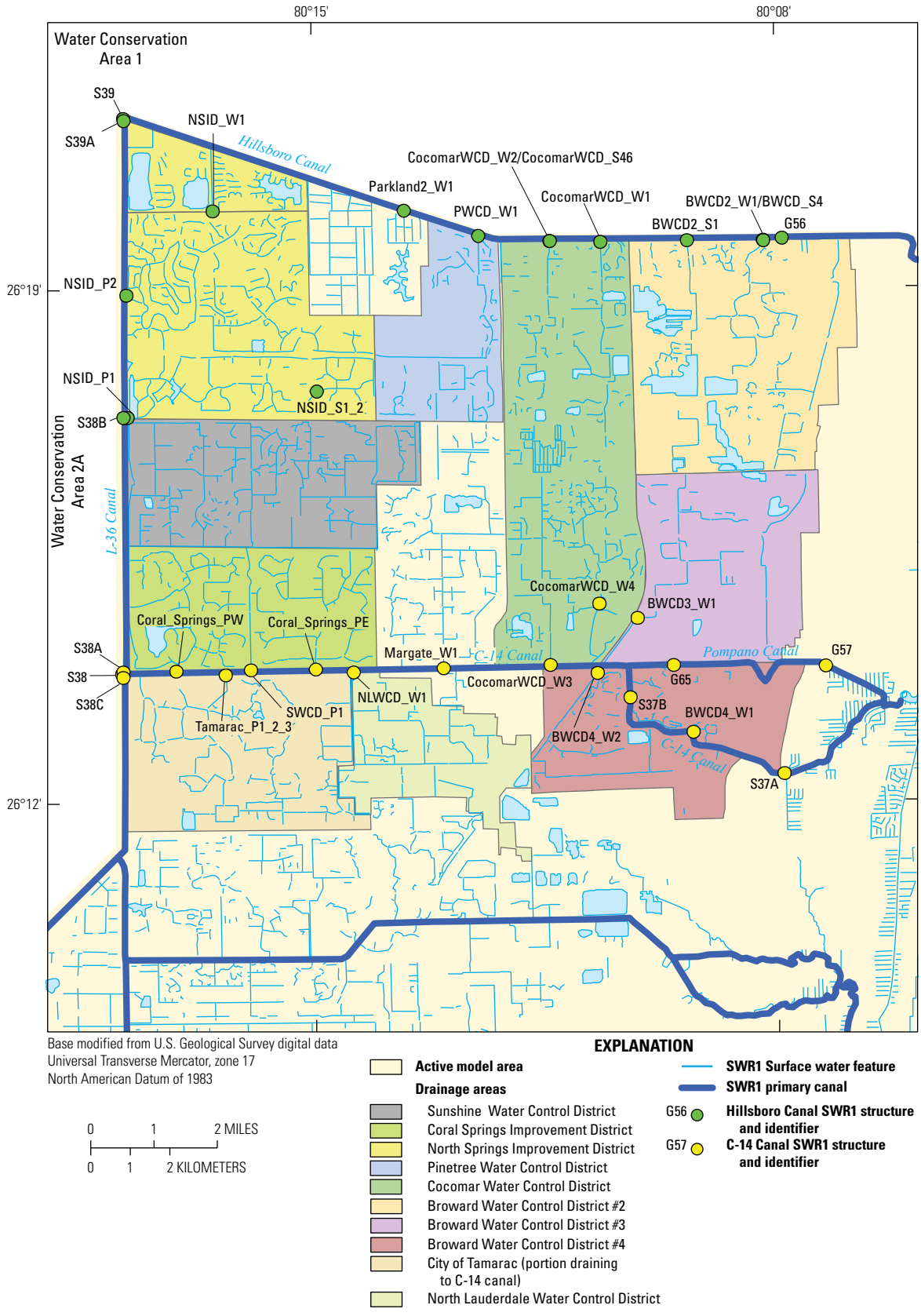

Figure E17. Locations of Surface-Water Routing (SWR) process surface-water flow connections for the Hillsboro and C-14 Canals.

Table E5. Surface-Water Routing process surface-water flow connections, types, and control elevations for the C-14 Canal.

[ft, foot; NAVD 88, North American Vertical Datum of 1988; WCA, water conservation area; N/A, not applicable]

Model designation	Location	Connection 1	Connection 2	Control elevation (ft above NAVD 88)	Type of connection
S38	C-14 Canal	WCA 2A	C14	N/A	Specified flux
G65	C-14 Canal	C14	PC	2.49	Pump
G57	Pompano Canal (PC)	PC	Tide	2.99	Fixed gate
S37B	C-14 Canal	C14	C14	5.29	Fixed gate
S37A	C-14 Canal	C14	Tide	1.49	Fixed gate
S38A	L-36 Canal	L36-2	C14	6.14	Weir
S38C	C-14 Canal	C14	L36-3	5.49	Weir
Coral Springs PW	Coral Springs Improvement District	Coral Springs W	C14	4.99	Pump
Coral Springs PE	Coral Springs Improvement District	Coral Springs E	C14	4.99	Pump
SWCD P1	Sunshine Water Control District (SWCD)	SWCD	C14	5.99	Pump
Tamarac P1-2-3	City of Tamarac	Tamarac 1	C14	5.49	Pump
NLWCD W1	North Lauderdale Water Control District	NLWCD 1	C14	2.3	Weir
Margate W1	City of Margate	Margate 1	C14	5.99	Weir
CocomarWCD W3	Cocomar Water Control District	Cocomar SW	C14	7.49	Weir
CocomarWCD W4	Cocomar Water Control District	Cocomar SE	C14	7.99	Weir
BWCD3 W1	Broward Water Control District #3 (BWCD3)	BWCD3	C14	7.49	Weir
BWCD4 W2	Broward Water Control District #4 (BWCD4)	BWCD4 2	C14	5.49	Weir
BWCD4 W1	Broward Water Control District #4	BWCD4 1	C14	5.49	Weir

The steady-state model used an average of measured wet season tail water values for the historical period (2013–17). The tail water stage values used for future sea-level scenarios were calculated by adding the corresponding sea-level rise for each future sea-level scenario to the tail water stage values used for the historical simulation (table E12). For the steady-state model, a downstream stage for each of the coastal structures was specified for a single reach directly connected to the upstream reach of the structure (fig. E21). The stage of the downstream reach was specified as half the average daily tidal range of ±1.116 ft, or 0.558 ft, which was lower than the tail water stage. The discharge of a coastal structure was calculated using the head difference between the upstream and the downstream stages, not the tail water stage. This allows the coastal structures to discharge to a lower downstream value in the steady-state model and is representative of a movable gate coastal structure discharging more frequently during periods of lower tide. Specifying the entire tail water section at this lower stage value would result in lowered groundwater levels in the surrounding areas. This configuration, paired with the restriction of flow direction to only occur from inland toward the coast, allows a coastal structure to maintain an upstream stage that is slightly lower than the mean tidal level.

The leakance values for each reach were assigned on the basis of drainage areas and the connections between these drainage areas and the primary drainage canals (fig. A4). Reaches that were specified as tidal reaches were grouped together and assigned one leakance value. Any unassigned reaches that were not part of these designated groups were assigned one leakance value. The leakance values for each of the groups were calibrated using the steady-state model. The resulting calibrated leakances ranged from 0.5 to 9.983 day^{-1} (table E13).

Table E6. Surface-Water Routing process surface-water flow connections, types, and control elevations for the C-13 Canal.

[ft, foot; NAVD 88, North American Vertical Datum of 1988; NNR, North New River]

Model designation	Location	Connection 1	Connection 2	Control elevation (ft above NAVD 88)	Type of connection
S124	L-36 Canal	L36-3	NNR	5.99	Weir
S125	C-13 Canal	C13	NNR	3.39	Weir
S36	C-13 Canal	C13	Tide	2.49	Fixed gate
Sunrise W17	City of Sunrise	Sunrise 17	L36-3	3.99	Weir
Sunrise W15	City of Sunrise	Sunrise 15	C13	3.99	Weir
Sunrise W13-2	City of Sunrise	Sunrise 13	C13	3.79	Weir
Sunrise W13-1	City of Sunrise	Sunrise 13	C13	3.79	Weir
Sunrise P5	City of Sunrise	Sunrise 5	C13	2.99	Pump
Sunrise P6	City of Sunrise	Sunrise 6	C13	2.99	Pump
Sunrise P4	City of Sunrise	Sunrise 4	C13	2.99	Pump
Sunrise W11	City of Sunrise	Sunrise 11	C13	4.99	Weir
Sunrise P3	City of Sunrise	Sunrise 3	C13	2.99	Pump
Sunrise P2	City of Sunrise	Sunrise 2	C13	2.99	Pump
Lauderhill PA	City of Lauderhill	Lauderhill A	C13	4.85	Pump
Tamarac W1	City of Tamarac	Tamarac 2	C13	4.99	Weir

Simulation of Rainfall and Evapotranspiration Within the Steady-State Model

Rainfall and ET within the steady-state model are simulated using the Recharge and EVT packages. Measured rainfall data from 18 measurement locations were used to create the model input datasets (table E14). Recharge for each model cell was specified as the daily average wet season (2013–17) value using 18 different rainfall zones. Each model cell was assigned the rainfall zone corresponding to the nearest rainfall measurement station (fig. E22). The average daily wet season rainfall values for the 18 rainfall zones ranged from 0.197 to 0.249 inches (in.) with an average of 0.223 in. (table E14). The potential evapotranspiration (PET) input used in the EVT package was calculated from 2-kilometer scale Geostationary Operational Environmental Satellite (GOES) PET data for the State of Florida published by the U.S. Geological Survey (Shoemaker, 2017; Mecikalski and others, 2018). Daily GOES PET rates were averaged across each of the 18 rainfall zones for the 2013–17 wet seasons. The daily PET across the 18 zones was nearly spatially uniform, having a range of 0.195−0.199 in., with an average of 0.197 in. (table E14). The ET surface used within the EVT package was set to the land-surface elevations for each cell, which was consistent with the central and southern saltwater intrusion model. The ET extinction depths were based on the values used in the central and southern saltwater intrusion model (fig. E23). For that project, the extinction depth values were assigned on the basis of land use and then adjusted during the calibration process. The calibrated extinction depths from the central and southern saltwater intrusion model were scaled as part of the steady-state model calibration with an independent scale factor calculated for each rain zone (table E14).

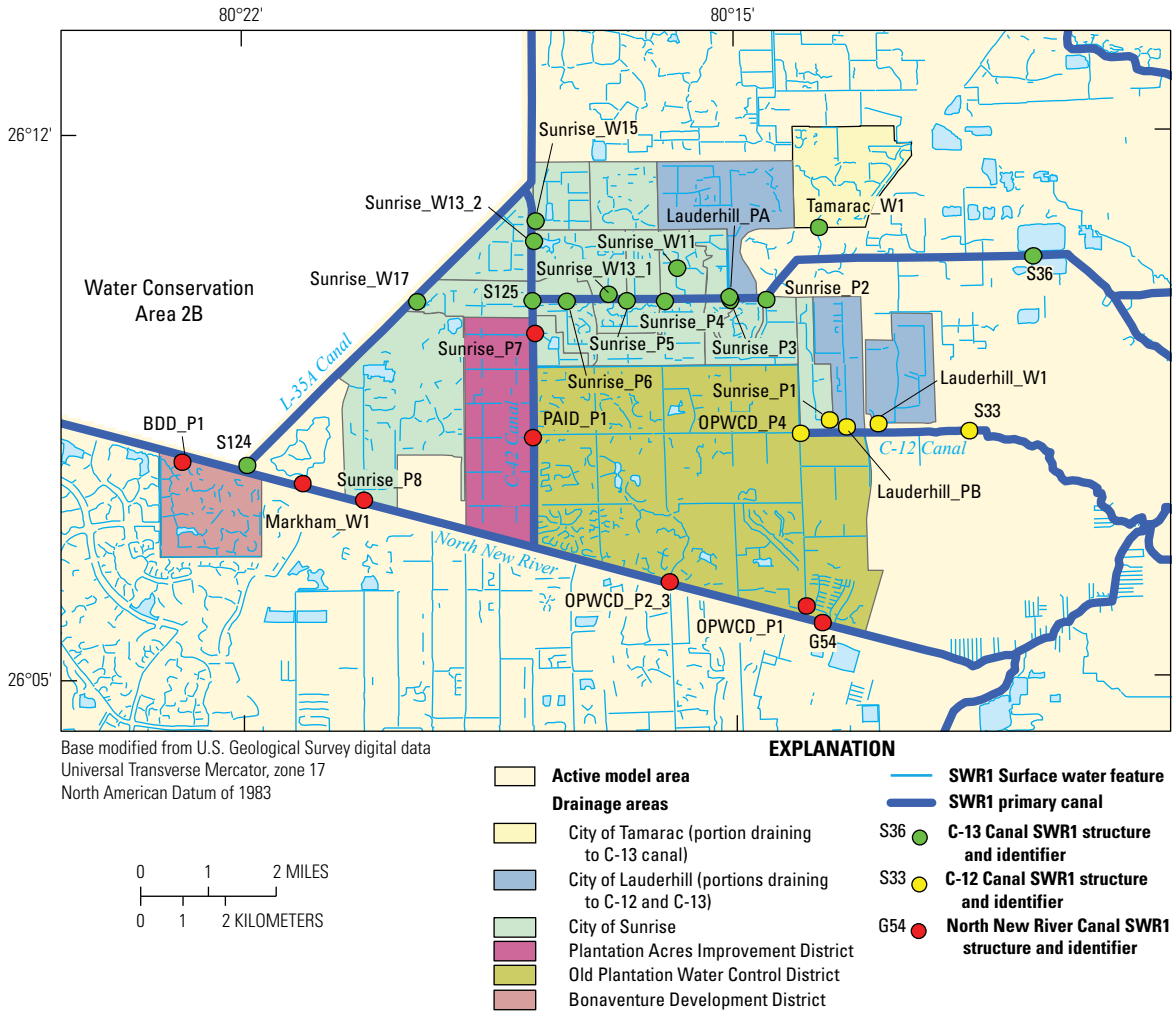

Figure E18. Locations of Surface-Water Routing (SWR) process surface-water flow connections for the C-13, C-12, and North New River Canals.

Table E7. Surface-Water Routing process surface-water flow connections, types, and control elevations for the C-12 Canal.

[ft, foot; NAVD 88, North American Vertical Datum of 1988]

Model designation	Location	Connection 1	Connection 2	Control elevation (ft above NAVD 88)	Type of connection
S33	C-12 Canal	C12	Tide	1.49	Fixed gate
OPWCD P4	Old Plantation Water Control District (OPWCD)	OPWCD	C12	2.74	Pump
Sunrise P1	City of Sunrise	Sunrise 1	C12	3.49	Pump
Lauderhill W1	City of Lauderhill	Lauderhill C	C12	4.49	Weir
Lauderhill PB	City of Lauderhill	Lauderhill B	C12	4.89	Pump

Table E8. Surface-Water Routing process surface-water flow connections, types, and control elevations for the North New River Canal.

[ft, foot; NAVD 88, North American Vertical Datum of 1988; WCA, water conservation area; NNR, North New River; N/A, not applicable]

Model designation	Location	Connection 1	Connection 2	Control elevation (ft above NAVD 88)	Type of connection
S34	North New River Canal	WCA	NNR	N/A	Specified flux
G54	North New River Canal	NNR	Tide	1.99	Fixed gate
BDD P1	Bonaventure Development District (BDD)	BDD	NNR	2.99	Pump
Markham W1	Markham Park	Markham	NNR	2.99	Weir
Sunrise P8	City of Sunrise	Sunrise 8	NNR	2.99	Pump
Sunrise P7	City of Sunrise	Sunrise 7	NNR	2.99	Pump
PAID P1	Plantation Acres Improvement District (PAID)	PAID	NNR	2.99	Pump
OPWCD P2-3	Old Plantation Water Control District (OPWCD)	OPWCD	NNR	2.99	Pump
OPWCD P1	Old Plantation Water Control District	OPWCD	Tide	2.89	Pump

Table E9. Surface-Water Routing process surface-water flow connections, types, and control elevations for the C-11 Canal.

[ft, foot; NAVD 88, North American Vertical Datum of 1988; WCA, water conservation area]

Model designation	Location	Connection 1	Connection 2	Control elevation (ft above NAVD 88)	Type of connection
S9	C-11 Canal	C11W	WCA	1.75	Pump
S13 S	C-11 Canal	C11E	Tide	−0.11	Weir
S13 P	C-11 Canal	C11E	Tide	0.74	Pump
S9XN	L-37 Canal	L37	C11W1	6.49	Weir
S9XS	L-33 Canal	L33	C11W1	4.49	Weir
G86N	C-11 Canal	US27	C11W1	3.99	Weir
G86S	C-11 Canal	US27	C11W1	3.99	Weir
S381	C-11 Canal	C11W1	C11W2	4.49	Weir
SBDD S9-10W	South Broward Drainage District (SBDD)	SBDD S9-10	C11W2	2.49	Weir
SBDD S8P	South Broward Drainage District	SBDD S8-1	C11W2	1.99	Pump
SBDD S8W	South Broward Drainage District	SBDD S8-2	SBDD S8-1	2.49	Weir
ITDD P1	Indian Trace Development District (ITDD)	ITDD	C11W2	2.99	Pump
S13A G	C-11 Canal	C11W2	C11E	1.00	Fixed gate

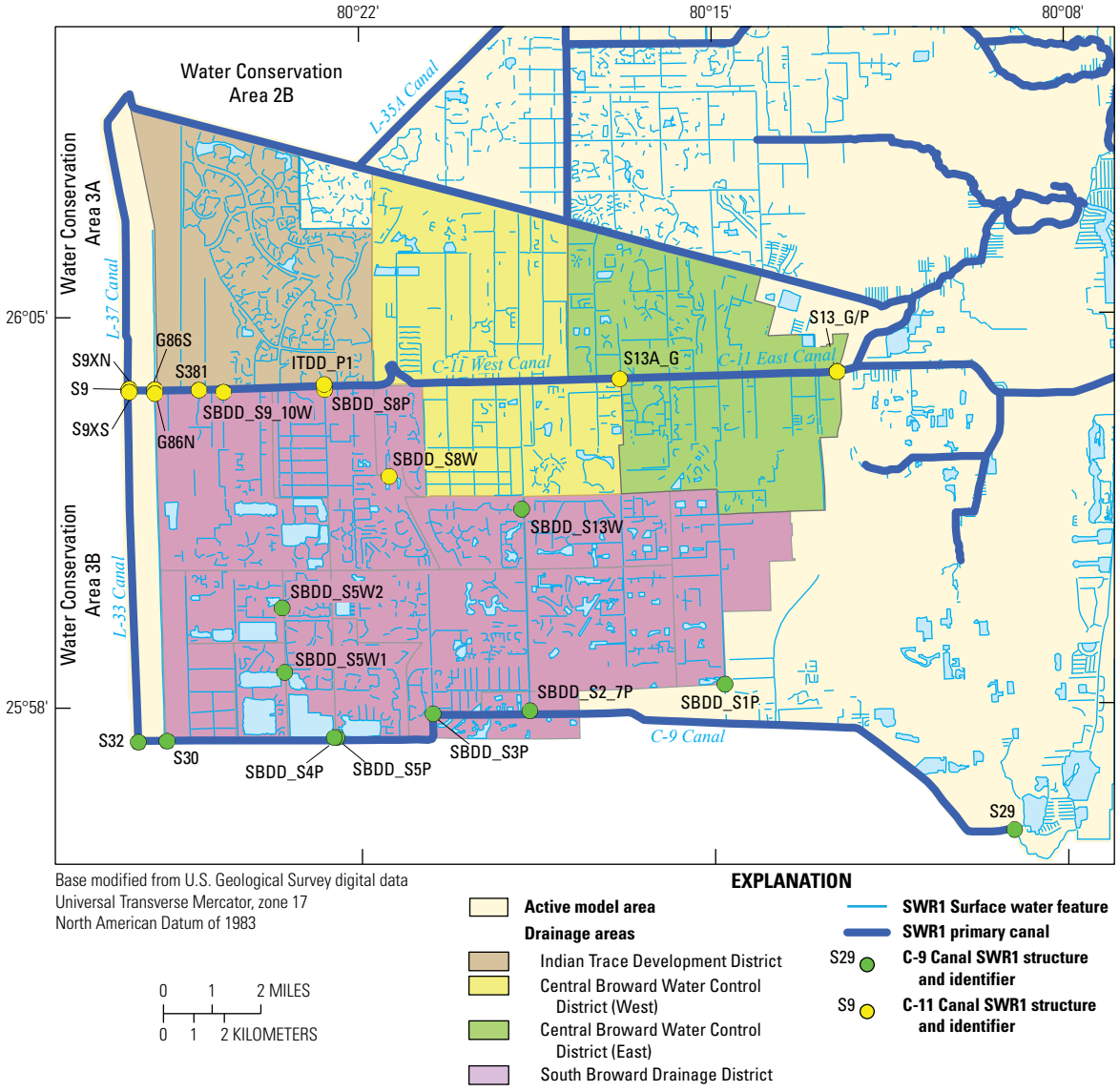

Figure E19. Locations of Surface-Water Routing (SWR) process surface-water flow connections for the C-11 and C-9 Canals.

Table E10. Surface-Water Routing process surface-water flow connections, types, and control elevations for the C-9 Canal.

[ft, foot; NAVD 88, North American Vertical Datum of 1988; N/A, not applicable]

Model designation	Location	Connection 1	Connection 2	Control elevation (ft above NAVD 88)	Type of connection
S32	L-33 Canal	L33	N/A	4.99	Weir
S30	C-9 Canal	L33	C9	4.49	Weir
S29	C-9 Canal	C9	Tide	−0.01	Fixed gate
SBDD S5P	South Broward Drainage District (SBDD)	SBDD S5-1	C9	2.49	Pump
SBDD S5W1	South Broward Drainage District	SBDD S5-3	SBDD S5-1	2.99	Weir
SBDD S5W2	South Broward Drainage District	SBDD S5-2	SBDD S5-1	2.74	Weir
SBDD S4P	South Broward Drainage District	SBDD S4	C9	1.99	Pump
SBDD S3P	South Broward Drainage District	SBDD S3	C9	1.99	Pump
SBDD S2 7P	South Broward Drainage District	SBDD S2-7	C9	1.19	Pump
SBDD S13W	South Broward Drainage District	SBDD S13	SBDD S2-7	1.49	Weir
SBDD S1P	South Broward Drainage District	SBDD S1	C9	0.99	Pump

Simulation of Rainfall, Evapotranspiration, Infiltration, and Recharge Within the Transient Model

The development of the transient model used the URO process to calculate surface-water storage, unsaturated zone storage, infiltration into the unsaturated zone, and recharge from the unsaturated zone into the underlying MODFLOW groundwater cells. Daily measured rainfall rates from the 18 measurement locations (table E14) were applied to the active URO cells contained within each rainfall zone (fig. E22). If a model cell contained a SWR1 reach, the URO process was not active within that cell, and rainfall for that model cell was directly applied to the SWR1 reach; evaporation was removed from that cell by applying the PET rate to the SWR1 reach. The maximum daily rainfall value averaged across the 18 measurement locations for the historical period was 5.76 in. (fig. E24). The maximum daily rates across the 18 zones indicate that there were 12 days where rainfall exceeded 5.0 in. within at least one zone, 3 days where rainfall exceeded 7.5 in. within at least one zone, and 1 day where rainfall exceeded 10.0 in. within at least one zone. The daily PET rate averaged across the 18 zones ranged from 0.18 to 3.72 inches per day (in/d), with an average of 1.91 in/d.

The URO process calculates ET by first removing water from surface-water storage at the full potential rate. If the potential rate is not satisfied, water is then removed from the unsaturated zone at a reduced rate using a linear, water-content dependent relation. Lastly, if any potential rate remains, water is removed from the underlying groundwater cell at a linearly reduced rate down to zero at a user-defined extinction depth (Decker and Hughes, 2013) similar to the EVT package within MODFLOW. The same scaled extinction depth used within the steady-state model was used within the transient model (figs. E22 and E23, table E14).

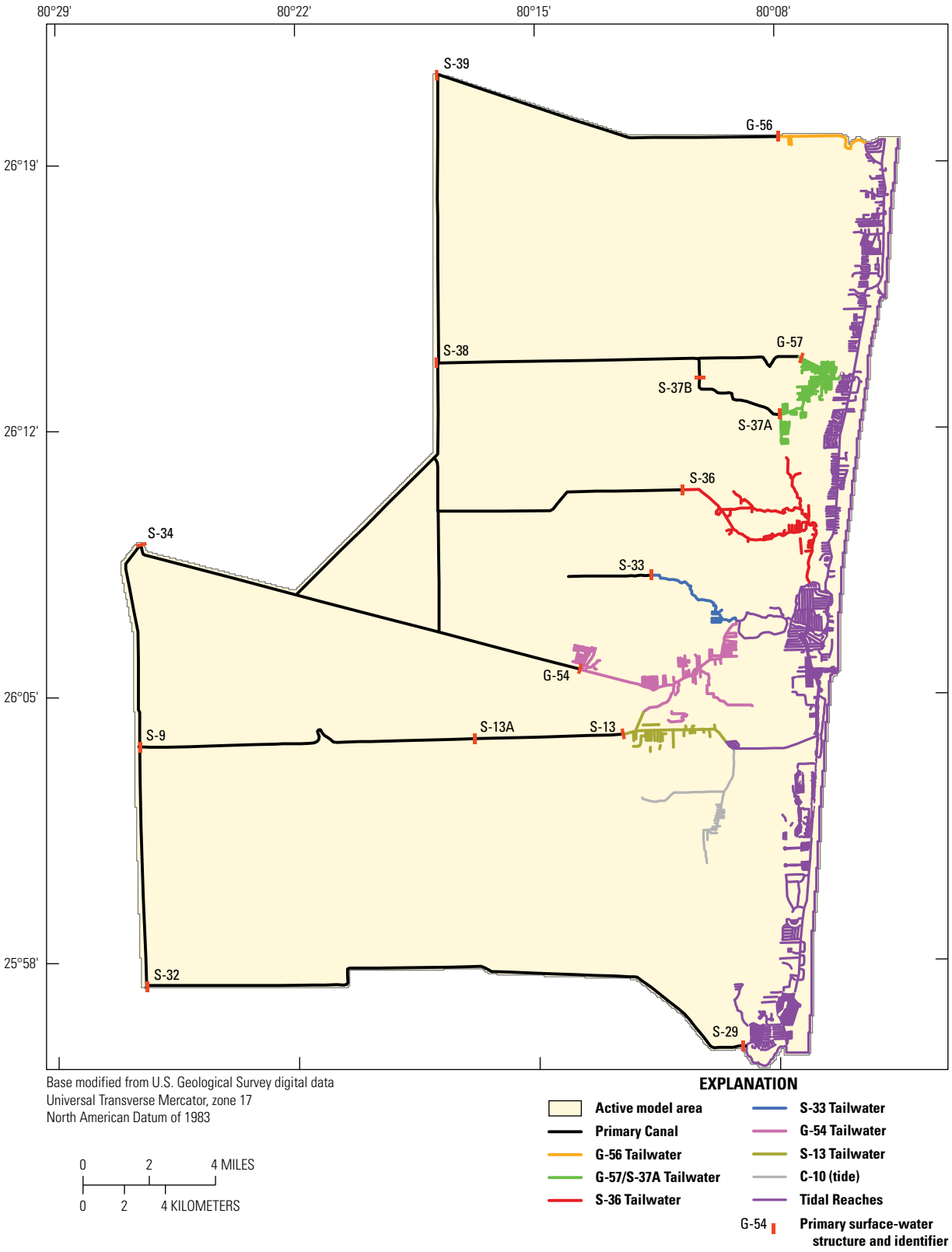

Figure E20. Specified stage reaches within the Surface-Water Routing process representing tide and tail water sections.

Table E11. Monthly tide offsets used to specify tail water stages within the Surface-Water Routing process.

[All values are in feet]

Month	Surface-water Control Structures					
	G-56	S-37A/G-57	S-36	S-33	G-54	S-13
January	0.325	0.218	0.290	0.306	0.500	0.243
February	0.346	0.203	0.310	0.300	0.515	0.263
March	0.300	0.174	0.246	0.253	0.447	0.108
April	0.238	0.164	0.251	0.249	0.438	0.136
May	0.307	0.165	0.310	0.283	0.480	0.209
June	0.678	0.213	0.432	0.388	0.734	0.352
July	0.441	0.186	0.437	0.372	0.716	0.365
August	0.418	0.186	0.385	0.336	0.671	0.365
September	0.505	0.286	0.545	0.465	0.834	0.483
October	0.408	0.285	0.442	0.395	0.684	0.403
November	0.358	0.258	0.385	0.366	0.574	0.374
December	0.307	0.229	0.375	0.361	0.608	0.403
Mean	0.386	0.214	0.367	0.340	0.600	0.309

Table E12. Specified stage values used within the Surface-Water Routing process for tail water sections for the historical and increased sea-level scenarios.

[All specified stage values are in feet above the North American Vertical Datum of 1988. ft, foot]

Designation	Sea-level scenario				
	Historical	0.5 ft	2.0 ft	2.5 ft	3.0 ft
Tide	−0.5	0.55	2.05	2.55	3.05
G-56	−0.04	1.01	2.51	3.01	3.51
G-57/S-37A	−0.28	0.77	2.27	2.77	3.27
S-36	−0.08	0.97	2.47	2.97	3.47
S-33	−0.13	0.92	2.42	2.92	3.42
G-54	0.18	1.23	2.73	3.23	3.73
S-13	−0.14	0.91	2.41	2.91	3.41
S-29	−0.50	0.55	2.05	2.55	3.05

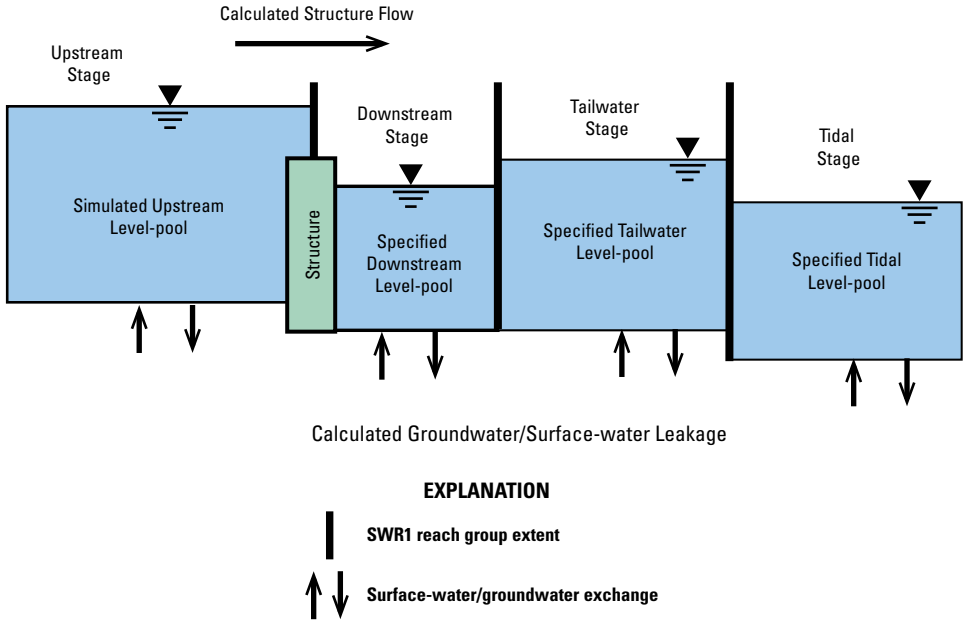

Figure E21. Model implementation of stream/canal reaches represented using the Surface-Water Routing (SWR1) process within the steady-state model.

Table E13. Leakances assigned within the Surface-Water Routing process to drainage areas and canals and the connected primary drainage canal.

[N/A, not applicable]

Drainage area(s) or canal designation(s)	Leakance (day^{-1})	Connected primary canal(s)
North Springs Improvement District, Pine Tree Water Control District, Broward Water Control District #2, and Hillsboro Canal	0.618	Hillsboro Canal
Cocomar Water Control District	0.991	Hillsboro Canal, C-14
City of Tamarac, North Lauderdale Water Control District, Coral Springs Improvement District, Sunshine Water Control District, Broward Water Control District #3, Broward Water Control District #4, C-14 Canal, Pompano Canal, Cypress Creek Canal, and City of Margate	2.969	C-14
City of Sunrise	1.768	C-12, C-13, C-42, North New River, L-36
City of Lauderhill	1.239	C-12, C-13
Bonaventure Development District, Plantation Acres Improvement District, Old Plantation Water Control District, C-42 Canal, and North New River	2.788	North New River
Indian Trace Development District, C-11 Canal, and L-37 Canal	2.432	C-11
Central Broward Water Control District	0.500	C-11
South Broward Drainage District	5.160	C-9, C-11
L-33 Canal and C-9 Canal	9.983	C-9
Tidal reaches	0.507	N/A
Unassigned reaches	2.213	Varies

Table E14. Rainfall measurement station locations and average daily wet season rainfall and Geostationary Operational Environmental Satellite (GOES) evapotranspiration (ET) data used in the steady-state model.

[ft, foot; in., inch]

Station name	Station location Florida State Plane (ft)		Average daily wet season (2013–17)		ET extinction depth scale factor
	Easting	Northing	Rainfall (in.)	GOES ET (in.)	
S9_R	838772.7	628469.7	0.197	0.195	0.280
S124_R	864386.8	653203.0	0.203	0.196	1.773
S125_R	886568.9	666012.0	0.224	0.197	1.904
S38_R	886166.9	689837.8	0.224	0.196	0.319
S39_R	886355.9	735683.0	0.229	0.196	0.743
NSID1_R	886322.7	710928.2	0.249	0.199	1.902
G56_R	940840.3	725811.7	0.217	0.196	1.551
S37B_R	928186.2	687965.5	0.209	0.199	0.783
S37A_R	940882.6	681555.9	0.217	0.196	1.800
G57_R	943261.7	690689.8	0.217	0.198	0.552
S36_R	925366.6	669527.0	0.225	0.196	1.091
S33_R	920335.7	655807.7	0.24	0.198	0.980
G54_R	908925.6	640922.9	0.238	0.199	0.496
S13_R	915840.7	630454.5	0.221	0.195	0.266
SBDD	865563.9	619965.2	0.247	0.196	1.798
S30_R	842873.3	590337.2	0.211	0.197	0.265
S29Z_R	898413.0	592592.1	0.233	0.197	0.628
S29_R	935011.7	580704.5	0.204	0.199	0.392

The URO process used to estimate infiltration at the soil surface and recharge at the water table can be viewed as a simplified bucket-style model of water stored in the unsaturated zone. In this model, infiltration of rainfall is inversely proportional to soil moisture storage within the unsaturated zone, whereas recharge to the saturated zone is released from the unsaturated zone storage at a rate assumed directly proportional to the soil moisture storage within the unsaturated zone. This simple model is utilitarian in approach, neglecting many physics-based features of flow within the unsaturated zone for computational ease and unsaturated zone data sparseness. Values of the maximum infiltration and recharge rates used for this process correspond to values used in the previous inundation model (figs. E25 and E26). Within the URO process, the infiltration and recharge are calculated on the basis of linear, water-content dependent relationships (Decker and others, 2019):

$$h_{inf} = k_{inf0}(1 - \theta)\Delta t, \tag{2}$$

$$h_{rec} = k_{rec0}\theta\Delta t, \text{ and} \tag{3}$$

$$\theta = \frac{L_{UZS}}{L_{UZSmx}}, \tag{4}$$

where

h_{inf} is the infiltration depth (L),
k_{inf0} is the maximum infiltration rate (L/T),
θ is the water content,
Δt is the URO time step (T),
h_{rec} is the recharge depth (L),
k_{rec0} is the maximum recharge rate (L/T),
L_{UZS} is the current unsaturated zone storage (L), and
L_{UZSmx} is the maximum storage depth of the unsaturated zone (L) and is updated each MODFLOW time step.

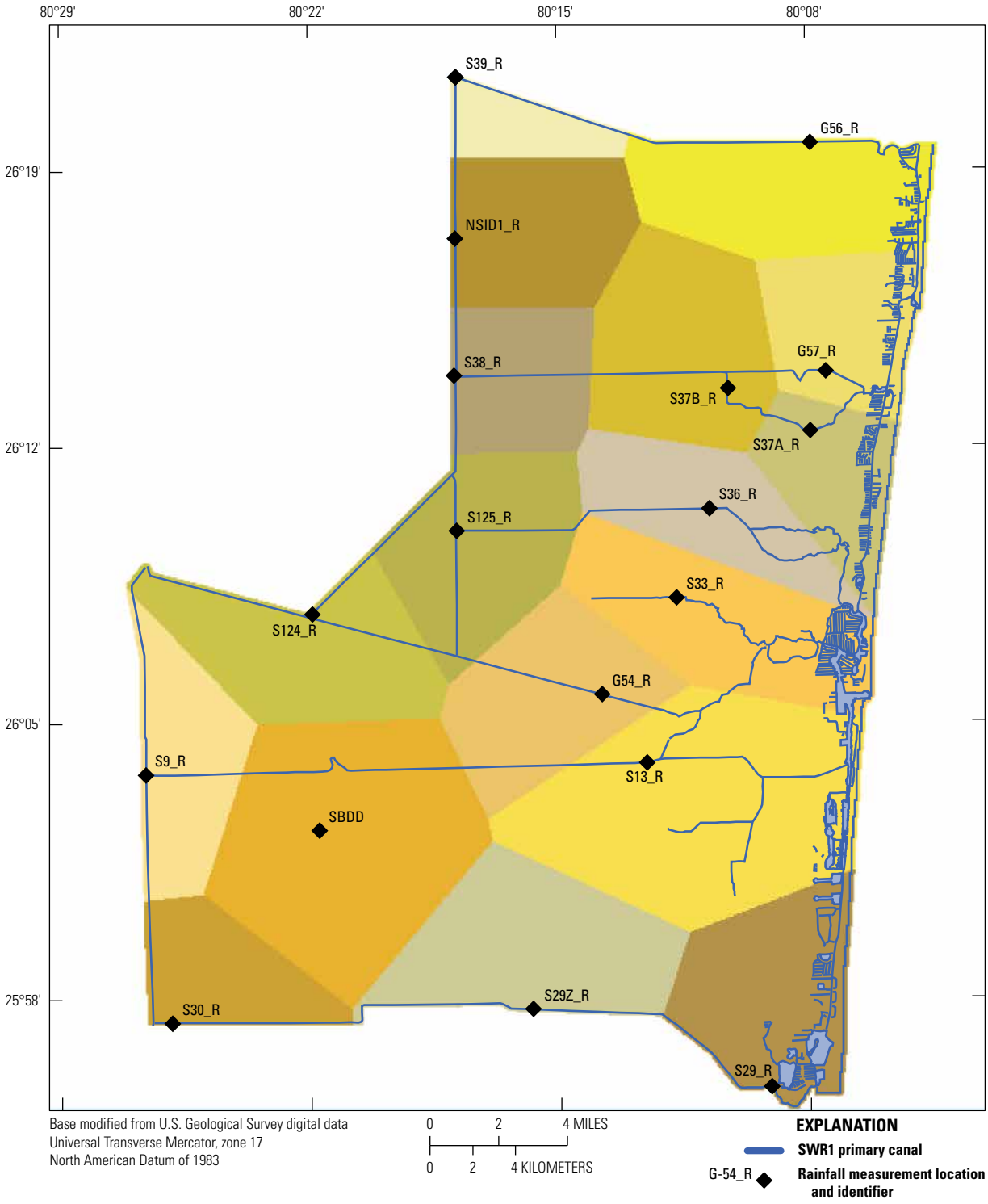

Figure E22. Rainfall measurement stations and resulting rainfall zones used in the creation of Modular Finite-Difference Groundwater Flow Model (MODFLOW) Recharge (RCH) and Evapotranspiration (EVT) datasets. SWR1, Surface-Water Routing process.

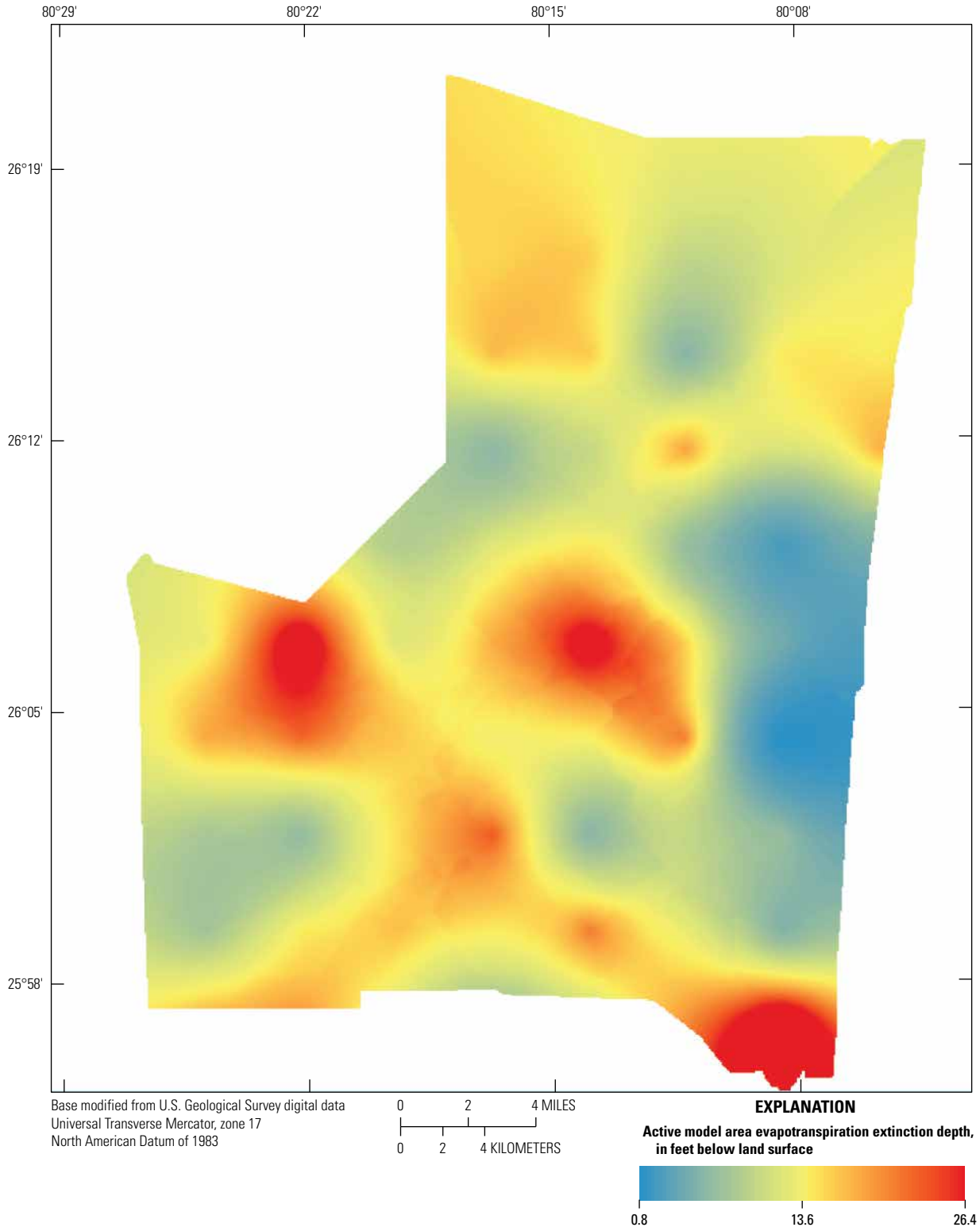

Figure E23. Evapotranspiration extinction depths, in feet, used for Modular Finite-Difference Groundwater Flow Model (MODFLOW) Evaporation (EVT) package.

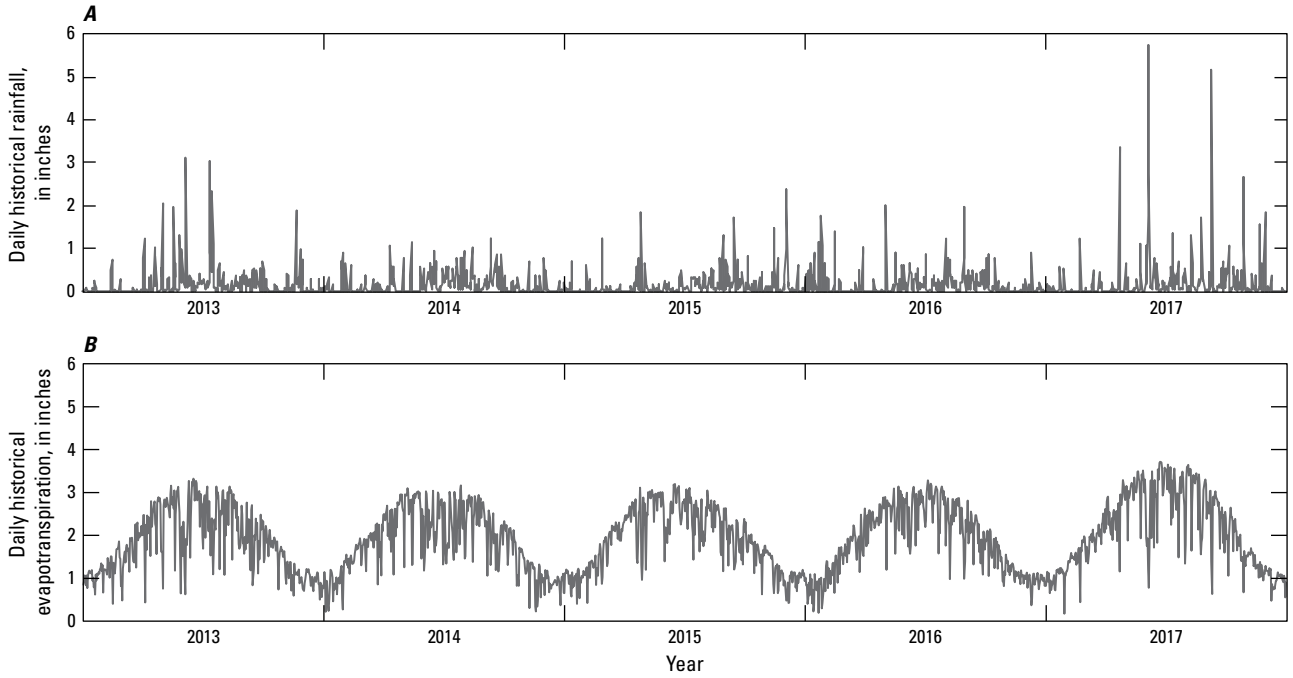

Figure E24. Daily historical rainfall in inches per day and daily historical potential evapotranspiration in feet per day averaged across the 18 rainfall zones.

Assigned Surface-Water Fluxes

Surface-water fluxes representing flow through the S-39, S-38, and S-34 structures were assigned to the corresponding SWR1 reaches within the Hillsboro, C-14, and North New River Canals (fig. A1). Measured flow from the historical period (2013–17) was assigned as inflows through these structures for all scenarios. Wet season average flow was used within the steady-state model. All flow was specified as positive into the simulated surface-water system. The average measured flow through the S-39 structure during the entire historical period was 163.3 cubic feet per second (ft^3/s), compared to 208.5 ft^3/s during the wet season (fig. E27). The average measured flow through the S-38 structure during the entire historical period was 271.9 ft^3/s, compared to 337.4 ft^3/s during the wet season (fig. E27). The average measured flow through the S-34 structure during the entire historical period was 66.2 ft^3/s, compared to 95.8 ft^3/s during the wet season (fig. E27).

Additional fluxes were assigned along the Hillsboro and C-9 Canals representing the inflows from parts of the drainage areas beyond the active model extent. The average contribution of rainfall into the Hillsboro Canal was estimated by first calculating the difference in flow out of the Hillsboro Canal through G-56 and the flows into the Hillsboro Canal from S-39 and leakage into the L-36 Canal adjacent to WCA 2A (fig. A1). Then the volumetric rate of wet season average (2013–17) rainfall over the Hillsboro Canal drainage area was calculated as 538.7 ft^3/s using a drainage area of 89.99 mi^2 and the average of the S39_R and G56_R (fig. E22) rainfall measurements which are 0.229 and 0.217 in/d, respectively (table E15). The wet season average (2013–17) flow rates through the G-56 and S-39 structures are 250.9 and 163.3 ft^3/s, respectively. Preliminary steady-state model results indicated that leakage into the L-36 Canal, which flows into the Hillsboro Canal, was approximately 40 ft^3/s. The average contribution of rainfall to the Hillsboro Canal from the entire drainage area is then estimated as the difference between the flows at G-56 and the combined flows from the S-39 structure and the L-36 Canal, which is 102.6 ft^3/s, or 19.1 percent of the total wet season average rainfall. The part of the drainage area not within the active model extents is 51.8 mi^2, or 57.6 percent of the total drainage area. Therefore, the additional inflows caused by rainfall from the part of the Hillsboro Canal drainage area missing from the model extents was approximated as 57.6 percent of the 19 percent of total rainfall for the area, or 10.9 percent. This value was used for the steady-state and transient models. The wet season average inflow to the Hillsboro Canal was estimated to be 59.1 ft^3/s (table E15, fig. E28).

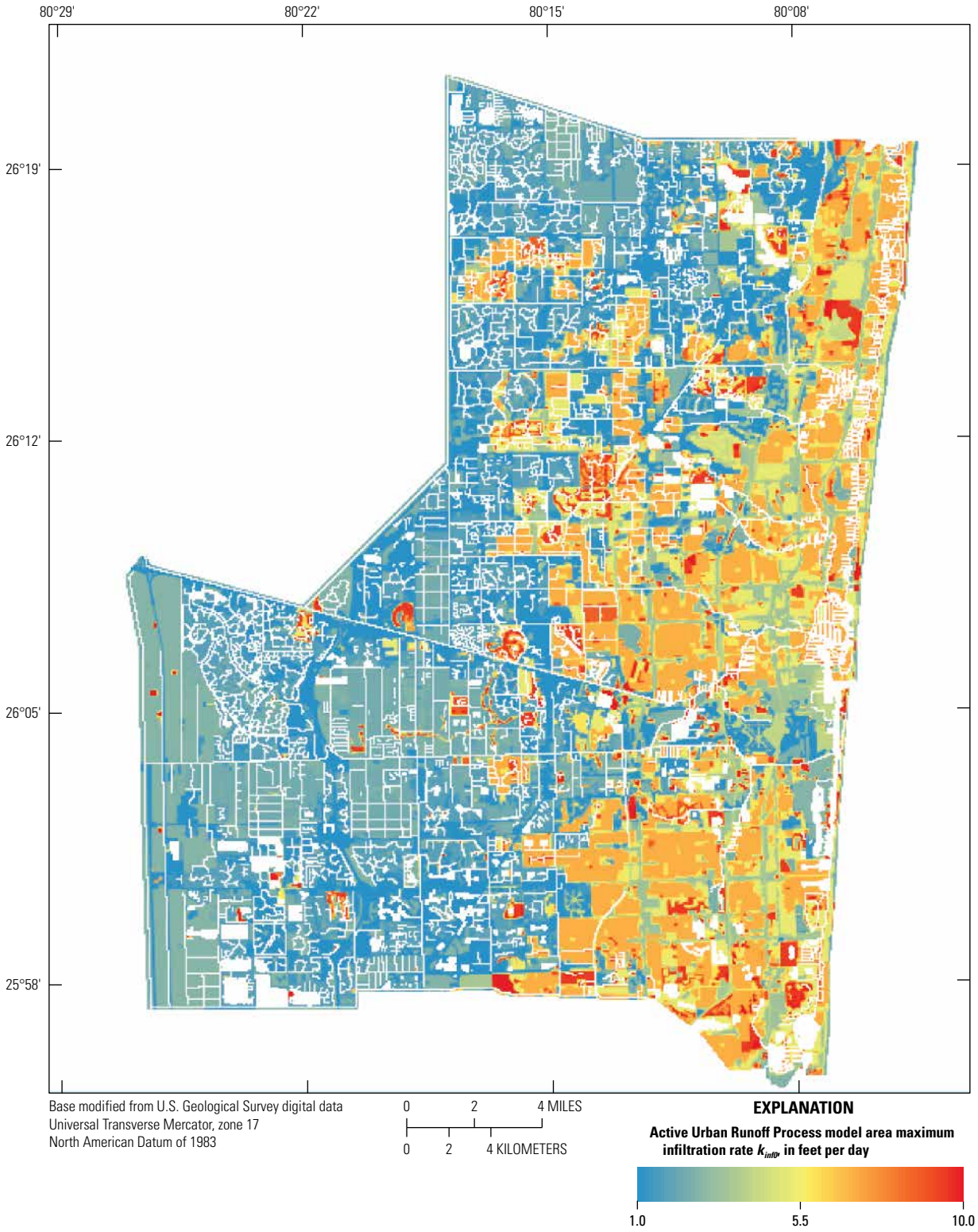

Figure E25. Calculated maximum infiltration rates in feet per day used by the Urban Runoff process within the active model area.

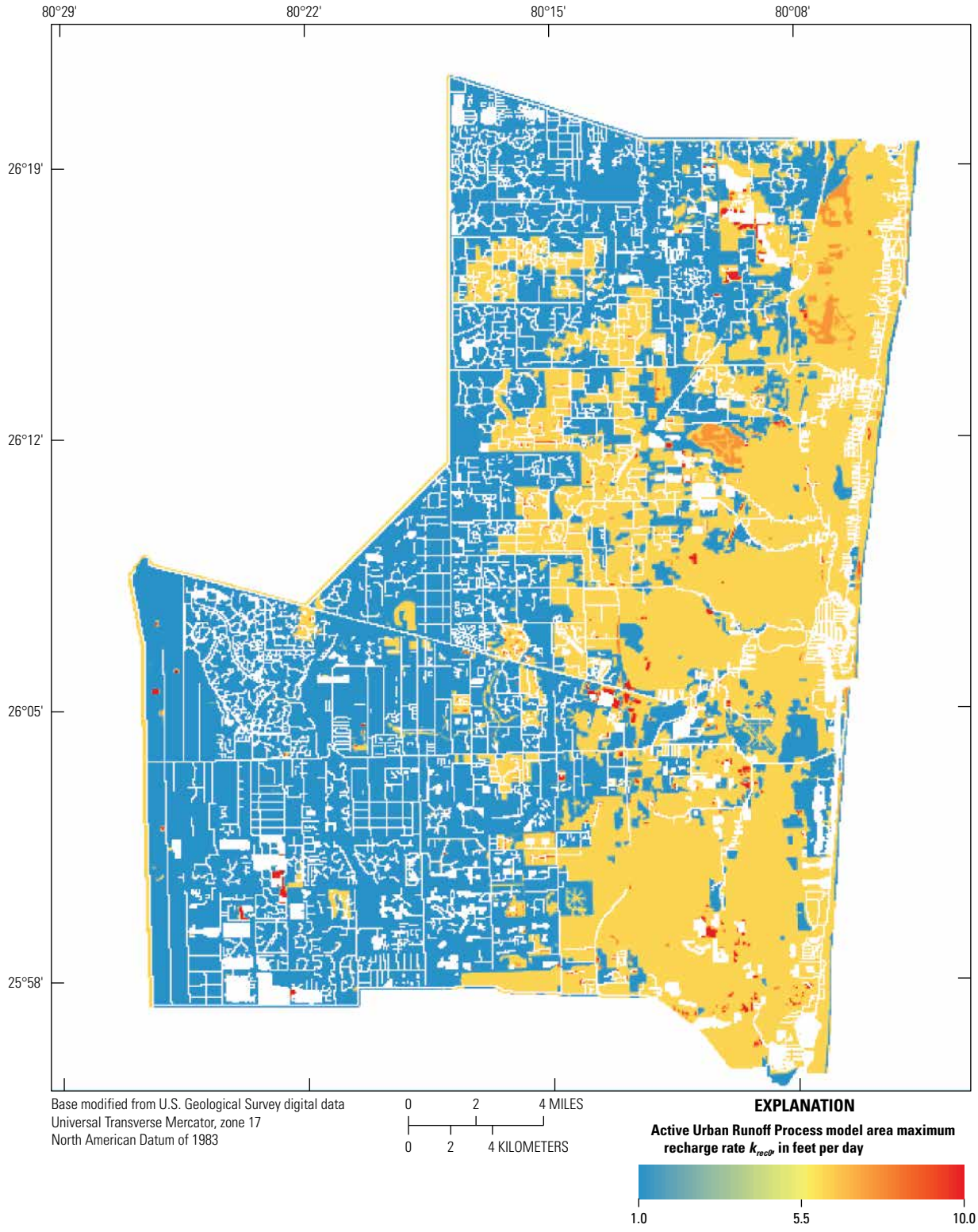

Figure E26. Calculated maximum recharge rates in feet per day used by the Urban Runoff process within the active model area.

The average contribution of rainfall into the C-9 Canal was estimated by first calculating the difference in flow out of the C-9 Canal through the S-29 structure and the flows into the C-9 Canal from S-30 (fig. A1). Then the volumetric rate of wet season average (2013–17) rainfall over the C-9 Canal drainage area was calculated as 581.9 ft^3/s using a drainage area of 99.4 mi^2 and an average of the S30_R, S29Z_R, and S29_R (fig. E22) rainfall measurements which were 0.211, 0.233, and 0.204 in/d, respectively (table E16). The wet season average (2013–17) flow rates through the S-29 and S-30 structures were 453.2 and 13.0 ft^3/s, respectively. The calculated difference between flows through the S-29 and S-30 structures was 414.2 ft^3/s or 75.7 percent of the total wet season rainfall over the entire drainage area. The part of the drainage area not within the active model extents was 33.7 mi^2, or 33.9 percent of the total drainage area. Therefore, the additional inflows caused by rainfall from the part of the C-9 Canal drainage area missing from the model extents was approximately 33.9 percent of the 75.7 percent of total rainfall for the area, or 25.7 percent. This value was used for the steady-state and transient models. The wet season average inflow to the C-9 Canal was estimated to be 149.3 ft^3/s (table E16, fig. E29).

Estimation of Selected Model Parameters Under Steady-State Average Wet Season Conditions (2013–17)

A limited set of model parameters were adjusted to improve model fit to steady-state wet season average conditions using the automated Parameter ESTimation software (PEST) (Doherty, 2010). Because of the increased likelihood of inundation during the wet season from increased precipitation, capturing the system's behavior during this period was the focus of the parameter estimation. Canal leakance, general-head boundary conductance values, and ET extinction depths were adjusted to obtain better matches for flow out of the primary structures within the model. Flow through the nine primary structures was used as an observation, with S-37B replacing S-37A because of discrepancies in the S-37A flow measurements (table E17). Groundwater level observations were not included because of the strong influence of surface-water stage on groundwater levels and the deviation between simulated surface-water structure operations and actual operations.

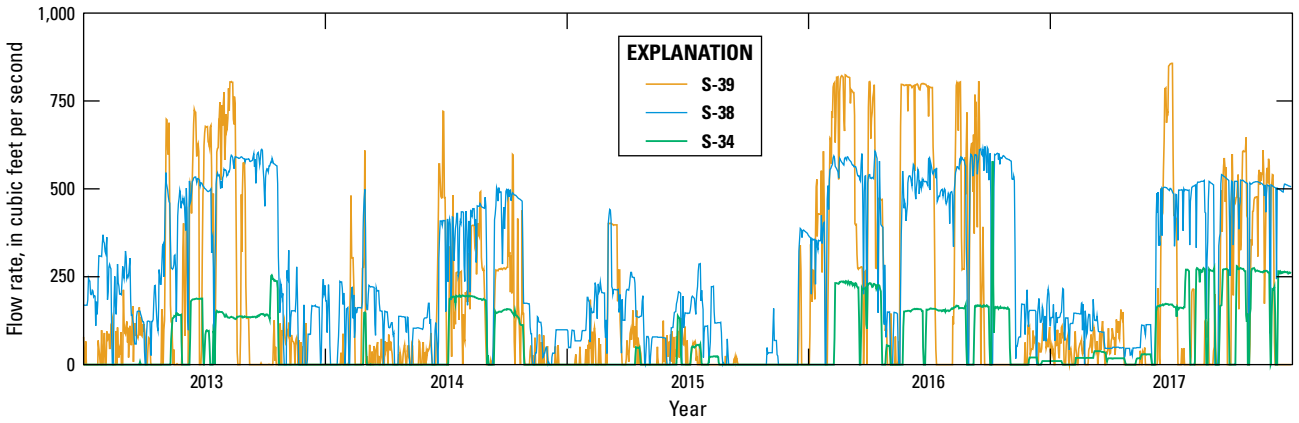

Figure E27. Measured flow through the S-39, S-38, and S-34 structures during the historical period.

Table E15. Information about the Hillsboro Canal drainage area and the estimated inflow into the Surface-Water Routing (SWR1) process surface-water model.

[WCA, water conservation area; mi^2, square mile; %, percent; ft^3/s, cubic foot per second]

Hillsboro Canal drainage area		Average wet season values					
Total drainage area	Missing drainage area	Total rainfall	Flow through G-56 structure	Flow through S-39 structure	Estimated inflow into L-36 from WCA 2A	Estimated rainfall contribution	Estimated inflow from missing area (wet season)
90.0 mi^2	51.8 mi^2 (57.6%)	538.7 ft^3/s	351.1 ft^3/s	208.5 ft^3/s	40 ft^3/s	102.6 $ft^3/2$ (19.1% rainfall)	59.1 ft^3/s

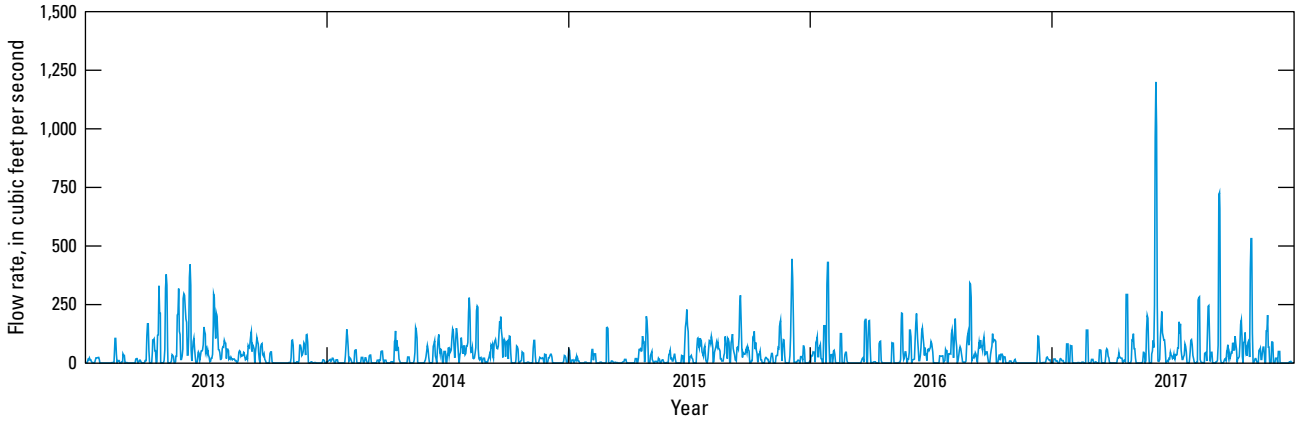

Figure E28. Estimated inflow rate into the Hillsboro Canal from the missing part of the drainage area for the historical period.

Table E16. Information about the C-9 Canal drainage area and the estimated inflow into the Surface-Water Routing (SWR1) process surface-water model.

[mi², square mile; %, percent; ft³/s, cubic foot per second]

C-9 Canal drainage area		Average wet season values				
Total drainage area	Missing drainage area	Total rainfall	Flow through S-29 structure	Flow through S-30	Estimated rainfall contribution	Estimated inflow from missing area (wet season)
99.4 mi²	33.7 mi² (33.9%)	581.9 ft³/s	453.2 ft³/s	13.0 ft³/s	440.2 ft³/s (75.7% rainfall)	149.3 ft³/s

The assignment and calibration of canal leakance values were based on drainage area and connection to primary drainage canals and primary structures. This methodology was used to divide the surface-water reaches into 11 designations with an additional designation used for all unassigned reaches (table E13). Upper and lower bounds of 0.50 and 10.00 day^{-1} were used for calibrating the leakance parameter based on parameters from the previous inundation and southern and central saltwater intrusion models. The resulting range of leakance parameters ranged from 0.50 to 9.983 day^{-1} with a mean of 2.60 day^{-1}.

The conductance values used for the general-head boundaries along the western extent (fig. A1) were scaled independently for each boundary section corresponding to a WCA during calibration. Initial estimates of conductance values along a WCA for each of the three layers were calculated using the hydraulic conductivity, layer thickness, and an estimated distance (eq. 1). These initial estimates were averaged along each boundary to obtain one value for each layer along a WCA. Each boundary was assigned a scaling factor that was applied to all layers equally and allowed to be adjusted during model calibration. Upper and lower bounds of 0.5 and 5.00 were used during calibration. The resulting scaling factors ranged from 0.583 to 3.169 and correspond to conductance values ranging from 2,160.5 to 38,332.3 ft²/d (table E1).

The user-defined extinction depth used by the EVT package was also adjusted during model calibration. The field of spatially variable extinction depths calibrated during the development of the southern and central saltwater intrusion model was used as the initial estimate for the extinction depth values (figs. E22 and E23). Eighteen scaling factors were assigned on the basis of rainfall zones, and upper and lower limits of 0.25 and 2.00 were used during calibration. The resulting scale factors ranged from 0.28 to 1.904 (table E14).

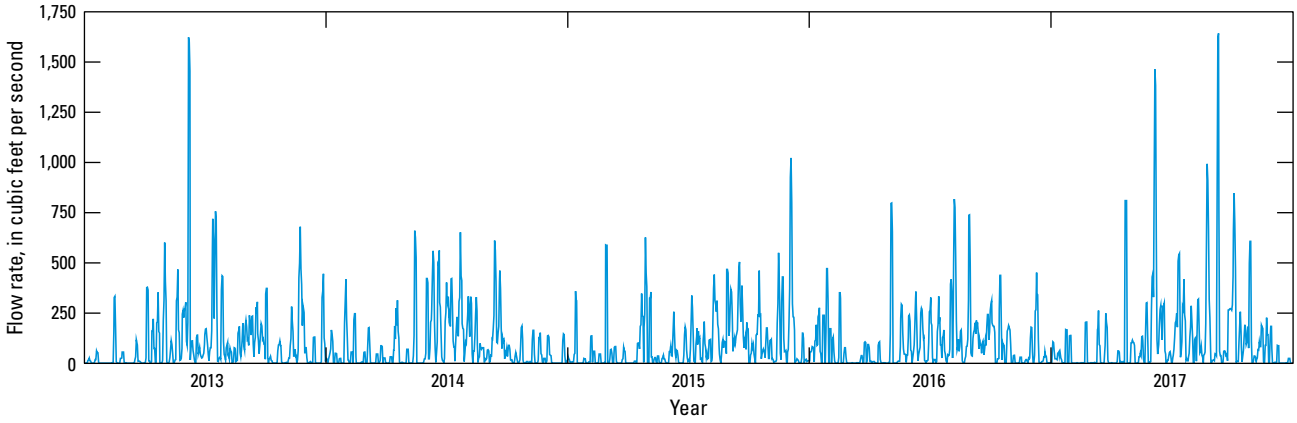

Figure E29. Estimated inflow rate into the C-9 Canal from the missing part of the drainage area for the historical period.

The differences between simulated and measured primary structure flow for the calibrated wet season average simulation ranged from −57.4 to 29.8 ft^3/s, with a mean of −5.5 ft^3/s (table E17). The total difference between simulated and measured flow out of the surface-water model through these structures was −49.5 ft^3/s (−2.5 percent). Two of the largest differences occurred at the G-56 and S-29 structures. The G-56 structure is located at the end of the Hillsboro Canal, and the S-29 structure is located at the end of the C-9 Canal, which are both adjacent to the model's northern and southern boundaries. These canals were assigned estimated surface-water inflows to represent flow from parts of the drainage area not actively simulated in the model extents. The adjusted model parameters that influence the flow at these two structures also tended to be nearer to the upper and lower bounds of the assigned ranges within PEST, indicating that the flows through the G-56 structure were generally biased lower and those through the S-29 structure were generally biased higher. The adjusted scaling factor for the conductance along WCA 2A, which would mostly affect flow through G-56, was 0.583 whereas the adjusted scaling factor for the conductance along WCA 3B, which would most affect flow through S-29, was 3.169 (table E1). Leakance values for the drainage areas associated with the Hillsboro Canal were adjusted to 0.618 day^{-1} whereas those associated with the C-9 were adjusted to 5.160 and 9.983 day^{-1} (table E13). The adjusted extinction depth scaling factors for the areas near the C-9 Canal were lower than the average with values of 0.265, 0.392, and 0.628 for the rainfall zones designated as S30_R, S29_R, and S29Z_R, respectively (table E14). The adjusted extinction depth scaling factors for the areas near the Hillsboro Canal did not show a consistent pattern. These results indicate that the simulated flows of drainage basins that are only partially simulated are subject to poorer matching to observations within the model.

Though the parameter estimation process was focused on wet season conditions, the model produced similar results to measured values throughout the entire historical period. Analysis of the model's fit to historical transient groundwater levels at 23 monitoring locations throughout the entire historical period resulted in mean groundwater level differences and mean root-mean squared differences (RMSDs) of −0.28 and 0.89 ft, respectively. Analysis of the model's fit to historical transient upstream stage at the primary structures resulted in a mean difference and RMSD of −0.155 and 0.678 ft, respectively. Analysis of the model's fit to historical transient flow through the primary structures resulted in a mean difference and RMSD of −0.7 and 106.5 ft^3/s, respectively (chapter B).

Table E17. Measured and simulated wet season average structure flows for the historical period (2013–17) after model calibration.

[ft^3/s, cubic foot per second]

Structure name	Wet season structure flow (ft^3/s)		Difference (ft^3/s)
	Measured average	Steady-state simulated	
G-56	351.1	345.5	−5.7
G-57	15.4	16.0	0.6
S-37B	472.9	444.2	−28.7
S-36	112.9	142.7	29.8
S-33	9.5	8.8	−0.7
G-54	166.6	164.2	−2.4
S-9	85.5	90.1	4.6
S-13	272.1	282.5	10.4
S-29	453.2	395.9	−57.4
Total	1,939.3	1,889.7	−49.5

References Cited

Decker, J.D., 2022, MODFLOW-NWT datasets for the simulation of drainage infrastructure and groundwater system response to changes in sea-level and precipitation, Broward County, Florida: U.S. Geological Survey data release, https://doi.org/10.5066/P9ITQBFZ.

Decker, J.D., and Hughes, J.D., 2013, Urban runoff (URO) process for MODFLOW 2005—Simulation of sub-grid scale urban hydrologic processes in Broward County, Florida, *in* MODFLOW and more 2013—Translating Science into Practice [Proceedings]: Golden, Colo., Colorado School of Mines, Integrated Groundwater Modeling Center, p. 216–221.

Decker, J.D., Hughes, J.D., and Swain, E.D., 2019, Potential for increased inundation in flood-prone regions of southeast Florida in response to climate and sea-level changes in Broward County, Florida, 2060–69: U.S. Geological Survey Scientific Investigations Report 2018–5125, 106 p., accessed November 3, 2021, at https://doi.org/10.3133/sir20185125.

Doherty, J.E., 2010, PEST, model-independent parameter estimation—User manual (5th ed.): Brisbane, Australia, Watermark Numerical Computing, 336 p.

Harbaugh, A.W., 2005, MODFLOW-2005, the U.S. Geological Survey modular groundwater model—The groundwater flow process: U.S. Geological Survey Techniques and Methods, book 6, chap. A16, 253 p.

Hindle, T., and Restrepo, J., 1999, Broward County hydrographic survey report: Boca Raton, Fla., Florida Atlantic University Department of Geography & Geology.

Hughes, J.D., Langevin, C.D., Chartier, K.L., and White, J.T., 2012, Documentation of the Surface-Water Routing (SWR1) process for modeling surface-water flow with the U.S. Geological Survey Modular Ground-Water Model (MODFLOW-2005): U.S. Geological Survey Techniques and Methods, book 6, chap. A40 (ver. 1.0), 113 p.

Hughes, J.D., Sifuentes, D.F., and White, J.T., 2016, Potential effects of alterations to the hydrologic system on the distribution of salinity in the Biscayne aquifer in Broward County, Florida: U.S. Geological Survey Scientific Investigations Report 2016–5022, 114 p., accessed November 3, 2021, at https://doi.org/10.3133/sir20165022.

Langevin, C.D., and Zygnerski, M., 2013, Effect of sea-level rise on saltwater intrusion near a coastal well field in southeastern Florida: Ground Water, v. 51, no. 5, p. 781–803.

Mecikalski, J.R., Shoemaker, W.B., Wu, Q., Holmes, M.A., Paech, S.J., and Sumner, D.M., 2018, High-resolution GOES insolation–evapotranspiration data set for water resource management in Florida—1995–2015: Journal of Irrigation and Drainage Engineering, v. 144, no. 9, 04018025, accessed November 3, 2021, at https://doi.org/10.1061/(ASCE)IR.1943-4774.0001312.

Niswonger, R.G., Panday, S., and Ibaraki, M., 2011, MODFLOW-NWT—A Newton formulation for MODFLOW-2005: U.S. Geological Survey Techniques and Methods, book 6, chap. A37, 44 p.

Patino, E., Conrads, P., Swain, E.D., and Beerens, J., 2017, Everglades Depth Estimation Network (EDEN)—A decade of serving hydrologic information to scientists and resource managers: U.S. Geological Survey Fact Sheet 2017–3069, 6 p.

Perkins, R.D., 1977, Depositional framework of Pleistocene rocks in south Florida, *in* Enos, P., and Perkins, R.D., eds., Quaternary sedimentation in south Florida: Geological Society of America Memoir, v. 147, p. 131–198.

Shoemaker, W.B., 2017, Daily reference (RET) and potential (PET) evapotranspiration data over Florida: U.S. Geological Survey data release, accessed May 27, 2020, at https://www.usgs.gov/centers/car-fl-water/science/reference-and-potential-evapotranspiration?qt-science_center_objects=0#qt-science_center_objects.

South Florida Water Management District [SFWMD], 2007, 2007 Broward 5-ft DEM in NAVD 1988, release version 1: South Florida Water Management District, accessed August 4, 2021, at https://geo-sfwmd.hub.arcgis.com/documents/broward-2007-fdem-5-ft/about.

South Florida Water Management District [SFWMD], 2016, Structure books: West Palm Beach, Fla., South Florida Water Management District, 597 p., accessed May 19, 2016, at ftp://ftp.sfwmd.gov/pub/hehmke/AsBuilts/Other%20Reports/OCC%20Structure%20Book.pdf.

For more information about this publication, contact
Director, Caribbean-Florida Water Science Center
U.S. Geological Survey
4446 Pet Lane, Suite 108
Lutz, FL 33559

For additional information, visit
https://www.usgs.gov/centers/car-fl-water

Publishing support provided by
Lafayette Publishing Service Center

ISSN 2328-0328 (online)
https://doi.org/10.3133/sir20225074